

**DESIGN OF A HYDROSTATIC ACTUATOR  
FOR USE IN FLIGHT SIMULATION MOTION SYSTEMS**

**Constantine Calogeropoulos**

**A Major Technical Report  
in  
The Department  
of  
Mechanical Engineering**

**Presented in Partial Fulfillment of the Requirement  
for the degree of Masters of Engineering at**

**Concordia University  
Montreal, Quebec, Canada**

**June, 1981**

**© Constantine Calogeropoulos, 1981**

## ABSTRACT

### Design of a Hydrostatic Actuator For Use in Flight Simulation Motion Systems

Constantine Calogeropoulos

A high performance servo-actuator has been designed and tested for use in flight simulator motion systems. The frequency response and smoothness of the resulting system are significantly improved over previous systems. The servo-actuator has hydrostatic piston and rod-end bearings, internal cushioning and it uses an ultrasonic position transducer mounted inside the piston rod. Force feedback is provided both by an instrumented rod-end pin and by pressure transducers.

The servo-valve has been optimized for the application and a drive circuit has been developed which blends position and acceleration commands to provide excellent controllability.

The report reviews the design requirements and development. Rationale and results are presented indicating frequency response which is flat to 10Hz with a 18,000 lb. payload.

### ACKNOWLEDGEMENT

I would like to express my thanks and gratitude to a number of people that contributed to the completion of this report.

First and foremost I wish to thank Dr. M. McKinnon, CAE Electronics R & D Manager, under whose advice and experience this study was completed.

I wish to thank my professor and advisor Dr. J.V. Svoboda, Concordia University for his guidance and extensive collaboration in the preparation of this report.

I am grateful to the CAE Electronics Ltd. administration for giving permission to use some unpublished material and the company resources.

My thanks are due to other CAE Colleagues for their help to prepare the graphs, tables and illustrations. Special thanks to Jackie Lambe and Donna Masterson for the presentation of this report.

## TABLE OF CONTENTS

<u>SECTION</u>	<u>TITLE</u>	<u>PAGE</u>
	LIST OF FIGURES	iii
	LIST OF TABLES	vi
	NOMENCLATURE	vii
1.0	INTRODUCTION	1
	1.1 Motion System Requirements	5
	1.2 Motion System Performance	6
	1.3 Description of Previous Design	14
2.0	BASIC DESIGN	17
	2.1 Critical Parameters	17
	2.2 Cylinder Stress Calculations	20
	2.2.1 Stress Analysis of the Rods	20
	2.2.2 Stress Analysis of the Cylinder	29
	2.2.3 Summary of Stress Analysis	42
	2.3 Vibration Characteristics	44
	2.3.1 Hydraulic Modes	45
	2.3.2 Mechanical Modes	50
	2.3.3 Hydraulic Oil Spring Stiffness	51
	2.3.4 Cylinder Hydraulic Resonance	52
	2.3.5 Summary	55
3.0	HYDROSTATIC BEARING ANALYSIS	57
	3.1 Basic Design Theory	57
	3.1.1 Introduction	59
	3.1.2 Single Bearing	60
	3.1.3 Double Bearing	63
	3.2 Calculation of Parameters	66
	3.2.1 Leakage Flow Calculations	66
	3.2.2 Bearing Centering Force Calculations	74
	3.3 Design Critical Parameters	81



## TABLE OF CONTENTS (Cont'd)

<u>SECTION</u>	<u>TITLE</u>	<u>PAGE</u>
4.0	CUSHION DESIGN	84
	4.1 Mathematical Model	91
	4.2 Calculation of Cushion Forces	93
5.0	SERVO VALVE CHARACTERISTICS	98
	5.1 Introduction	98
	5.2 Types of Lap and Their Characteristics	102
	5.3 Position Accuracy	104
	5.4 Servovalve Important Parameters	109
	5.5 Servovalve Asymmetry	112
	5.6 Servovalve Evaluation	115
6.0	SERVO JACK CONTROL	121
	6.1 Mathematical Model	121
	6.2 Damping Methods	127
	6.3 Load Compensation	129
	6.4 Effects of Coulomb Friction	131
	6.5 Preliminary Design Performance	133
	6.6 Cue Generation and Wash-Out	138
	6.7 Servo Jack Control Block Diagram	142
7.0	SERVO JACK PERFORMANCE	151
	7.1 Results	155
	7.2 Conclusion	172
8.0	REFERENCES	175
9.0	BIBLIOGRAPHY	177

## LIST OF FIGURES

<u>FIGURE</u>	<u>TITLE</u>	<u>PAGE</u>
1.1	Block Diagram of Typical Simulator	3
1.2	Series 400 Motion System	8
1.3	Series 400 Motion System Frequency Response	11
1.4	Hydraulic Schematic Series 400	12
1.5	Conventional Hydraulic Cylinder Series 400	13
2.1	Tie Rod Variation with Pressure	26
2.2	Sodeberg Diagram for Tie Rod Infinite Fatigue Life	26
2.3	Typical Cylinder	31
2.4	Critical Load Versus Slenderness Ratio	39
3.1	Hydrostatic Actuator	58
3.2	Dimensions of Single Conical Hydrostatic Bearing	61
3.3	Double Conical Hydrostatic Piston Bearing	61
3.4	Double Conical Hydrostatic Rod End Bearing	64
3.5	Leakage Flow Piston Bearing Single	70
3.6	Leakage Flow Rod End Bearing (Lower)	71
3.7	Leakage Flow Rod End Bearing (Upper)	72
3.8	Bearing Forces Piston Bearing (Single)	75
3.9	Bearing Forces Rod End Bearing (Lower)	76
3.10	Bearing Forces Rod End Bearing (Upper)	77
4.1	Cushion Typical Performance Curves	86
4.2	Lower Cushion	87
4.3	Upper Cushion	87
4.4	Cylinder Cushion Parameters	89
4.5	Cushion Orifice Area vs Travel (Log Scale)	92
4.6	Cushion Orifice Area vs Travel (Linear Scale)	92
4.7	Lower Cushion Acceleration and Velocity Profile	95
5.1	Two Stage Electrohydraulic Servo Valve	99
5.2	Servo Valve Flow-Input Current Relationship	101
5.3	Servo Valve Pressure-Input Current Relationship	101

# LIST OF FIGURES. (Cont'd)

<u>FIGURE</u>	<u>TITLE</u>	<u>PAGE</u>
5.4	Types of Spools	103
5.5	Frequency Response of a Typical Servo Valve.	110
5.6	Assymetric Cylinder with 4 Way Valve	113
5.7	Noise Acceleration	118
5.8	Actuator Velocity-Servo Valve Input Current (Moog)	119
5.9	Actuator Velocity-Servo Valve Input Current (Pegasus)	120
6.1	Block Diagram of Hydraulic Servo "Physical Model"	123
6.2	Block Diagram of Hydraulic Servo "Control Model"	123
6.3	Modified Block Diagram of Servo-Loop	125
6.4	Performance Diagram	137
6.5	Relationship Between Velocity, Displacement and Wash-out	139
6.6	Relationship Between Velocity, Cue Acceleration and Time	139
6.7	Relationship Between Velocity, Cue Acceleration, Wash-out Acceleration and Time	141
6.8	Relationship Between Velocity, Cue Acceleration and Travel	141
6.9	Block Diagram of Servo Jack Control	143
6.10	Simulated System Frequency Response	147
6.11	Simulated System Frequency Response	149
6.12	Simulated System Frequency Response	150
7.1	Hydraulic Schematic of Servo Jack Series 500	152
7.2	Motion System Series 500	153
7.3	Test Equipment Set-up	154
7.4	Frequency Response, Pitch Mode	156
7.5	Frequency Response, Roll Mode	157
7.6	Frequency Response, Yaw Mode	158
7.7	Frequency Response, Heave Mode	159
7.8	Frequency Response, Lateral Mode	160
7.9	Frequency Response, Longitudinal Mode	161
7.10	Frequency Response, Heave Mode without Elliptic Filter	162
7.11	Frequency Response, Heave Mode with Elliptic Filter	163

LIST OF FIGURES. (Cont'd)

<u>FIGURE</u>	<u>TITLE</u>	<u>PAGE</u>
7.12	Acceleration Noise, Excitation Mode: Roll	164
7.13	Acceleration Noise, Excitation Mode: Heave	165
7.14	Motion System Performance Diagram, Pitch Mode	166
7.15	Motion System Performance Diagram, Yaw Mode	166
7.16	Motion System Performance Diagram, Heave Mode	167
7.17	Motion System Performance Diagram, Roll Mode	167
7.18	Motion System Performance Diagram, Longitudinal Mode	168
7.19	Motion System Performance Diagram, Lateral Mode	168
7.20	Impulse Response Results	170
7.21	Series 500 Motion Simulator	171

# LIST OF TABLES

<u>TABLE</u>	<u>TITLE</u>	<u>PAGE</u>
1.1	Maximum Excursions of Series 500 Motion System	10
3.1	Dimensions and Parameters for Leakage Flow Calculations	68
3.2	Viscosity Versus Temperature	73
3.3	Dimensions and Parameters for Bearing Force Calculations	79
5.1	Servovalve Specification Comparison	117

## NOMENCLATURE

$a$	Cue acceleration
$a_w$	Wash-out acceleration
$a_{1,2,3,4}$	Servo valve spool opening area
$A$	Cylinder bore area, $\text{in}^2$
$A_c$	Cylinder body wall cross-section area, $\text{in}^2$
$A_e$	Cushion effective area, $\text{in}^2$
$A_o$	Cushion orifice area, $\text{in}^2$
$A_r$	Piston rod cross-section area, $\text{in}^2$
$A_t$	Tie rod cross-section area (sum of 4 rods), $\text{in}^2$
$A_{THD}$	Piston rod thread stress area, $\text{in}^2$
$A_y$	Servo valve uncovered slot area, $\text{in}^2$
$A_1$	Cylinder cap end area, $\text{in}^2$
$A_2$	Cylinder rod end area, $\text{in}^2$
$b$	Thread pitch, in.
$B$	Viscous friction
$c$	Hydrostatic bearing radial clearance
$c_h$	Hydraulic stiffness, $\text{lb/in}$
$c_o$	Hydraulic oil spring stiffness, $\text{lb/in}$
$C$	Orifice discharge coefficient
$C_t$	Thread stress concentration factor
$C'$	Column end condition constant
$d$	Hydrostatic bearing nominal diameter
$d_t$	Tie rod nominal diameter, in.
$D_1$	Cylinder bore diameter, in.
$D_o$	Cylinder outside diameter, in.

### NOMENCLATURE (Cont'd)

$D_{ri}$	Piston rod inside diameter, in.
$D_{ro}$	Piston rod outside diameter, in.
$e$	Cylinder-piston eccentricity
$E$	Eccentricity dimensionless parameter.
$E_k$	Kinetic energy
$E_p$	Potential energy
$E_1$	Cylinder body modulus of elasticity, psi
$E_2$	Tie rod modulus of elasticity, psi
$f$	Hydrostatic bearing radial force
$F$	Load, lbs.
$F_c$	Axial contact reaction load of cylinder body, lbs.
$F_{cr}$	Critical load, lbs.
$F_e$	External load, lbs.
$F_f$	Coulomb friction, lbs.
$F_j$	Servojack load due to payload, lbs.
$F_r$	Cushion resistive load, lbs.
$F_{st}$	Static load, lbs.
$F_t$	Tie rod load due to internal pressure (sum of 4 rods), lbs.
$F_{tav}$	Average load on all tie rods, lbs.
$F_{tr}$	Range load on all tie rods, lbs.
$F_{t1}$	Tie rod load with pressure, at beginning of stroke, lbs.
$F_{t2}$	Tie rod load with pressure, at full stroke, lbs.
$F_{t3}$	Tie rod minimum load with pressure, at full stroke, lbs.
$g$	Gravity constant, in/sec <sup>2</sup>
$G(s)$	Transfer function

# NOMENCLATURE (Cont'd)

$h$	Hydrostatic conical-bearing radial distance
$h_t$	Thread height, in.
$H$	Transfer function
$i$	Servo valve current, amps.
$I_1$	Moment of inertia of cylinder body, $\text{in}^4$
$I_2$	Moment of inertia of piston rod, $\text{in}^4$
$k$	Torque friction factor
$k_c$	Stiffness coefficient of cylinder body, $\text{lb/in}$
$k_t$	Stiffness coefficient of tie rod, $\text{lb/in}$
$K$	Cylinder geometry constant
$K_c$	Servo valve position feedback constant
$K_f$	Force feedback constant
$K_p$	Pressure feedback constant
$K_v$	Servo valve velocity gain
$K'_v$	Servo valve-actuator velocity gain
$K_s$	Servo valve gain
$K_1$	Position loop damping
$K_2$	Position loop gain
$K_3$	Feed-forward velocity correction
$l$	Hydrostatic conical bearing length
$l_1$	Oil column in cylinder cap end, $\text{in}^3$
$l_2$	Oil column in cylinder rod end, $\text{in}^3$
$L$	Piston rod length, in.
$L_c$	Cylinder body length, in.
$L_t$	Tie rod length, in.



## NOMENCLATURE (Cont'd)

M	Mass Load
$M_b$	Bending moment due to cylinder curvature.
$M_1$	Bending moment due to cylinder external load.
n	Number of piston rod threads subject to load.
N	Number of tie rods.
p	Internal cylinder pressure, psi,
$p_s$	Cylinder-cap separation pressure, psi
P	Cylinder maximum load due to internal pressure, lbs.
$P_L$	Load pressure, psi
$P_s$	Supply pressure, psi
$P_t$	Preload on tie rods due to nut torque (sum of 4 rods), lbs.
$P_1$	Cylinder cap end pressure, psi
$P_2$	Cylinder rod end pressure, psi
$P_3$	Return line pressure, psi
q	Hydrostatic bearing leakage flow.
Q	Servovalve output flow.
$Q_1$	Oil flow into cylinder cap end.
$Q_2$	Oil flow into cylinder rod end.
r	Radius of gyration, piston rod, in.
$r_m$	Thread mean radius, piston rod, in.
s	Laplace transform operator
S	Piston stroke, in.
$S_b$	Bending stress at root of thread, psi
$S_c$	Cylinder body stress, psi
$S_{cb}$	Cylinder bending stress, psi

# NOMENCLATURE (Cont'd)

$S_{ch}$	Cylinder hoop stress, psi
$S_e$	Endurance limit of material, psi
$S_{eq}$	Equivalent column stress, psi
$S_i$	Initial tie rod thread stress due to preload, psi.
$S_s$	Mean transverse thread shear stress, psi
$S_{tav}$	Average tie rod thread stress during cyclic loading, psi
$S_{tr}$	Range stress in tie rods, psi.
$S_u$	Ultimate tensile strength of material, psi
$S_y$	Yield Strength of material, psi
$t$	Hydrostatic conical bearing laper
$t_a$	Cue acceleration duration time, sec.
$t_c$	Cushion duration time, sec
$T$	Hydrostatic conical bearing geometry parameter
$T'$	Tie rod preload torque per rod, ft-lbs.
$U$	Servo valve spool underlap, in.
$v$	Hydrostatic bearing axial speed
$v_1$	Maximum piston velocity entering cushion, in/sec
$v_0$	Maximum permissible velocity at end of cushion, in/sec.
$V$	Hydrostatic bearing velocity parameter, single bearing
$V^*$	Hydrostatic bearing velocity parameter, double bearing
$V_c$	Velocity parameter where cavitation might occur.
$V_1$	Volume of cap end oil column, in <sup>3</sup>
$V_2$	Volume of rod end oil column, in <sup>3</sup>
$w$	Natural frequency rad/sec
$w_b$	Servojack bandwidth, rad/sec

# NOMENCLATURE (Con'd)

$w_0$	Servojack undamped frequency rad/sec
$w_{ov}$	Servo valve natural frequency
$W$	Static dead weight, lbs
$x$	Axial, horizontal co-ordinate
$x_1$	Servo valve spool displacement
$X$	Cushion travel
$y$	Servojack model piston displacement
$y_c$	Cylinder initial lateral deflection at interface, in.
$y_1$	Cylinder lateral deflection
$y_2$	Rod lateral deflection
$Z_c$	Cylinder body section modulus, in <sup>3</sup>
$Z_r$	Piston rod section modulus, in <sup>3</sup>
$\alpha$	Cushion deceleration, in/sec <sup>2</sup>
$\beta$	Oil Bulk modulus, psi
$\delta$	Differential increment
$\delta_c$	Cylinder deflection in compression, in.
$\delta_t$	Tie rod deflection in tension, in.
$\epsilon$	Signal error
$\epsilon_c$	Cylinder body linear strain, in/in
$\epsilon_t$	Tie rod linear strain, in/in
$\zeta$	Relative damping
$\zeta_v$	Servo valve relative damping

NOMENCLATURE (Cond't)

$\eta$	Pressure load coefficient
$\theta$	Crack Angle, degrees
$\mu$	Dynamic Viscosity
$\mu'$	Poisson's ratio
$\nu$	Kinematic viscosity
$\rho$	Fluid density, lb-sec <sup>2</sup> /in <sup>4</sup>
$\omega$	Fluid specific weight, lb/in <sup>3</sup>

## 1.0 INTRODUCTION

The object of this report is to summarize the study and development of an improved hydraulic servojack designed to replace an existing, conventional servojack in a six degrees of freedom synergistic motion system used in aircraft simulator motion systems.

This report shall describe the motion system requirements and performance, basic design concepts, the analysis of the hydrostatic bearings used, the design of the energy absorbing cushion, servovalve characteristics and servojack control circuits.

The motion system consists of a fixed triangular base and moving upper frame connected at the vertices by six independent hydraulic servojacks pivotted at both ends. This motion system provides a six degrees of freedom motion to the flight compartment which is mounted on top of the upper frame.

The purpose of the flight simulator is to stimulate the trainee pilot's sensory inputs in a manner similar to that which occurs in an actual flight, to provide a realistic environment and to simulate those motion cues which are useful to a pilot in controlling an aircraft.

The motion system hydraulic servojacks are powered by a hydraulic power supply which contains three electric motor driven variable displacement pressure compensated pumps, supplying 120 US gallons per minute at 1500 psi.

Electrical position command and acceleration signals, computed by a digital computer according to simulated flight conditions, are fed into the servojack of the motion system, so that the simulator will generate motions which will seem to the trainee pilot, to be similar to normal aircraft motions.

The motion system provides excursions, velocities, and accelerations in six orthogonal axes, vertical, lateral, longitudinal, pitch, roll and yaw. Combinations of these motions are used to provide special motion effects such as, rough air turbulence, engine effects, stall, buffet, stall onset, stall recovery, high speed buffet and background movement.

The computer software contains algorithms which determine all simulated motion system command signals. These command signals will be dependent upon aircraft flight conditions such as aircraft loading, control positions, atmospheric turbulence, autopilot command signals and simulated ground roughness and should be consistent with human sensory system requirements.

Figure 1.1 shows a schematic diagram of a typical simulator.

The motive for the development of a new design was to improve the fidelity and accuracy of motion. In the previous standard Series 400 motion system, conventional hydraulic servo-actuators were used.

Due to the use of conventional piston seals in this actuator, friction up to 300 lbs was measured. The presence of Coulomb friction and breakaway friction affected considerably the stability and accuracy

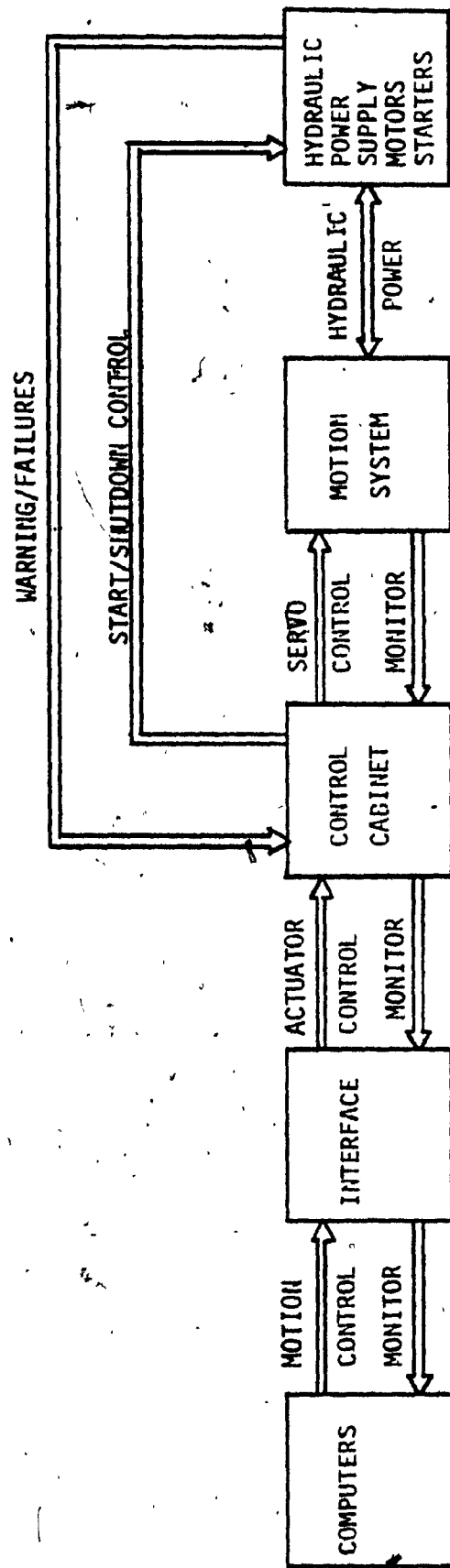


**FIGURE 1.1**  
**SCHEMATIC DIAGRAM OF MOTION SYSTEM**

of the system as well as the bandwidth. A reversal bump, an unwanted acceleration noticeable inside the flight compartment, was present at velocity reversal.

The design and development of hydraulic actuators with hydrostatic piston and rod end bearings offers a major opportunity to improve control accuracy and smoothness, as it eliminates Coulomb friction completely.

In conventional motion systems, acceptable positional accuracy could be achieved by the use of a high loop gain which, due to inherent nonlinearities present in the servojack transfer function, resulted in a system which was noise sensitive or rough. In the new design an acceleration servo is introduced to augment the position servo. The acceleration servo allows low position gain for steady state positional stability and a wide bandwidth for acceleration cues.



## 1.1 Motion System Requirements

The motion system will be a six degree-of-freedom electro-hydraulic servo system capable of providing realistic pitch, roll and yaw plus lateral, longitudinal and vertical translations in response to electrical command signals from the computer interface. The design approach will reflect state of the art techniques with due consideration given to simplicity, weight, reliability and maintainability requirements, while maximizing performance under the constraint that safety must be maintained.

The motion simulation must be capable of providing acceleration velocity and position cues to the occupants of the simulator, in a similar manner to the same cues experienced in the actual aircraft cockpit during flight and ground handling. These cues must be applied to the simulator occupants in the absence of a view outside the simulator cockpit. The movement of the cockpit will therefore be sensed only by the vestibular and haptic sensory systems of the occupants. The movements sensed by the occupants must be compatible with the movements of the simulated scene presented through the simulator visual system.

## 1.2 Motion System Performance

The essential performance requirements of the motion system are:

- Resolution, the ability to respond accurately to small amplitude inputs both in position and acceleration.
- Smoothness, the absence of self-generated or spurious acceleration disturbances.
- Stability, the absence of mechanical or electrohydraulic resonances which would adversely affect simulation.
- Frequency response, the ability of the motion system to respond to a wide range of frequencies. This is a particularly important parameter in the simulation of cues such as landing bumps, jerks or buffets which have significant high frequency components.

Generally, good simulation depends on judicious compromise between fidelity and stability. A high closed loop gain generally tends to improve fidelity as indicated by frequency response bandwidth and immunity to external disturbances; however, an excessive loop gain results in ringing due to sustained oscillations. The use of force feedback and careful selection of servovalve characteristics allow gains to be increased while maintaining or improving stability.

The quality of the overall system depends on the final tuning of the motion system, the selection of gains for position, velocity and force feedback and the tuning of the associated compensators and filters.

There are several parameters which must be optimized to achieve good simulation including motion envelope, system frequency response and the ability of the motion system to faithfully respond to low amplitude inputs with minimal self induced disturbance.

The performance requirements for a larger motion envelope is compromised by the design criterion for a simple and efficient motion system. The geometry of the six degrees of freedom synergistic motion system is determined by many parameters such as room size, required travels and crew compartment size and weight.

For the second performance measure, frequency response experience has shown that in conventional motion systems, attempts to maximize bandwidth are misdirected in terms of overall system performance. High frequency components are not normally as significant in flight simulation as smoothness. More significant for simulation is the elimination of low frequency structural resonances. It is only with the improvements described in this report that a wide bandwidth and smooth motion can be achieved simultaneously.

The reduction of acceleration noise is an important design goal particularly in the case of random discontinuities which can be interpreted as false motion cues and the reversal bump that traditionally has served the trainee with a constant reminder that he is in a simulator.

At the beginning of this study the standard CAE motion system was the Series 400 which is shown in Figure 1.2. In this 400 Series the flight compartment was installed on top of the upper triangular frame.

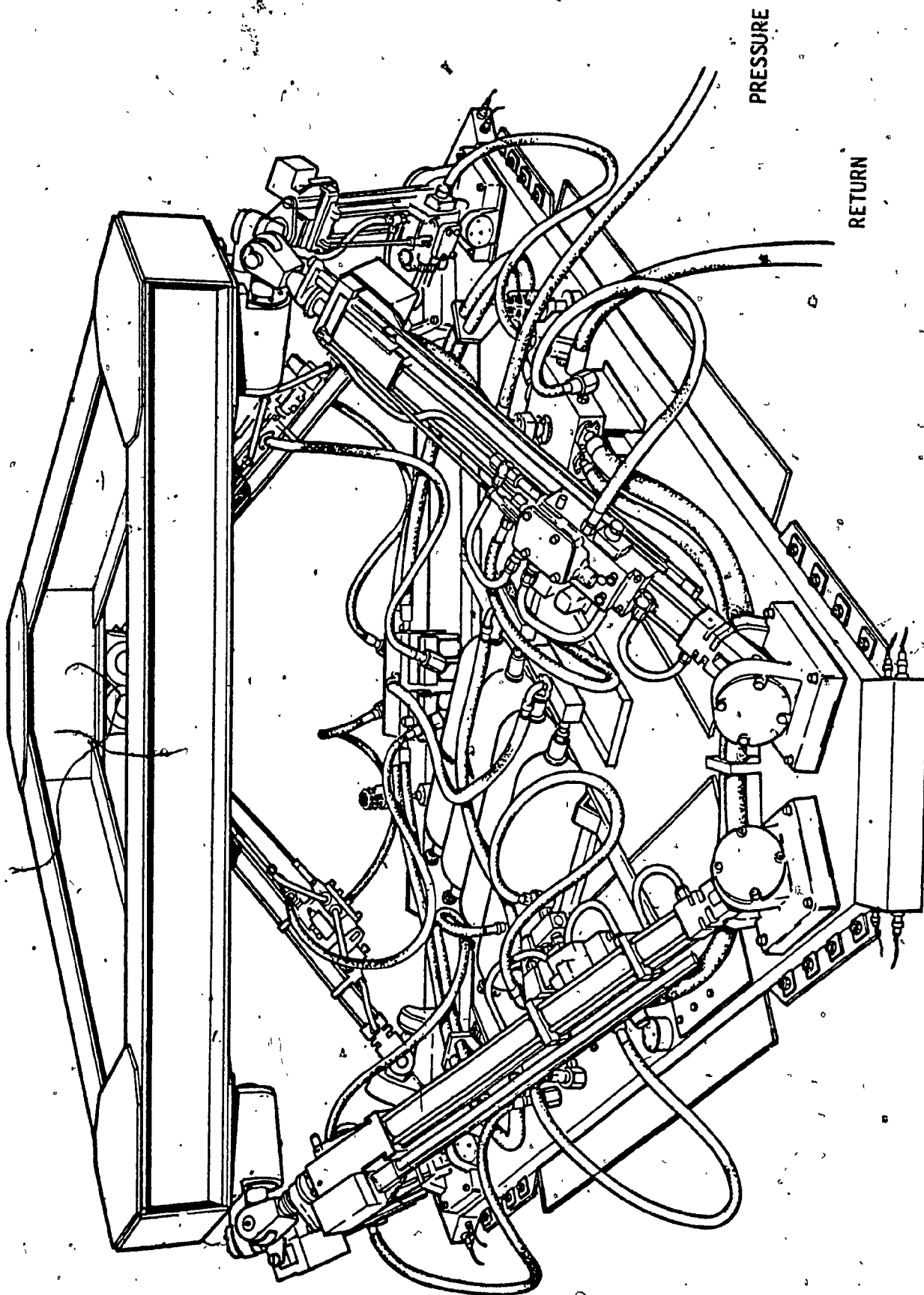


FIGURE 1.2 SERIES 400 MOTION SYSTEM

Its performance presented in table 1.1 is based on a payload of 12,500 lbs. The maximum excursions listed are functional limits, that is those which can be used in normal simulation, as measured without distortion of a 0.1 Hz sinusoidal drive signal.

The values in parenthesis are maximum possible or stop to stop values.

The values listed are measured independently in each axis about the neutral position except for the values for lateral and longitudinal motions which are about the neutral heave position. The motion system can achieve any combination of 20% of the maximum excursions. The lowest structural resonant frequency in Series 400 motion system will occur above 5 Hz. The closed loop frequency response is shown in Figure 1.3.

Figure 1.4 shows the hydraulic schematic diagram of the servojack, motion system and hydraulic power supply. The servojack shown in Figure 1.5 is the conventional jack used for CAE motion system at the start of the new design development.

TABLE 1.1

## MAXIMUM EXCURSIONS SERIES 400 MOTION SYSTEM

PARAMETER	PITCH	ROLL	YAW	VERTICAL	LATERAL	LONGITUDINAL
EXCURSION (DEG.)	$\pm 22$ ( $\pm 22$ )	$\pm 22$ ( $\pm 28$ )	$\pm 28$ ( $\pm 34$ )	$\pm 30$ , ( $\pm 33$ )	80, (88)	86, (95)
EXCURSION (IN)						
VELOCITY (DEG/SEC)	20	20	20	24	28	28
VELOCITY (IN/SEC)						
ACCELERATION (DEG/SEC <sup>2</sup> )	100	100	100	0.8	0.6	0.6
ACCELERATION (g)						
ONSET (DEG/SEC <sup>3</sup> )	300	300	300	4	3	3
ONSET (g/SEC)						

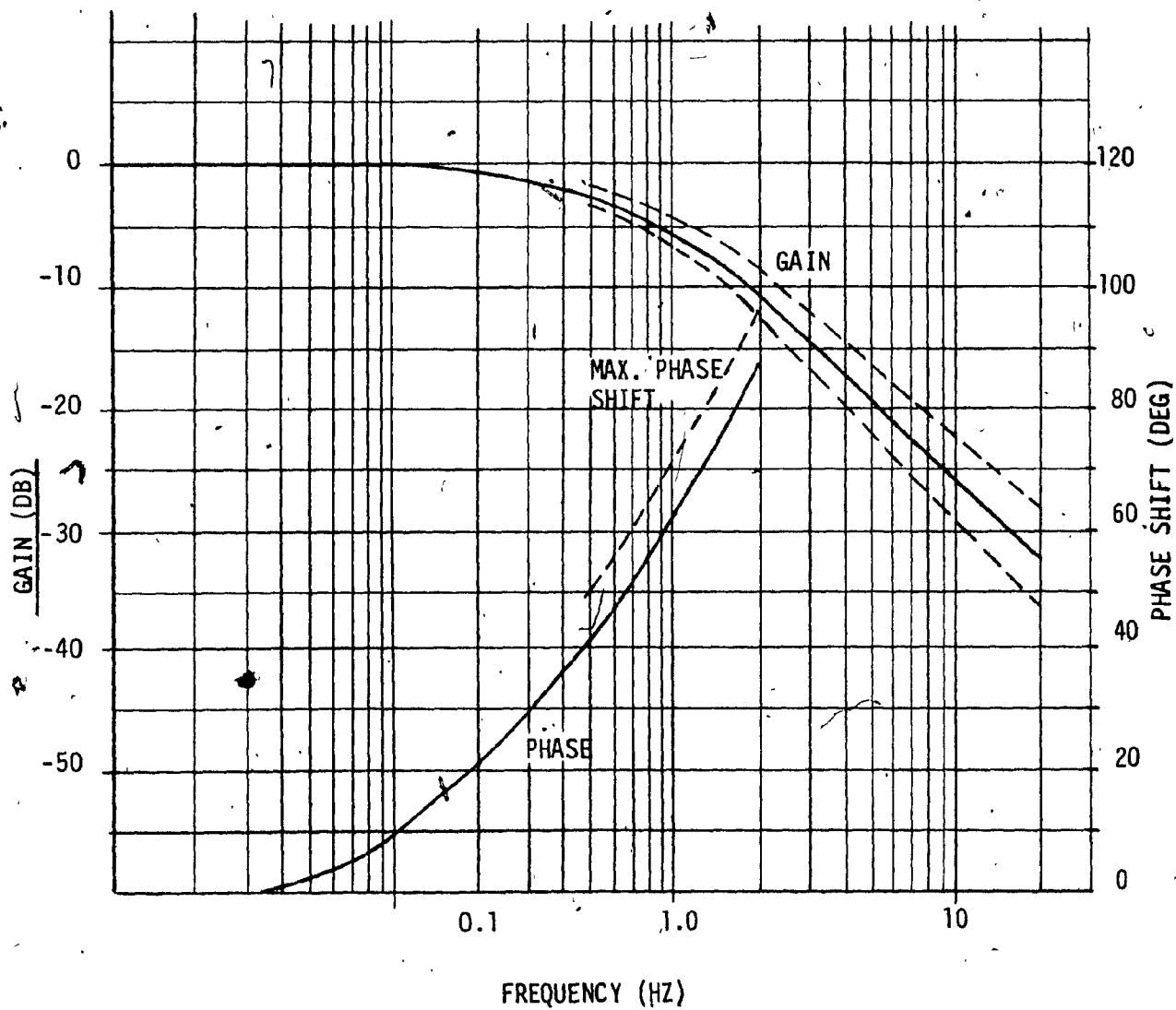


FIGURE 1.3.

SERIES 400 MOTION SYSTEM FREQUENCY RESPONSE (WITHOUT INPUT FILTERS)

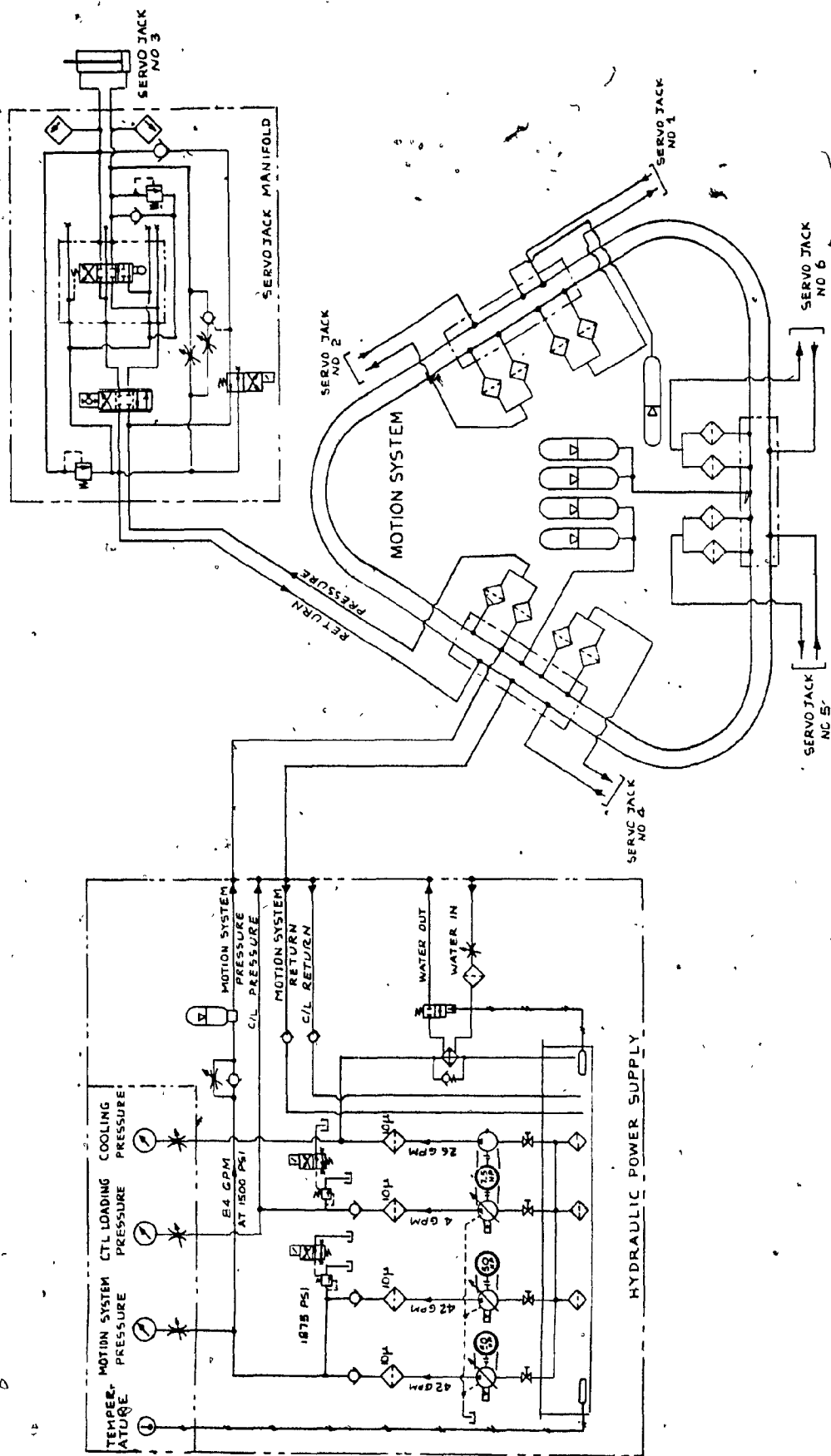


FIGURE 1.4 HYDRAULIC SCHEMATIC OF SERIES 400 MOTION SYSTEM



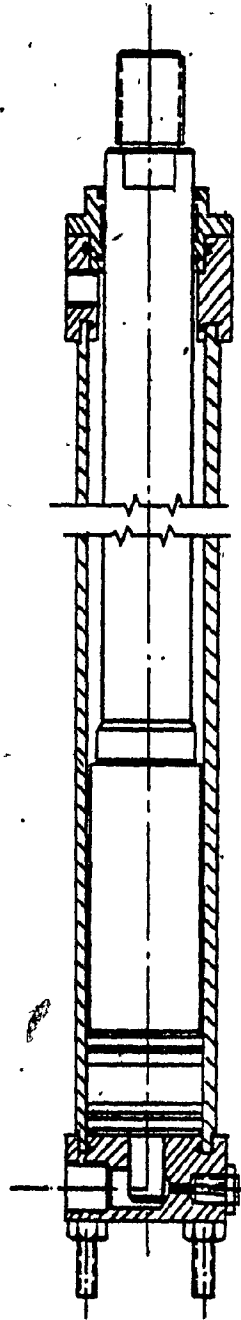


FIGURE 1.5

CONVENTIONAL HYDRAULIC CYLINDER

FOR SERIES 400 MOTION SYSTEMS

### 1.3 Description of Previous Design

Each servojack consists of a hydraulic cylinder (Figure 1.5) provided with hydraulic cushions at each end. The piston rod is hardened and chrome plated to provide resistance to wear and to prevent inadvertent damage to its surface. Dimensions and materials bearing surfaces, wiper rings and seals are selected so as to reduce leakage, maintain low friction levels and to provide wear resistance.

Friction levels for a fully loaded and pressurized servo-actuator are approximately 300 lbs. Each servojack is fitted with unidirectional metering orifice cushions at either end of full stroke. In addition, a cam operated deceleration valve provides controlled deceleration at the ends of stroke and in the event of servovalve runaway.

The deceleration valve operates progressively over a range of 7.5 inches from the end of the rod end stroke and 12.0 inches from the cap end stroke. The deceleration valve is adjusted to ensure an entrance velocity in the cushion of less than 2 in/sec. The cushion region includes 1.25 inches at either extremity.

The servojack can operate in the deceleration region during normal simulation; however, performance is reduced as the end stroke is approached. The jack is not normally operated in the cushion region and a limit switch at each end of the stroke provides an electrical signal to indicate that motion is out of limits.

A solenoid valve is included in the hydraulic circuit so that in the case of electrical power failure, the rod end of every servojack is connected to system pressure and the cap end to return through a metering orifice preset to control the rate of retraction (See Figure 1.4)

In addition, the servo valves are set with a small positive mechanical bias so that the servo jacks retract on loss of power.

Anticavitation check valves are mounted at either end of the servo jack to prevent either rod end or cap end pressure from dropping below return pressure.

The valve used to control the servojack is an asymmetric four way critically lapped two stage electrohydraulic servo valve. The metering orifice of the valve are sized to match the differential areas of the single acting cylinder to reduce discontinuities in pressure as the piston velocity reverses direction. Pressure discontinuities at zero velocity are contributors to reversal bump. The amount of underlap is selected for minimal disturbance.

The servojack incorporates pressure relief valves at both ends set at 2000 psi. It also incorporates a tacho generator and a ten turn potentiometer position transducer driven by a common rack mounted on the cylinder and mechanically connected to the piston rod.

Pressure transducers are mounted close to the inlet ports at either end of the cylinder to provide signals for the computation of a force feedback term.

All valves are manifold mounted to reduce oil volume and for piping simplicity.

All components are rated for at least 3000 psi working pressure but restricted to 1500 psi operating pressure.

## 2.0 BASIC DESIGN

The design of the hydrostatic servojack must be capable of meeting the requirements and performance of the motion system as stated in the introduction. The basic design shall define the critical parameters, strength and vibration characteristics of the servojack.

### 2.1 Critical Parameters

When the maximum excursions of the motion system as shown in Table 1.1 are transformed into the servojack coordinates, the critical parameters can be determined. The critical parameters to be considered for the servojack design are the following:

Response: The system shall have a response time of less than .05 seconds. The acceleration frequency response for actual vertical acceleration divided by acceleration command input to the analog circuit shall be at least 3 Hz at -3db and 90° phase. The design objective is to have a maximum bandwidth. The system must perform smoothly at all times and friction should not induce spurious acceleration transients at the pilot station, with any or all of the rams being driven with a sinusoidal input signal of 10% of maximum voltage at 0.5 Hz frequency. The perception level of an attentive pilot is normally assumed to be 0.02g, however, accelerations as small as 0.005g can be sensed in some circumstances.

The motion must be able to produce vibrations of at least 0.25g up to 10 Hz and detectable vibrations up to 30 Hz. The following dimensions have been selected based on experience with the Series 400 motion system:

Maximum Displacement	54.0 inches
Maximum Velocity	2.0 ft/sec
Maximum Acceleration	1.2g
Cylinder Bore Diameter	3.5 inches
Piston Rod Diameter	2.5 inches
Effective Stroke ( minus cushions)	50.25 inches
Servojack Length Pivot to Pivot	
Minimum	92.0 inches
Neutral	119.0 inches
Maximum	146.0 inches
Platform Mass Total	16,000 lbs.
System Safety Factor (minimum)	4:1
Hydraulic Supply Specification:	
Oil Flow (pump at 1800 RPM)	125 U.S. GPM
System Operating Pressure	1500 psi
System Maximum Pressure	2000 psi
System Rated Pressure	3000 psi
System Operating Temperature	100-115° F
Hydraulic Oil	Shell Tellus 46
Hydraulic Servovalve Capacity	80 GPM @ 1000 psi
Hydraulic Oil Bulk Modulus	120,000-150,00 psi
Pressure Line Accumulators	15 Gal U.S. (Qty. 3)
Return Line Accumulator	15 Gal U.S. (Qty. 1)

The factor that limits maximum acceleration is the operating pressure. It is important to have a constant pressure supply of sufficient capacity to be capable of producing the desired maximum accelerations. Maximum velocities are limited by the oil flow supply and the rating of the servo valve. Hydraulic pumps shall supply the required oil flow to build up the desired pressure. At higher velocities the pressure line accumulators precharged to 50-60% of system pressure shall supply extra flow during transients.

A hydraulic pulsation dampener downstream of the pumps removes pump pulsations which would otherwise cause noise and vibration.

The hydraulic cylinder is sized such that it shall be able to carry the desired payload and produce the required motions with a smooth operation and minimum friction.

## 2.2 Cylinder Stress Calculations

Stress calculations are required to determine the maximum load capacity of the servo jack cylinder assembly. Points of interest shall be the tie rods pre-torque, the cylinder body, the piston rod and the buckling stress analysis of the assembly.

### 2.2.1 Stress Analysis of the Rods

This analysis is based on the method described in Reference 1.

This method shows how tie rod loading in hydraulic cylinders is affected by Poisson ratio effects in the cylinder body and by the cylinder body and seals. Tie rod loading varies with cylinder length and position of the piston along the stroke. The tie rod assembly preload and the pressure at which separation of head and cylinder body will occur, can be determined. The section includes the dimensional data required for stress analysis of the tie rods together with the calculations and the results obtained.



Tie Rods and Cylinder Dimension Data.

$$\begin{array}{ll} L_c = 62 \text{ in.} & L_t = 65.75 \text{ in.} \\ E_c = 30 \times 10^6 \text{ psi} & E_t = 30 \times 10^6 \text{ psi} \\ A = 9.62 \text{ in}^2 & A_c = 6.283 \text{ in}^2 \\ A_t = 1.227 \text{ in}^2 & A_{THD} = .242 \text{ in}^2 \\ N = 4 & C = 2.5 \\ \mu' = .25 & d = .625 \text{ in.} \end{array}$$

$$\begin{array}{ll} p = 2000 \text{ psi} & k = .2 \\ P = pA = 2000 \times 9.62 = 19,240 \text{ lbs.} \end{array}$$

$$T' = 62 \text{ ft-lbs}$$

$$P_t = \frac{12 T'}{kd} \cdot N$$

$$P_t = \frac{12 \times 62}{.2 \times .625} \times 4 = 23,808 \text{ lbs}$$

$$k_c = \frac{A_c E_c}{L_c} = \frac{6.283 \times 30 \times 10^6}{62} = 30.4 \times 10^5 \text{ lb/in}$$

$$k_t = \frac{A_t E_t}{L_t} = \frac{1.227 \times 30 \times 10^6}{65.75} = 5.6 \times 10^5 \text{ lb/in}$$

$$k_c / k_t = 5.4$$

The tie rod thread is .625-18 UNF, with AN315-10R nut.

The tie rod material specifications are:

$$S_u = 145,000 \text{ psi}$$

$$S_y = 132,000 \text{ psi}$$

$$S_e = 85,000 \text{ psi}$$

### Tie Rod Preload

The tie rod preload (sum of all tie rods) is the load produced by pre-torque (tension)

$$P_t = \frac{12T'}{kd} \times 4 = \frac{12 \times 62}{.2 \times .625} \times 4 = 23,808 \text{ lbs.}$$

The same load is applied as compression on the cylinder body.

The initial stress applied to the tie rods will be

$$S_1 = \frac{P_t}{NA_{THD}} = \frac{23,808}{4 \times .242} = 24,595 \text{ psi per tie rod.}$$

The deflection from Hookes law is given by

$$\epsilon_t = \frac{S_1}{E_t} = \frac{24,595}{30 \times 10^6} = .0008 \text{ in/in}$$

$$\text{where } \epsilon_t = \frac{\delta_t}{L_t}$$

$$\text{then } \delta_t = L_t \epsilon_t = 65.75 \times .0008 = .054 \text{ in.}$$

Similarly the deflection in compression for the cylinder body will be

$$\delta_c = \frac{P_t L_c}{A_c E_c} = \frac{23,808 \times 62}{6.283 \times 30 \times 10^6} = .008 \text{ in.}$$

When internal pressure is applied the tie rods will stretch additionally and the cylinder stress in compression will be reduced and the additional tie rod stretch  $\Delta$ , will equal the cylinder body axial expansion (relaxation).

However, the axial deflection must take into account Poisson ratio effects caused by hoop and radial stresses from the internal pressure.

In order to calculate the tie rod loads the pressure co-efficient factor  $\eta$  has to be calculated first. This factor will take into consideration Poisson ratio effects and sizes of cylinder body and tie rods.

### Pressure Load Coefficient ( $\eta$ )

The value of  $\eta$  depends upon the length, area, and material of the cylinder body and tie rods. The pressure load coefficient varies also with the piston position. At the beginning of the stroke the internal pressure is not applied at the full length of the cylinder, thus hoop and radial stresses do not exist in this condition. However with the piston fully extended the cylinder is subjected to full system pressure and the Poisson ratio  $\mu'$  effect must be included in the calculations.

- a) When the piston is at full stroke the pressure load coefficient is minimum

$$\eta = \frac{1-2\mu'}{1+k_c/k_t} = \frac{1-2 \times .25}{1+5.4} = .08$$

- b) When the piston is at the beginning of stroke the Poisson ratio effect does not apply and the pressure load coefficient is maximum

$$\eta_{\max} = \frac{1}{1+k_c/k_t} = \frac{1}{1+5.4} = .16$$

- c) For minimum tie rod stress calculation the value of  $\eta$  is given by

$$\eta' = \frac{2\mu'}{1+k_c/k_t} = \frac{2 \times .25}{1+5.4} = .08$$

### Tie Rod Load Stress with Internal Pressure

The total load (sum for all tie rods) varies with applied internal pressure and position of piston. The equations used below were derived from reference 1.

- a) When internal pressure is not applied ( $p = 0$ ) and no other external loads are applied

The tie rod load ( $F_t$ ) = Preload ( $P_t$ ) = 23,808 lbs.

- b) When internal pressure is applied (2000 psi) and piston is at the beginning stroke (Poisson ratio effect does not apply), the tie rod load is maximum and is given by

$$\begin{aligned} F_{t1} &= P_t + \eta_{\max} (pA) \\ &= 23,808 + .16 (19,240) = 26,886 \text{ lbs.} \end{aligned}$$

- c) With internal pressure applied and piston at full stroke (Poisson ratio effect applies), the tie rod load is given by

$$F_{t2} = 23,807 + .08 (19,240) = 25,347 \text{ lbs.}$$

- d) The minimum tie rod load is given by

$$\begin{aligned} F_{t3} &= P_t - \eta' (pA) \\ &= 23,808 - .08 (19,240) = 22,268 \text{ lbs.} \end{aligned}$$

### Cylinder Axial Load $F_c$

The maximum cylinder axial load in compression is the preload of the tie rods with no internal pressure, or external loads applied.

The cylinder axial load will be decreased when pressure is applied and is given by

$$\begin{aligned} F_c &= P_t - (1 - \eta) pA \\ &= 23,808 (1 - .08) 19,240 = 6,107 \text{ lbs.} \end{aligned}$$

### Separation Pressure

Separation pressure, the pressure at which the cylinder body loses contact with the heads, is dependent on the preload force of tie rods.

Under the condition  $F_c = 0$ , the separation pressure is given by

$$P_s = \frac{P_t}{A(1-\eta)} = \frac{23,808}{9.62(1-.08)} = 2,690 \text{ psi}$$

Note that system operating pressure is 1500 psi and the maximum system relief pressure is 1,875 psi.

Figure 2.1 summarizes the tie rod load variation with pressure.

1. The total internal pressure load is represented by line  $F_t = pA$ , with no external load or preload applied.
2. The tie rod load with zero pressure is 23,808 lbs.
3. If the internal pressure is increased but piston rod motion is externally restrained the tie rod load is represented by  $F_{t1} = P_t + \eta_{\max} (pA)$  line (maximum load).
4. If the internal pressure is increased after piston rod has completed its stroke the tie rod load is represented by  $F_{t2} = P_t + \eta(pA)$  line (normal load).

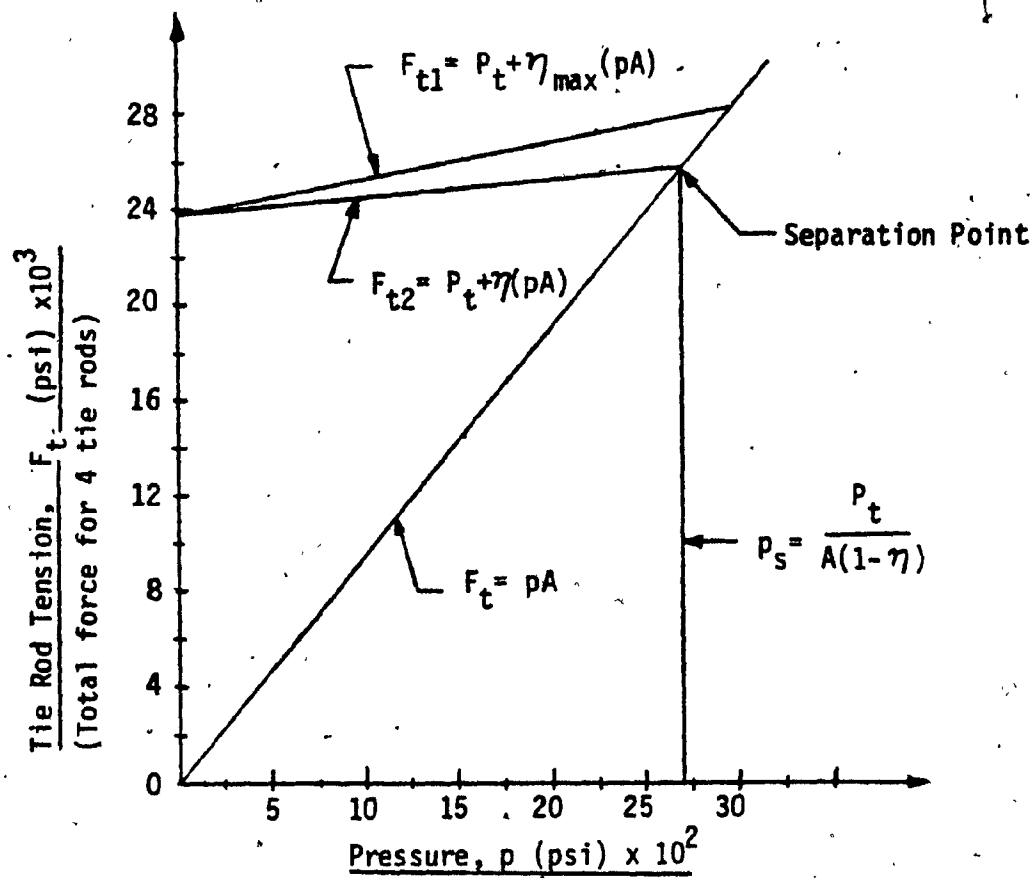


FIGURE 2.1 TIE ROD VARIATION WITH PRESSURE

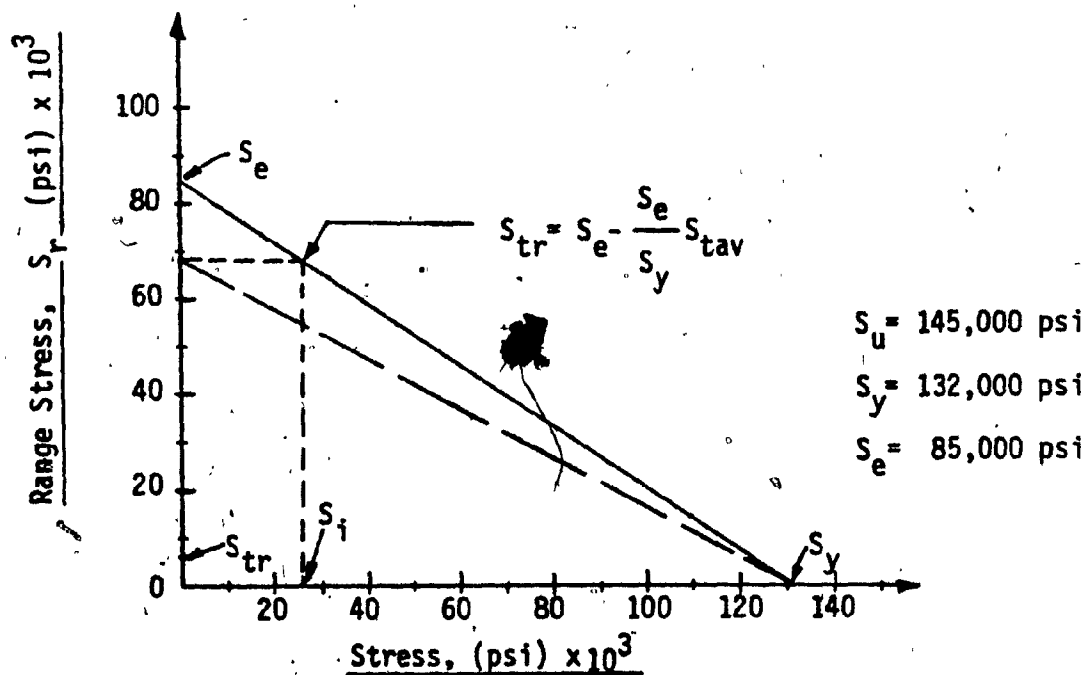


FIGURE 2.2 SODERBERG DIAGRAM FOR TIE ROD INFINITE FATIGUE LIFE

5. Separation of cylinder body from heads occur where either of the load lines intersect the  $F_t = pA$  line. The lowest value of separation pressure  $p_s$  is 2,690 psi.
6. At pressures beyond the separation point (2,690 psi), tie rod loading follows the  $F_t = pA$  line until tie rods fail.

#### Fatigue Analysis

Since tie rod loading fluctuates during normal operation a fatigue analysis is required.

The tie rod average load is given by

$$F_{tav} = \frac{F_{t1} + F_{t3}}{2} = 24,577 \text{ lbs.}$$

The tie rod range load is

$$F_{tr} = \frac{F_{t1} - F_{t3}}{2} = 2,309 \text{ lbs.}$$

The average stress in the tie rod thread area is

$$\begin{aligned} S_{tav} &= S_i + \frac{pA}{2NA_{THD}} (\eta_{max} - \eta') \text{ per tie rod} \\ &= 24,595 + \frac{19,240}{2 \times 4 \times .242} (.08) \\ &= 25,390 \text{ lbs per tie rod.} \end{aligned}$$

$$\text{Safety factor} = \frac{S_y}{S_{tav}} = \frac{132,000}{25,390} = 5.2$$

The range stress in the tie rod thread, assuming a thread stress concentration factor  $C_t = 2.5$ , is

$$S_{tr} = \frac{C_t p A}{2 N A_{THD}} (\eta_{max} + \eta)$$
$$= \frac{2.5 \times 19,240}{2 \times 4 \times .242} (.24) = 5,962 \text{ psi}$$

In order to determine a finite fatigue life the Sodeberg diagram for the tie rod is shown in Figure 2.2.



### 2.2.2 Stress Analysis of Cylinder

The hydraulic cylinder will properly perform its design function only if the stresses and deflections in the components do not exceed allowable limits. Stresses and deflections result from combined effects of axial load and bending as well as the hydraulic pressure in the cylinder.

The sliding connection between the cylinder and rod portions permits an initial angular deflection which interacts with the axial load to amplify bending moments and deflections.

However, in the case of the hydraulic cylinder with conical hydrostatic bearings, even though diametrical clearances may be larger than those in conventional cylinders, as the piston rod is extended or retracted under system pressure, the piston and piston rod are centered by the hydraulic pressure. Thus the initial deflection is almost cancelled during the operation.

An initial eccentricity may exist, however, during the assembly of the cylinder components.

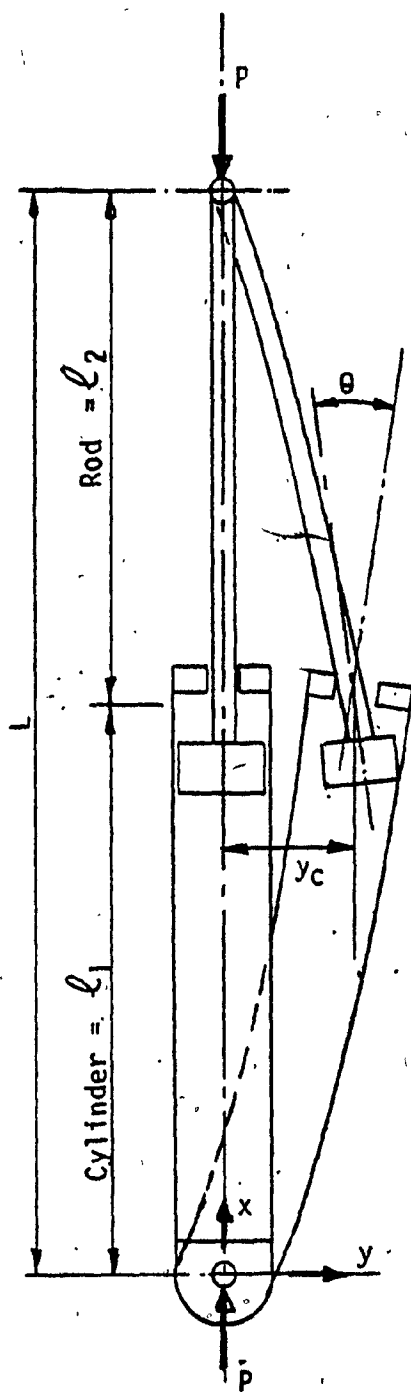
The pinned mounting of the hydraulic cylinder prevents the cylinder from being subjected to any applied bending moment, except those due to the jack itself. Any moments created by misalignment of the components and friction

at bearings of pivot points will be very small and should not affect the cylinder performance. Thus these effects will be omitted in this analysis.

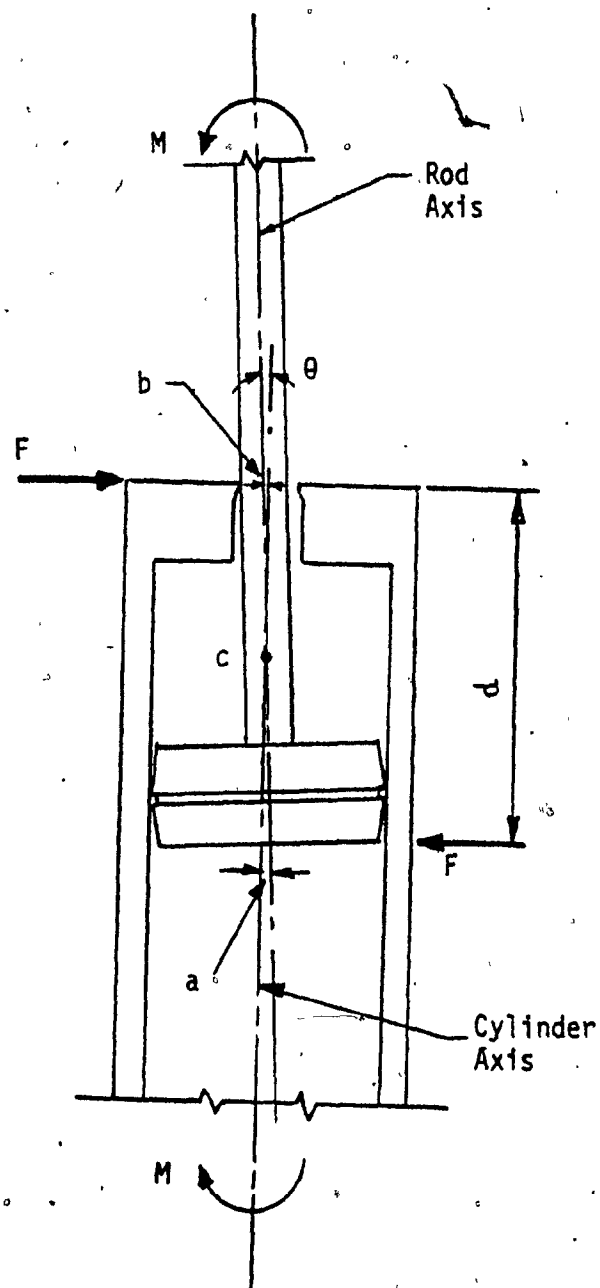
The method used in this analysis which includes both cylinder and rod, is that of the stepped continuous column. Although the stress distribution in the stepped column is not the same as the actual cylinder stress distribution, this method can be applied for buckling analysis. In this case the cylinder internal pressure replaces the axial load acting on the wall of the cylinder. It should be noted that this analysis cannot be used to determine stress failure of the cylinder, since the stress distribution in the cylinder due to internal pressure is completely different from that due to axial loading.

#### Development Analysis

A typical hydraulic cylinder is shown in Figure 2.3 in two possible positions: perfectly straight; and with an initial crookedness angle  $\theta$ , due to clearances at no load. The system is assumed to be operating vertically, to be linearly elastic, and to be pin supported at both ends. If it is further assumed that the total deflections, due to initial crookedness and component bending are also small and that the length of interface (piston length and rod and bearing length) is small compared to the total length, then the



(a) Deflection



(b) Cylinder/Rod Interface

FIGURE 2.3  
TYPICAL CYLINDER

following relationships between deflections and loads describe the behaviour of the system (Reference 2).

$$E_1 I_1 \frac{d^2 y_1}{dx^2} + P y_1 = 0$$

$$E_2 I_2 \frac{d^2 y_2}{dx^2} + P y_2 = 0$$

Where  $y_1, y_2$  are deflections of cylinder and rod, and  $x$  is the distance from the cylinder pin, and  $I_1, I_2$  are the moments of inertia of cylinder and piston rod cross sections.

Boundary condition and compatibility of the system as shown in Figure 2.3 are:

$$y_1 = 0 \quad \text{at} \quad x = 0$$

$$y_2 = 0 \quad \text{at} \quad x = x_2$$

$$y_1 = y_2 \quad \text{at} \quad x = x_1$$

$$\frac{dy_1}{dx} + \frac{dy_2}{dx} = \theta \quad \text{at} \quad x = x_1$$

where  $\theta$  is the crookedness angle at the interface.

The angle  $\theta$  is a function of the axial load, clearances between cylinder and piston head, and clearances between piston rod and rod end bearing. It is also a function of the modulus of elasticity of the elements in contact at the interface.

In the study done by Oklahoma State University (Reference 2), the analysis was based on a conventional cylinder taking into consideration the compressibility of the piston, and rod end bearing seals under axial load. However, in the case of the hydrostatic cylinder there are no seals, but there is a film of hydraulic oil under system pressure. The hydrostatic cylinder with conical piston and rod end bearing has the advantage due to the centering force applied by the system pressure during operation.

Considering the oil bulk modulus, the oil film thickness, and possible contact area at interface, the additional deflection (increase) of the crookedness angle  $\theta$  due to axial load is very small compared to the initial angle  $\theta$ , therefore it can be neglected.

The bending moment due to curvature obtained from ordinary bending theory is

$$M_i = -E I \frac{d^2 y}{dx^2}$$

The bending moment at the same location due to external load is

$$M_b = P y$$

where  $E$  &  $I$  are the modulus of elasticity and moment of inertia of the cylinder or rod,  $P$  is axial load and  $y$  is the lateral deflection. At equilibrium the internal and external moments must be equal as

$$\frac{d^2 y}{dx^2} + \frac{P}{E I} y = 0$$

and  $\frac{dy_2^2}{dx^2} + \frac{p}{E_2 I_2} y_2 = 0$

The initial deflection,  $y_c$ , with piston fully extended was calculated to .03 inches considering the dimensional tolerances without internal pressure applied. (see Section 3.3).

The bending stress in the cylinder is then

$$S_{cb} = \frac{P y_c}{Z_c} = \frac{19,240 \times .030}{5.67} = 102 \text{ psi}$$

The hoop stress in the cylinder is

$$S_{ch} = \frac{D_o^2 + D_i^2}{D_o^2 - D_i^2} p = \frac{(4.5)^2 + (3.5)^2}{(4.5)^2 - (3.5)^2} \times (2000) = 8,125 \text{ psi}$$

where  $Z_c$  = section modulus of cylinder = 5.67 in.<sup>3</sup>

$D_o$  = outside diameter of cylinder = 4.5 in.

$D_i$  = inside diameter of cylinder = 3.5 in.

$p$  = internal pressure = 2000 psi.

Total cylinder stress =  $S_{cb} + S_{ch} = 8,125 + 102 = 8,225 \text{ psi}$

From cylinder material (MT1018)

$S_u$  = 85,000 psi, ultimate strength

$S_y$  = 65,000 psi, yield strength

The cylinder safety factor =  $\frac{65,000}{8,225} = 7.9$

Using Barlow's formula for cylinder stress

$$S_c = \frac{p D_i}{D_o - D_i} = \frac{2000 \times 3.5}{1.0} = 7000 \text{ psi}$$

The maximum stress in the rod section is

$$S_r = \frac{4P}{\pi[(D_{ro})^2 - (D_{ri})^2]} + \frac{Py}{Z_r}$$
$$= \frac{4 \times 19,240}{\pi[(2.5)^2 - (.78)^2]} + \frac{19,240 \times .030}{1.52} = 4,722 \text{ psi}$$

Where  $D_{ro}$  = outside diameter of piston rod = 2.5 in.

$D_{ri}$  = inside diameter of piston rod = .78 in.

$Z_r$  = section modulus of piston rod = 1.52 in<sup>3</sup>

From rod material specifications,

$$S_u = 115,000 \text{ psi}$$

$$S_y = 85,000 \text{ psi}$$

$$\text{Safety factor} = \frac{85,000}{4,722} = 18 \text{ (in tension)}$$

#### Critical Load of Piston Rod

Compressive loading of long members (columns) may result in buckling in which the members experience lateral deflections that are excessive. Buckling is a stability failure and the resultant lateral deflection is not related to the applied load by a direct proportion. Consequently, the relation between load, dimensions, material properties and conditions of loading must be examined in column analysis.

A compressed column acts like a spring and resists any lateral deflection. The lateral deflection can be initiated by eccentricities due to: deviations from absolute straightness of the column and error in alignment when load is supplied. A small increase in load above the critical load will significantly increase the

initial deflection. This increase may be enough to induce inelastic action in the material of column which will be sufficient to cause collapse (stability failure).

A column will be stable if it is able to return to its neutral equilibrium after removal of the applied load, (which will have produced a lateral deflection). The point at which the column will become unstable (collapse) is the point where the stresses due to the applied load are equal or above the material proportional limit. Since the proportional limit strength of a material is hard to calculate, the yield strength is used.

The maximum load that can be applied on a column, before the column becomes unstable is the critical load.

The critical load for slender (long) columns of uniform cross section is given by the Euler equation (Reference 3)

$$F_{cr} = \frac{C\pi^2 EA_r}{(L/r)^2} = \frac{C\pi^2 EI}{L^2} \quad (2.1)$$

The critical load for moderate length columns of uniform cross section is given by the J.B. Johnson equation (Reference 3)

$$F_{cr} = S_y A_r \left[ 1 - \frac{S_y (L/r)^2}{4C\pi^2 E} \right] \quad (2.2)$$

where  $A_r$  = Piston rod area, 4.431 in<sup>2</sup>

$C$  = End condition constant, 1

$E$  = Material Modulus of Elasticity, 30 X 10<sup>6</sup> psi

$F$  = Maximum applied load, 6400 lbs.

$L$  = Piston rod length, 73 in.

$r$  = Piston rod radius of gyration 0.655 in.

$S_y$  = Piston rod yield strength, 85,000 psi



Which of the previous equations may be used is determined by the value of the slenderness ratio  $L/r$ . This ratio is obtained by equating the equations 2.1 and 2.2 from which

$$\left(\frac{L}{r}\right) = \sqrt{\frac{2C'\pi^2 E}{S_y}} \quad (2.3)$$

In order to use the Euler equation the condition is

$$\left(\frac{L}{r}\right)_{\text{actual}} > \left(\frac{L}{r}\right)_{\text{slenderness ratio}}$$

From the above data

$$\left(\frac{L}{r}\right)_{\text{actual}} = \frac{73.0}{0.655} = 111.45$$

$$\left(\frac{L}{r}\right) = \sqrt{\frac{2 \times 1 \times \pi^2 \times 30 \times 10^6}{85,000}} = 83.47$$

Since  $\left(\frac{L}{r}\right)_{\text{actual}}$  is greater than  $\left(\frac{L}{r}\right)$ , the Euler's equation must be used. The critical load then is given by

$$F_{cr} = \frac{C\pi^2 E A_r}{(L/r)^2} = \frac{1 \times \pi^2 \times 30 \times 10^6 \times 4.431}{(111.45)^2} = 105,624 \text{ lbs.}$$

$$\text{The critical stress is } \sigma_{cr} = \frac{F_{cr}}{A} = \frac{\pi^2 E}{(L/r)^2} = 23,837 \text{ psi.} \quad (2.4)$$

The equivalent column stress for an actual load  $F$ , is given by Euler's equation,

$$S_{eq} = \frac{F}{A_r} \left[ \frac{S_y (L/r)^2}{C\pi^2 E} \right] \quad (2.5)$$

$$= \frac{6400}{4.431} \left[ \frac{85,000 \times (111.45)^2}{1 \times \pi^2 \times 30 \times 10^6} \right] = 5,150 \text{ psi}$$

The equivalent stress is a fictitious stress related to the yield point stress, in the same way as the actual load is related to the critical load. Equivalent stress depends on the yield point stress. In a column of given proportions and lengths, changing the material does not change the critical load, but it does change the stress.

As shown in equation (2.1) the critical load depends on the modulus of elasticity of the material and the dimensions of the column. In order to increase the critical load, the moment of inertia must be increased. This may be done without changing the cross-sectional area  $A$ , but by distributing the material as far as possible from the principal axis of the cross-section, i.e. increasing the radius of gyration  $r$ .

Hence tubular sections are more economical than solid sections for compression members. However, the maximum value of the radius of gyration  $r$ , in equation (2.4) is limited by the material proportional limit or yield point stress.

Figure 2.4 shows the Euler's equation curve, with critical stress as a function of the slenderness ratio. The Euler equation is valid only for the portion BC of the curve (long columns).

The critical stress for  $(L/r) > 83.47$  depends on the slenderness ratio while for  $(L/r) < 83.47$  it depends on the material yield point stress or proportional limit. The value of  $(L/r)$  from equation (2.3) as a function of the yield point stress is 83.47.

Since the actual value of  $(L/r)$  is above 83.47 the use of the Euler's equation is justified.

$$\sigma_{cr} = \frac{\pi^2 E}{(L/r)^2} = \frac{F_{cr}}{A_r}$$

$$E = 30 \times 10^6 \text{ psi}$$

$$S_y = 85,000 \text{ psi}$$

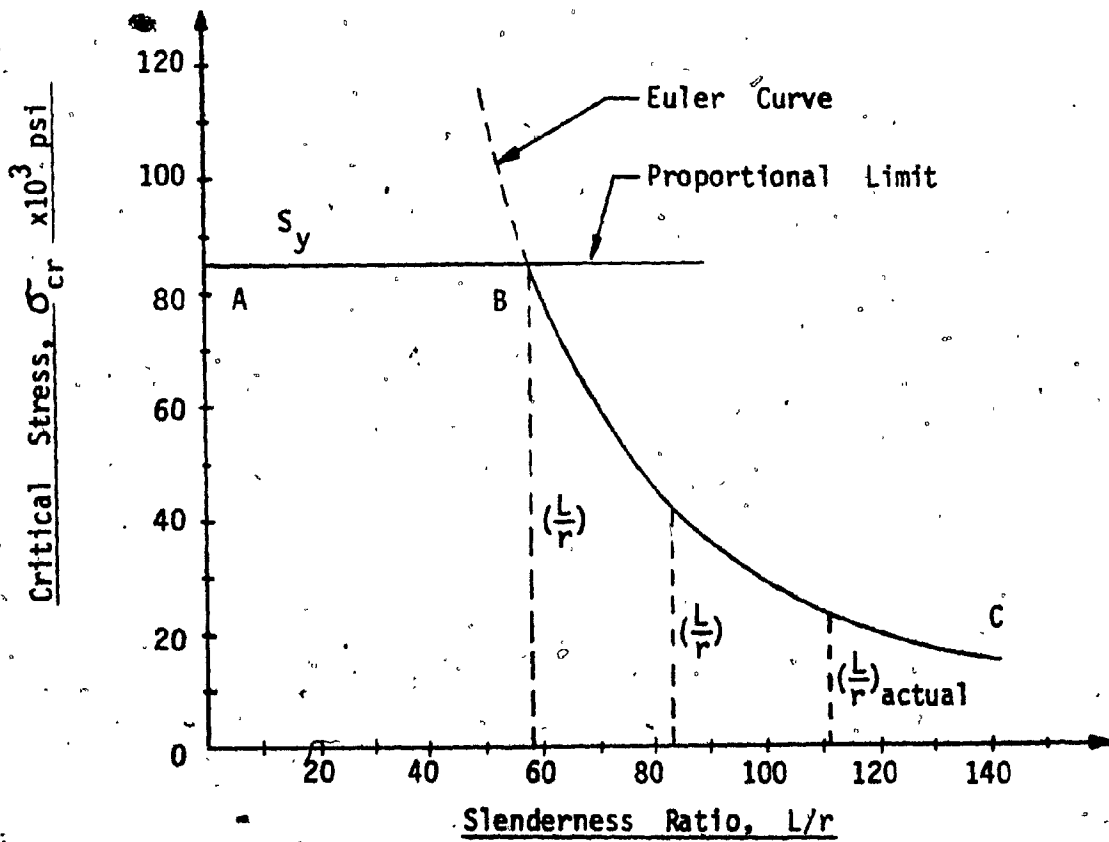


FIGURE 2.4 CRITICAL STRESS OF PISTON ROD

The safety factor for load and stress is

$$(SF)_{\text{load}} = \frac{S_y}{\sigma_{\text{eq}}} = \frac{F_{\text{cr}}}{F} = \frac{105,624}{6,400} = 16.5$$

$$(SF)_{\text{stress}} = \frac{\sigma_{\text{cr}}}{\sigma_{\text{eq}}} = \frac{23,837}{5,150} = 4.63$$

NOTES:

1. The length of the piston rod L, was taken when the piston was fully extended.
2. The end conditions were considered as both ends pinned thus having  $C' = 1$ .
3. The rod area and radius of gyration were calculated considering the rod as a circular tube with 2.5 in. O.D. and 0.78 in I.D.
4. The maximum actual load to be supported by the rod was measured to be 6400 lbs. This was the case where all jacks of the motion system are fully extended, and the motion system is subjected to an upward pitch at 1.25g acceleration.
5. All load is carried through the piston rod and supported by the hydraulic oil pressure applied on the piston head end. Stresses on the cylinder body were calculated in the previous section.
6. Any shocks applied on the rod, will be absorbed by the hydraulic oil which is of lower stiffness.

### Piston Rod Thread Stress

#### Dimensional data:

Thread Size: 1.875-12 UN-2A  
Thread Engagement Length: 1.70 inches  
Load to be Carried: 6,400 lbs. in compression

The bending stress at the root of the thread is given by (Reference 3)

$$S_b = \frac{3Fh_t}{2\pi n r_m b^2} \quad (2.6)$$

The mean transverse shear stress is

$$S_s = \frac{F}{2\pi n r_m b} \quad (2.7)$$

where  $F$  = load = 6,400 lbs.  
 $b$  = thread pitch = 0.083 in.  
 $h_t$  = thread height = 0.051 in.  
 $n$  = number of threads subject to load = 20  
 $r_m$  = mean thread radius = 1.806 in.

then  $S_b = \frac{3 \times 6,400 \times .051}{2 \times \pi \times 20 \times 1.806 \times (.083)^2} = 626 \text{ psi}$

$$S_s = \frac{6,400}{2 \times \pi \times 20 \times 1.806 \times .083} = 1,067 \text{ psi}$$

Above stresses are far below the material strength and they are satisfactory when piston is under compression.

Considering the case of motion system fall-out (point of no recovery), where full system pressure of 1500 psi is applied on the cylinder rod end, the applied force is  $F = pA = 1500 \times 4.71 = 7,065 \text{ lbs.}$  Tension stresses in this case are going to be slightly higher than those calculated above.

### 2.2.3 Summary of Stress Analysis

Stress analysis of tie rod indicates that selected material and sizes are capable of operating under normal loading with a safety factor of at least 5. Preloading on tie rods is sufficient in this application. Calculations show that separation of cylinder body from cylinder head will occur at approximately 2700 psi. The maximum system pressure, however, is 1,875 psi (relief valve setting), and the system operating pressure is limited to 1500 psi. The Soderberg diagram shows that the tie rods will have an infinite fatigue life.

The cylinder stresses due to bending are very small, almost negligible, while the hoop stresses will have a safety factor of at least 7.

The piston rod loading will have a safety factor of 16.5. Even though the load capacity is very high, it is not advisable to try to reduce the critical loading by changing the rod dimension, since this will affect the critical stress which has a safety factor of 4.63.

Thread stresses on the piston rod in compression and tension are very small compared to the rod material yield point stresses.

A factor that has not been included in the column stress analysis is the load eccentricity (Ref. 4). If the column is loaded axially, eccentricity will be zero. It is virtually impossible, however, to eliminate all eccentricity which might result from various factors such as the initial crookedness of the column, minute flaws in the material, and a lack of uniformity of the

cross-section as well as accidental eccentricity of the load.

However, the eccentricity affects greatly the critical stress at small slenderness ratios below  $L/r = 100$ . The critical stress,  $\sigma_{cr}$ , for  $L/r > 100$ , will be decreased slightly. Assuming that there is 0.030 in. eccentricity, the calculated critical stress of 23,837 psi will be reduced to approximately 22,000 psi, which still meets the safety factor requirements.

Comparing the column strength from the obtained results with Series 400 hydraulic servojacks, it was found that Series 500 piston rod is capable of carrying higher loads. If the Series 400 servojack were to be used under the present load requirements, its critical parameters will have the following values:

$$L/r = 116$$

$$F_{cr} = 69,093 \text{ lbs.}$$

$$S_{eq} = 7,873 \text{ psi.}$$

$$\sigma_{cr} = 22,000 \text{ psi.}$$

Eventhough its load carrying capacity is sufficient, the critical stress does not meet the safety factor requirements. In order that a safety factor of 4 to be met the maximum load to be carried by a Series 400 servojack is 4,500 lbs., which is equivalent to a platform payload of 15,000 lbs. approximately.

### 2.3 Vibration Characteristics

Previous models on motion systems have been treated as low frequency models. Effects due to oil compressibility and structure vibrations were not considered. Therefore, while the models can be used to answer questions pertaining to the main low frequency components of the motion, they remain mute on the subject of rapid spurious motions.

Since these spurious motions lead to appreciable accelerations, they are easily perceived by the simulator user. It is thus important to understand the causes of such motions and if possible to eliminate them.

The normal operating frequency of the motion system is below one or two Hz. However, it is required to simulate flight conditions under air turbulence, which will occur at much higher frequencies. Since it is desired to simulate the actual flight conditions as closely as possible, some low amplitude high frequency noise is frequently added to the motion commands.

Thus, it is important to know the hydraulic and mechanical vibration characteristics of the hydraulic actuators and motion system so that the high frequency noise will not excite the motion system resonances. The existence of a resonant vibration is obvious in that one can hear, feel and even at times see the vibration. However, the whole frame appears to be shaking and it is usually difficult to observe the mode shape.

This section will investigate the hydraulic and the mechanical vibration modes of the hydraulic actuator and motion system.



### 2.3.] Hydraulic Modes

Considering one servo cylinder and taking into account oil compressibility, the flows at each side of the cylinder are:

$$\begin{aligned} \text{Cap end} \quad Q_1 &= A_1 \dot{S} + \frac{V_1}{\beta} \cdot \frac{dP_1}{dt} \\ \text{Rod end} \quad Q_2 &= A_2 \dot{S} + \frac{V_2}{\beta} \cdot \frac{dP_2}{dt} \end{aligned} \quad (2.8)$$

An increment in flow  $Q_1$  will produce

$$Q_1 = Q_{10}(t) + \delta Q_1(t) \quad (2.9)$$

$$S = S_0(t) + \delta S(t)$$

$$V_1 = V_{10}(t) + A_1 \delta S(t)$$

$$P_1 = P_{10}(t) + \delta P_1(t)$$

Where subscripted zero variables correspond to ideal incompressible case, i.e.  $\beta = \infty$ .

Substituting equation (2.9) into (2.8) we have

$$Q_{10}(t) + \delta Q_1(t) = A_1 \dot{S}_0(t) + A_1 \delta \dot{S}(t) + \frac{V_{10}(t) + A_1 \delta S(t)}{\beta} \cdot \frac{dP_{10}(t) + d[\delta P_1(t)]}{dt}$$

$$\text{and } \delta Q_1 = A_1 \delta \dot{S} + \frac{1}{\beta} [V_{10} + A_1 \delta S] \left[ \frac{dP_{10}}{dt} + \frac{d\delta P_1}{dt} \right] \quad (2.10)$$

Since the time behaviour of  $P_{10}$  is slow compared to  $\delta P_1$  and since  $V_{10} \gg A_1 \delta S$ , we have

$$\delta Q_1 = A_1 \delta \dot{S} + \frac{V_{10}}{\beta} \cdot \frac{d\delta P_1}{dt} \quad (2.11)$$

and similarly

$$\delta Q_2 = -A_2 \delta \dot{S} + \frac{V_{20}}{\beta} \cdot \frac{d\delta P_2}{dt} \quad (2.12)$$

### CASE 1, VALVE CLOSED

If the valve is closed, then  $\delta Q_1 = \delta Q_2 = 0$  and by integrating both sides of Equations 2.11 and 2.12 we have,

$$\delta P_1 = -A_1 \frac{\beta}{V_{10}} \delta S \quad (2.13)$$

$$\text{and } \delta P_2 = A_2 \frac{\beta}{V_{20}} \delta S \quad (2.14)$$

If  $S$  is the distance between the piston and the cap end during stroke, then (with piston stroke = 52 inches)

$$V_{10} = A_1 S$$

$$V_{20} = A_2 (52 - S)$$

then

$$\delta P_1 = -\frac{\beta}{S} \delta S \quad (2.15)$$

$$\delta P_2 = \frac{\beta}{(52-S)} \delta S \quad (2.16)$$

The upward positive force will be

$$\begin{aligned} \delta F &= A_1 \delta P_1 - A_2 \delta P_2 = -A_1 \left[ \frac{\beta}{S} \delta S \right] - A_2 \left[ \frac{\beta}{(52-S)} \delta S \right] \\ &= -\beta \left[ \frac{A_1}{S} \delta S + \frac{A_2}{(52-S)} \delta S \right] \\ &= -\beta \left[ \frac{52A_1 + A_2 S - A_1 S}{S(52-S)} \right] \delta S \end{aligned} \quad (2.17)$$

Equation 2.17 is the Force-Length relationship of a spring with stiffness depending on the actuator position. The factor in this equation has a broad minimum value of .43 near  $S = 30$  inches and rises to about .68 for  $S = 15$  or 45 inches.

## CASE 2, VALVE OPEN

In this case we must express the flow variation in terms of pressure changes through the orifice relationship of the valve. For small changes

$$\delta Q_1 = - \frac{C i_o(t)}{2[P_s - P_{10}]^{1/2}} \delta P_1 \quad (2.18)$$

$$\delta Q_2 = - \frac{C i_o(t)}{2[P_{20} - P_3]^{1/2}} \delta P_2 \quad (2.19)$$

Above case is where pressure is supplied at cap end and return in rod end of the cylinder.

Combining Equations 2.11, 2.12, 2.18 and 2.19

$$\frac{V_{10}}{\beta} = \frac{\delta Q_1 - A_1 \delta \dot{S}}{d\delta P_1/dt}$$

$$\text{or } \frac{V_{10}}{\beta} \frac{d\delta P_1}{dt} = - \frac{C i_o(t)}{2[P_s - P_{10}]^{1/2}} \delta P_1 - A_1 \delta \dot{S} \quad (2.20)$$

$$\text{and } \frac{V_{20}}{\beta} = \frac{\delta Q_2 + A_2 \delta \dot{S}}{d\delta P_2/dt}, \quad \frac{V_{20}}{\beta} \frac{d\delta P_2}{dt} = - \frac{C i_o(t)}{2[P_{20} - P_3]^{1/2}} \delta P_2 + A_2 \delta \dot{S} \quad (2.21)$$

Equations 2.20 and 2.21 are linear but time varying because of the value of current,  $i_o$ . The pressure  $P_{10}$  and  $P_{20}$ , and volume  $V_{10}$  and  $V_{20}$  will change with time.

From previous study of heave motion the factor  $\frac{\beta}{V_{10}} \cdot \frac{C i_o}{2[P_s - P_{10}]^{1/2}}$  has

a peak magnitude of  $7 \times 10^5$  for variables in SI units, and it goes down to zero when valve is shut.

Equations 2.20 and 2.21 show that the pressure dynamics are of first order with a rapid time constant. In effect  $\delta P_1$  and  $\delta P_2$  are always nearly zero, so that,  $\delta P_1$  and  $\delta P_2$  are essentially at their equilibrium values. Thus, the pressure responds very fast with first order dynamics to changes in rod velocity. A sudden velocity change causes an almost instantaneous change in pressure to the equilibrium value. There are no oscillatory transients. The value of  $7 \times 10^5 \text{ sec}^{-1}$  corresponds to a time constant of 1.4 sec. In order to increase this to a value that might interact with order dynamics we need to bring the valve current  $i_0$  to a value quite near zero. In essence, this rapid first order dynamic behavior is obtained whenever the valve is fully opened.

#### Results from Analysis

The linearized model of the motion system is of the form

$$M \ddot{\underline{x}} = A \underline{x} + B \delta \underline{F} \quad (2.22)$$

$$\delta \underline{S} = B^T \underline{x} \quad (2.23)$$

where

$\underline{x} = [x, y, z, \phi, \theta, \psi]$  is the vector of position and angular deviations.

$M = \text{diag}[m, m, m, I_x, I_y, I_z]$  is the matrix of mass (m) and moments of inertia.

$\delta \underline{F}$  = Vector force increments from nominal, at six actuators.

$\delta \underline{S}$  = Vector of length increments at six actuators.

A, B = 6 x 6 matrices

Equation 2.17 can be rewritten as

$$\delta \underline{F} = -K \delta \underline{S} \quad (2.24)$$

$$\text{where } K = \beta \cdot \left[ \frac{52A_1 + (A_2 - A_1)S}{S(52 - S)} \right]$$

If we assume all six valves are shut the same value of  $K$  applies for all actuators (e.g. at mid-point), then we may write the vector equation

$$\delta \underline{F} = -K \delta \underline{S} \quad (2.25)$$

Substituting Equation 2.25 into Equation 2.22 and 2.23 we have

$$M \ddot{\underline{X}} = A \underline{X} - KBB^T \underline{X} \quad (2.26)$$

$$\text{or } \underline{X} = M^{-1} (A - KBB^T) \underline{X}$$

Let  $\lambda_1, \lambda_2, \dots, \lambda_6$  be the eigenvalues of the matrix  $M^{-1}(A - KBB^T)$ , it is easy to show that the system modes are  $\pm \sqrt{\lambda_1}, \dots, \pm \sqrt{\lambda_6}$

The modes were computed for values of  $K$  corresponding to  $S = 30$  in. and

$S = 45$  or  $15$  in. The eigenvectors were also computed, so that the modal components could be identified. The results are shown below:

Mode	Surge-Pitch	Surge-Pitch	Heave	Sway-Roll	Sway-Roll	Yaw
Freq. (Hz)	4.56	26.6	8.27	4.53	14.32	15.6
S = 30						
Freq. (Hz)	5.74	33.4	10.4	5.74	18.1	19.5
S = 45						

Above figures show that most of the hydraulic modes are located in the range 5 Hz to 20 Hz with surge-pitch mode to about 30 Hz.

These oscillatory modes occur only with closed or nearly closed valves. It is thus shown that it is impossible for a 50 Hz mode (which has been measured in the system) to have its origin in the compressibility of the oil.

### 2.3.2 Mechanical Modes

Since the upper and lower frames are quite rigid it is obvious that the sources of high frequency vibration are the axial flexibility of the cylinders due to oil compressibility and the transverse flexibility of the cylinders (beam vibration). Section 2.3.1 showed that vibrations of hydraulic origin are in the range of 5 Hz to 30 Hz. Thus, higher frequency vibration must originate from the cylinder mechanical components.

In a recent study (Reference 5) a standard finite element computer program SAP IV (Structural Analysis Program) was used to analyse the dynamic properties of a 3-dimensional mechanism, involving hydraulic cylinders. In this study the oil column was considered as a truss of a properly chosen serving stiffness. The hydraulic cylinder wall and piston rod were considered as beams, interacting at the piston and rod end bearing. After applying the end conditions at the upper and lower supports of the cylinder, 78 natural frequencies were obtained for a total of six cylinders per motion system.

In the case of the motion system analyzed the natural frequencies of the six degrees of freedom motion were calculated at the centroid of the upper platform. Some of the typical values obtained are listed below:

Horizontal Motion	6.1	Hz	2 modes
Vertical Motion	11.3	Hz	1 mode
Combined Pitch and Roll	18.2	Hz	2 modes
Yaw Motion	27.6	Hz	1 mode
Lateral Cylinder Vibration	14 to 48	Hz	11 modes

The evidence that the high frequencies were originated at the cylinder structure was that the platform motions were very small and that the frequencies in each group were the same.

### 2.3.3 Hydraulic Oil Spring Stiffness

Hydraulic fluids, though far less compressible than gas, when compressed in a cylinder compartment act like a spring and induce therefore a second order mass-spring system whose natural frequency limits the bandwidth of any hydraulic servo. The hydraulic stiffness  $c_o$  is defined as the ratio of change in force to piston displacement and is given by

$$c_o = \frac{dF}{dS} = \frac{A_1 dP_1}{dS} + \frac{A_2 dP_2}{dS} \quad (2.27)$$

Since the bulk modulus of oil (150,000)psi is given by

$$\beta = \frac{dP \cdot V}{dV} = \frac{dP}{dS} \cdot S \quad (2.28)$$

Substituting Equation 2.28 into Equation 2.27 the oil spring constant is given as a function of the oil bulk modulus, the cap and rod areas and of the piston displacement.

$$\text{thus } c_o = \beta \left[ \frac{A_1}{\ell_1} + \frac{A_2}{\ell_2} \right] \quad (2.29)$$

assuming that the oil volume in the hydraulic lines is negligible compared to the oil volume at both sides of piston.

The value of  $c_o$  will be minimum at either end of the stroke and maximum at mid-stroke. The oil spring stiffness constant for the hydrostatic cylinder is :

$$C_o(\text{lower end}) = 150,000 \left[ \frac{4.71}{52} \right] = 13.58 \times 10^3 \text{ lb/in}$$

$$C_o(\text{mid stroke}) = 150,000 \left[ \frac{9.62}{26} + \frac{4.71}{26} \right] = 82.67 \times 10^3 \text{ lb/in}$$

$$C_o(\text{upper end}) = 150,000 \left[ \frac{9.62}{52} \right] = 27.75 \times 10^3 \text{ lb/in}$$

#### 2.3.4 Cylinder Hydraulic Resonance

The estimated weight supported by the hydraulic fluid is 18,000 lbs. At neutral position with motion stationary, the average weight supported by each servojack is

$$F_j = \frac{18,000}{6 \cos (36.26)} = \frac{3,000}{.806} = 3,720 \text{ lbs.}$$

The load supported by each jack is a function of its position from neutral and is also a function of the axis from which that extension from neutral is measured. Heave is the stiffest axis and lateral is the weakest.

The hydraulic resonance will be calculated with both cylinder ports blocked. That is; the oil will be trapped in each cylinder side and cannot escape.

The volume in line connection (piping on cylinder cap end) is negligible, while on the rod end it is estimated to be 50 in<sup>3</sup>. The cylinder net stroke is 52 inches.

1) The blocked port resonance frequency at neutral is given by

$$\begin{aligned} f_{nB} &= \frac{A_1 + A_2}{2\pi} \sqrt{\frac{\beta \times 386}{F_j [ (A_1 + A_2) l + 50 ]}} \quad (2.30) \\ &= \frac{14.33}{2\pi} \sqrt{\frac{150,000 \times 386}{3,720 (14.33 \times 26 + 50)}} \\ &= 13.84 \text{ Hz} \end{aligned}$$



For the actual hydraulic resonance calculations we will assume all hydraulic resonances are calculated as the system is extending and retracting and the cap end and rod end of cylinder are alternately one pressurized and the other open to reservoir.

- 2) At maximum extension up and cap end of cylinder pressurized the jack load will be

$$F_{ju} = \frac{3,000}{\cos(28.82)} = 3,424 \text{ lbs.}$$

and the resonance

$$f_{nu} = \frac{9.62}{2\pi} \sqrt{\frac{150,000 \times 386}{3,424 \times 9.62 \times 52}} = 8.90 \text{ Hz}$$

- 3) At maximum retraction down and rod end of cylinder pressurized the jack load will be

$$F_{jd} = \frac{3,000}{\cos(49.92)} = 4,659 \text{ lbs.}$$

and the resonance

$$f_{nd} = \frac{4.71}{2\pi} \sqrt{\frac{150,000 \times 386}{4,659 \times (4.71 \times 52 + 50)}} = 4.87 \text{ Hz}$$

- 4) At neutral extension going up with cap end pressurized

$$f_n = \frac{9.62}{2\pi} \sqrt{\frac{150,000 \times 386}{3,720 \times 9.62 \times 26}} = 12.08 \text{ Hz}$$

- 5) At neutral extension going down with rod end pressurized

$$f_{nr} = \frac{4.71}{2\pi} \sqrt{\frac{150,000 \times 386}{(3,720 (4.71 \times 26 + 50))}} = 7.12 \text{ Hz}$$

Since all frequency response requirements are to be met at neutral position the average value of the hydraulic resonance about neutral position will be calculated. This average value is found by using the average piston area and the average volume of the fluid under compression at neutral.

$$f_{nav} = \frac{(A_1 + A_2)/2}{2\pi} \sqrt{\frac{150,000 \times 386}{3,720 \times 26 \times (A_1 + A_2)/2}} = 10.42 \text{ Hz}$$

$$= 65.5 \text{ rad/sec}$$

The damping ratio of a hydraulic spring based on other systems and other designs is between .03 and .08. It is worthwhile to note here that the oil bulk modulus can vary from 80,000 to 250,000 psi, thus the hydraulic resonance frequency of the jack can be higher than the above calculated values. Values of actual testing have been in the 14 Hz range.

### 2.3.5 Summary

The preceeding vibration analysis may be summarized as follows:

1. ~~Vibration~~ natural frequencies in the motion system have been measured and vary up to almost 50 Hz depending on the motion.
2. Hydraulic natural frequency modes vary from 5 Hz to 30 Hz; again depending on the system motion.
3. Natural frequencies due to oil compressibility vary from 6 Hz to 15 Hz depending on the extension of the servo-actuator.
4. Oscillatory modes in the hydraulic system occur when closed center valves are used. Actual valves used in the system have slight underlap, thus providing extra damping.
5. Natural frequency modes from 14 Hz to 48 Hz are caused by lateral cylinder vibration.
6. The oil column hydraulic spring stiffness varies from 13,580 lb/in with cylinder retracted to 82,670 lb/in with cylinder at neutral position. Oil spring stiffness may vary depending on the oil bulk modulus.
7. The hydraulic cylinder-mass system natural frequency is minimum 5 Hz when cylinder is retracted and maximum 14 Hz with cylinder at neutral position with closed center valve.

NOTES: In order to increase the frequency interval between the system excitation frequency and the system natural frequency to avoid resonance, the system must be as stiff as possible.

Natural frequency is proportional to the square root of the system stiffness. Increasing stiffness implies increase in cylinder, and piston rod area or decreasing the cylinder length. Cylinder length, however, is governed by the system motion requirements. The piston area on the other hand is affecting the system velocity requirements. A larger cylinder requires more oil flow. Thus compromise is required.

From control theory it is well known that introducing feedback control changes the overall dynamics of the system. In a second order position servo, if the amount of position feedback is increased, the natural frequency is increased, implying that the system has been made stiffer, similarly velocity feedback has the effect of damping and increase in natural frequency, current feedback (in recent study) has shown that it stabilizes a single cylinder but, in the six-degree-of-freedom case, one of the modes (45.6 Hz) primarily in roll, is unstable.

Force feedback has a stabilizing effect on all modes, similar to that of valve pressure gain. This approach, however, has the possible weakness that all modes are given additional damping. It is then preferred to simply damp only the unstable modes, without affecting the dynamics of the other modes.

### 3. HYDROSTATIC BEARING ANALYSIS

#### 3.1 Basic Design Theory

The hydrostatic servojack contains two double conical bearings. One tapered piston mounted on the piston rod lower end and one tapered bushing mounted on the cylinder upper end (Figure 3.1).

Performance characteristics are given to show the influence of the axial speed of the piston in relation to the piston centering force, influence of eccentricity, clearance and taper.

The following symbols - used in this section - are also defined in the general Nomenclature. In this section English and metric units will be used, with the metric values shown in brackets.

$c$  = Radial clearance (at  $e=0$ ,  $x=0$ ), in. (mm)

$d$  = Nominal diameter of bearing, in. (mm)

$e$  = Eccentricity, in. (mm)

$f$  = Radial bearing force, lbs. (Newtons)

$h$  = Film thickness, in. (mm)

$l$  = Axial bearing length, in. (mm)

$P$  = Pressure, psi (bar)

$P$  = Pressure drop =  $P_2 - P_1$ , psi (bar)

$q$  = Leakage flow, U.S. gpm (lit/min)

$t$  = Bearing taper, in. (mm)

$x$  = Axial coordinate

$y$  = Tangential coordinate

$\mu$  = Dynamic viscosity, lb-sec/in<sup>2</sup> (N-sec/m<sup>2</sup>)

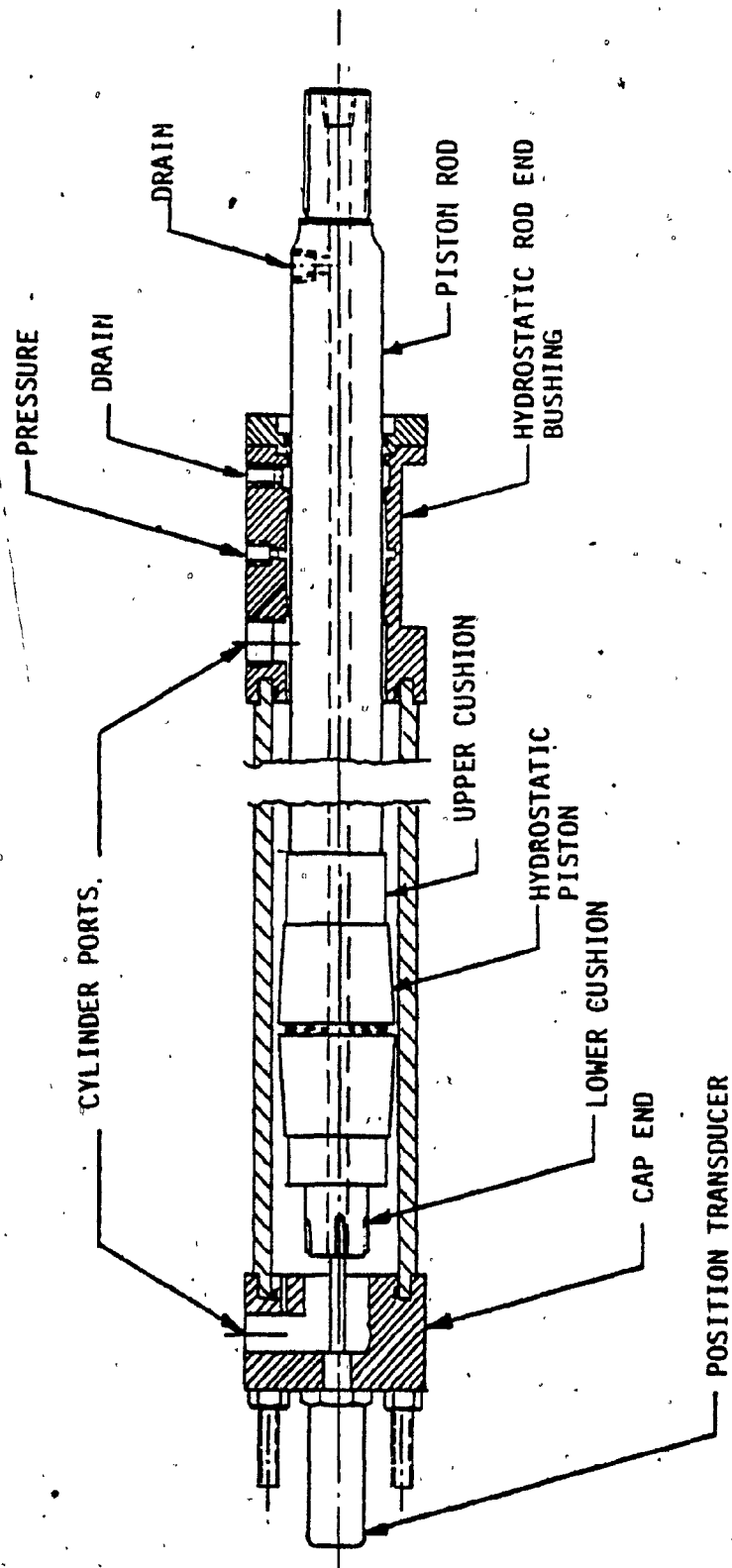


FIGURE 3.1 HYDROSTATIC ACTUATOR SERIES 500

### Dimensionless Quantities

$$E = e/c$$

$$\bar{F} = \frac{f}{0.25\pi d^2 (P_2 - P_1)}$$

$$L = \ell/d$$

$$T = t/c$$

$$V = \frac{\mu dv}{c^2(P_2 - P_1)} \quad \text{refers to single bearings}$$

$$V^* = \frac{\mu dv}{c^2(P_2 + P_1)} \quad \text{refers to double bearings}$$

$$V_c = \text{Value of } V^* \text{ where cavitation might occur}$$

Subscript 1 refers to the narrow end (2 to the wide end) of bearing gap, and 0 to the return line pressure.

#### 3.1.1 Introduction

Since closed loop hydraulic servo-actuators are used for accurate control of displacements, forces or varying speed, control accuracy is the most important factor in the performance of the servo system.

An important factor that affects control accuracy is Coulomb friction of piston and rod in its cylinder and bearing. Coulomb friction may reach from 5% to 15% of the load capacity in a conventional hydraulic cylinder.

The design of hydrostatic bearings offers a major opportunity to improve control accuracy as Coulomb friction is effectively eliminated.

Taking into consideration the results of the design study made at Delft University of Technology, (Ref.6), the tapered bearings were selected and this section will be on this type of bearing design.

The derivation of the equations used will not be presented here but can be found in Reference 6.

Since in this application formulae of both single and double bearings will be used, a summary of the characteristics of both designs is included.

### 3.1.2 Single Bearing

Conical hydrostatic bearings provide centering forces if the greater of the two pressures adjoining the bearing gap prevails at the wide side of the gap. Figure 3.2 shows a typical conical hydrostatic bearing. As long as pressure  $P_2$  is greater than  $P_1$ , a centering force exists and a permanent oil film can be maintained, eliminating metal to metal contact and Coulomb friction.

Using the Reynold's equation for two dimensional laminar flow around a tapered piston in a perfect cylindrical bore we have

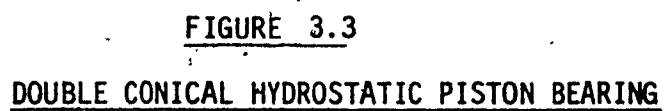
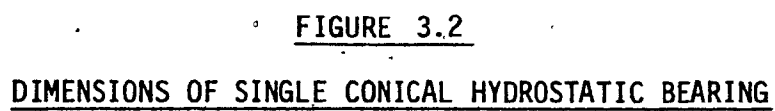
$$\frac{\partial}{\partial x} \left[ \frac{h^3}{12\mu} \frac{\partial P}{\partial x} - \frac{vh}{2} \right] + \frac{\partial}{\partial y} \left[ \frac{h^3}{12\mu} \frac{\partial P}{\partial y} \right] = 0 \quad (3.1)$$

Solving the above equation by first assuming one dimensional flow ( $\partial P / \partial y = 0$ ) and with  $h = h_1 + \frac{tx}{\ell}$ ,  $h_2 = h_1 + t$ ,

the pressure distribution around the piston becomes

$$P = P_1 + (P_2 - P_1) \cdot \frac{\frac{1}{h_2^2} - \frac{1}{h_1^2}}{\frac{1}{h_2^2} - \frac{1}{h_1^2}} + \frac{6\mu\ell v}{t} \cdot \frac{\left[ \frac{1}{h} - \frac{1}{h_1} \right] \left[ \frac{1}{h^2} - \frac{1}{h_2^2} \right]}{\left[ \frac{1}{h_2} + \frac{1}{h_1} \right]} \quad (3.2)$$





Proper integration around the piston gives the lateral force  $f$ .

The result in dimensionless form is

$$\frac{F}{L} = \frac{T}{E} \left[ \frac{2+T}{\sqrt{(2+T)^2 - 4E^2}} - 1 \right] - \left( \frac{24VL}{TE} \left[ \frac{\sqrt{(1+T)^2 - E^2} - \sqrt{1-E^2}}{T} - \frac{2+T}{\sqrt{(2+T)^2 - 4E^2}} \right] \right) \quad (3.3)$$

$$\text{where } T = \frac{t}{c}, \quad F = \frac{f}{.25\pi d^2 (P_2 - P_1)}$$

$$E = \frac{e}{c}, \quad V = \frac{\mu dv}{c^2 (P_2 - P_1)}$$

$$L = \frac{\ell}{d}$$

Applying hydrostatic bearings in a cylinder a certain leakage flow must be accepted, so that the bearing can operate. Knowing the pressure distribution of Equation 3.2 around the piston, the starting point for the calculation of the leakage flow is

$$dq = \frac{h^3}{12\mu} \frac{\partial P}{\partial x} dy \quad (3.4)$$

In an one dimensional flow model straight forward integration at a constant  $x$  yields

$$q = \frac{\pi c^3 \Delta P}{12\mu L} \left[ \frac{2(1+T)^2}{2+T} + \frac{3}{4} (2+T)E^2 + \frac{T^4}{8(2+T)} \left[ \frac{2+T}{(2+T)^2 - 4E^2} - 1 \right] \right]$$

which is approximated by (3.5)

$$q = \frac{\pi c^3 \Delta P}{12\mu} \cdot \frac{1 + 1.75T + 1.5 (1 + .5T)E^2}{L} \quad (3.6)$$

Since the leakage flow is quite small in comparison to the displacement flow the influence of the speed is omitted.

### 3.1.3 Double Bearing

The design of the single bearing limits its application to one-directional load because the bearings provide centering forces only when the greater of the two adjoining pressures prevails at the wide side of the gap. Otherwise a decentering force will occur. For this reason, a single bearing will not support a reversing load.

Another limiting factor is the speed, which directly influences the bearing forces.

However, both limitations can be overcome by using a double bearing which consists of two identical single bearings with opposite tapers (Figures 3.3 and 3.4). In this arrangement it is ascertained first of all that no "negative" pressure drop can occur, so a positive bearing force is guaranteed. Furthermore, the influence of speed is eliminated by the negative influence of the same speed on the other bearing half. But even the double bearings have limitations and further analysis is necessary.

From Equation 3.3 we see that the speed  $V$  does not directly influence the bearing as the negative half is cancelled by the positive influence of the speed on the other bearing half. In one dimensional flow model the total bearing force of a symmetric bearing can be found by

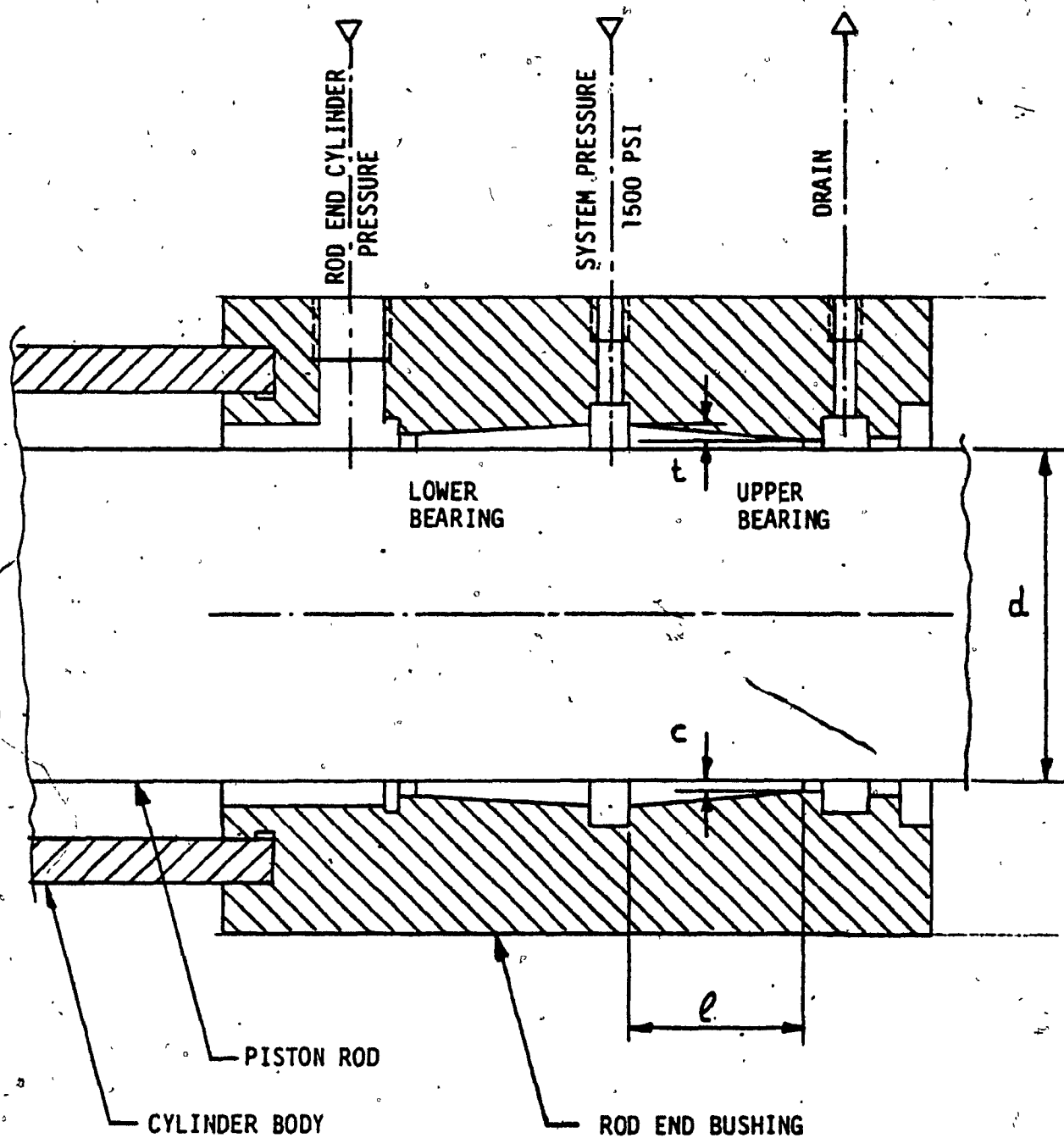


**FIGURE 3.4**

**DOUBLE CONICAL HYDROSTATIC ROD END BEARING**

$$f = \frac{TL}{E} \left[ \sqrt{\frac{2+T}{(2+T)^2 - 4E^2}} - 1 \right] \frac{\pi}{4} d^2 (\Delta P_I + \Delta P_{II}) \quad (3.7)$$

where  $\Delta P_I$  and  $\Delta P_{II}$  are the pressure drops across both bearing halves.

Even though the speed does not directly influence the bearing force, indirectly it does influence the maximum force.

Since negative pressures are physically impossible, we have assumed that the pressure is always positive, and in order to verify this assumption we examine the minimum pressure  $P_{\min}$

Introducing in Equation 3.2  $P_{\min} = 0$  and solving the equation

we get

$$\frac{\mu dv}{c^2} = \frac{(1-E)(1+T-E)^2}{3TL} \left[ \Delta P + \frac{2+T-2E}{1+T-E} \left[ P_1 + \sqrt{P_1^2 + P_1 \Delta P} \right] \right] \quad (3.8)$$

Equation 3.8 shows that speed  $V$  increases with  $E$ . By increasing the speed, the cavitation risk increases, and if we allow  $E = 0.75$

Equation 3.8 can be approximated by

$$V_c = \frac{\mu dv}{c^2 (P_2 + P_1)} \approx 0.1 \frac{T}{L} \quad (3.9)$$

In order to avoid possible cavitation the bearing speed must be less than  $V_c$ .

Introducing  $V^*$ , speed where cavitation might occur the characteristics are

$$f' = \frac{\pi}{4} d^2 (\Delta P_I + \Delta P_{II}) F \quad (3.10)$$

$$V^* = \frac{dv \mu}{c^2 (P_2 + P_1)} \ll 0.1 \frac{T}{L} \Rightarrow \text{then } F = \bar{F} \quad (3.11)$$

$$V^* = \frac{dv \mu}{c^2 (P_2 + P_1)} > 0.1 \frac{T}{L} \Rightarrow \text{then } F = \frac{\bar{F}}{3} \left( 4 - \frac{LV^*}{10T} \right) \quad (3.12)$$

### 3.2 Calculation of Parameters

#### 3.2.1 Leakage Flow Calculations

The leakage flow through a single conical bearing is given by Equation 3.6

$$q = \frac{\pi c^3 \Delta P}{12 \mu} \left[ \frac{1 + 1.75T + 1.5(1 + .5T)E^2}{L} \right]$$

The above equation shows that leakage flow depends on the following parameters:

- The radial clearance  $c$  between piston outside diameter and cylinder inside diameter (or piston rod diameter and upper bearing inside diameter).
- The pressure drop  $\Delta P$  across the bearing
- The viscosity  $\mu$  of the oil, which in turn depends on the type of hydraulic oil and on the operating temperature.
- The taper  $t$  of the conical bearing.
- The length  $L$  of the conical bearing.
- The eccentricity  $e$  of the bearing.

All the above parameters can be calculated or measured with the exception of the eccentricity.

The critical parameters in the above equation are, the radial clearance, pressure drop, viscosity and eccentricity.

The leakage flow is calculated for three different sizes of single bearings. The values used for radial clearance  $c$  and taper  $t$  in the leakage flow equation are the mean or average values. The viscosity was taken at operating temperature near the bearing area of 140° F.

Table 3.1 shows the numerical values to be used for calculations.

Figures 3.5, 3.6, and 3.7 show the leakage flow for three different sizes of hydrostatic bearing, as a function of eccentricity and pressure drop.

The leakage flow curves were obtained with an average value of radial clearance (.0017 in.) calculated from the bearing dimensional tolerances. An increase or decrease in clearance will increase or decrease the leakage flow by a factor of almost three.

Another factor that directly affects the leakage flow is the oil temperature. The temperature effect is present in two areas. First, the viscosity of the oil is decreased with increased temperature, thus the oil becomes less viscous and higher leakage flow is expected.

The flow curves were obtained with a dynamic viscosity of  $2.59 \times 10^{-6}$  lb-sec/in<sup>2</sup> at 140°F (20.5 cst kinematic viscosity) with a Shell Tellus 46 hydraulic oil. Table 3.2 shows the kinematic and dynamic viscosity values at different temperatures of Shell Tellus 46 hydraulic oil. The operating temperature near the piston bearing area is estimated to be 140°F, a value higher than the system operating temperature (110°F) due to heat generated by the pressure drop across the piston bearing.


TABLE 3.1

DIMENSION/ PARAMETER	PISTON BEARING	ROD END BEARING		UNITS *
		LOWER	UPPER	
d	3.500 (88.90 )	2.500 (63.50 )	2.50 (63.50 )	in. (mm)
ℓ	2.585 (65.66 )	1.450 (36.83 )	1.60 (40.64 )	in. (mm)
c	0.0017 ( 0.0432)	0.0019 ( 0.0483)	0.0016 ( 0.0406)	in. (mm)
t	0.007 ( 0.1778)	0.0025 ( 0.0635)	0.0027 ( 0.0686)	in. (mm)
$T = \frac{t}{c}$	4.12	1.316	1.25	-
$L = \frac{\ell}{d}$	0.739	0.580	0.660	-
μ	$2.59 \times 10^{-6}$ ( 0.018 )	$2.59 \times 10^{-6}$ ( 0.018 )	$2.59 \times 10^{-6}$ ( 0.018 )	lb-sec/in <sup>2</sup> (N-sec/m <sup>2</sup> )

- Dimensions and Parameter values to be used with Equation 3.6 for calculating leakage flow, q.

\* Dimensions in brackets are in metric units.





Another affect of oil temperature is the change of radial clearance between the piston bearing outside diameter and the cylinder body diameter. Due to the difference in thermal expansion of the piston bearing and cylinder body materials the radial clearance will be different from that calculated using the dimensional tolerances of the hydraulic cylinder.

Thermal expansion effects were considered in sizing the bearing and cylinder diameter. Eccentricity introduced by assembly of the components will greatly increase leakage flow at higher pressure drops. However, the centering force will tend to eliminate any introduced eccentricity. This implies that the leakage flow values should be taken at an eccentricity value,  $e$ , less than 50% of the radial clearance.

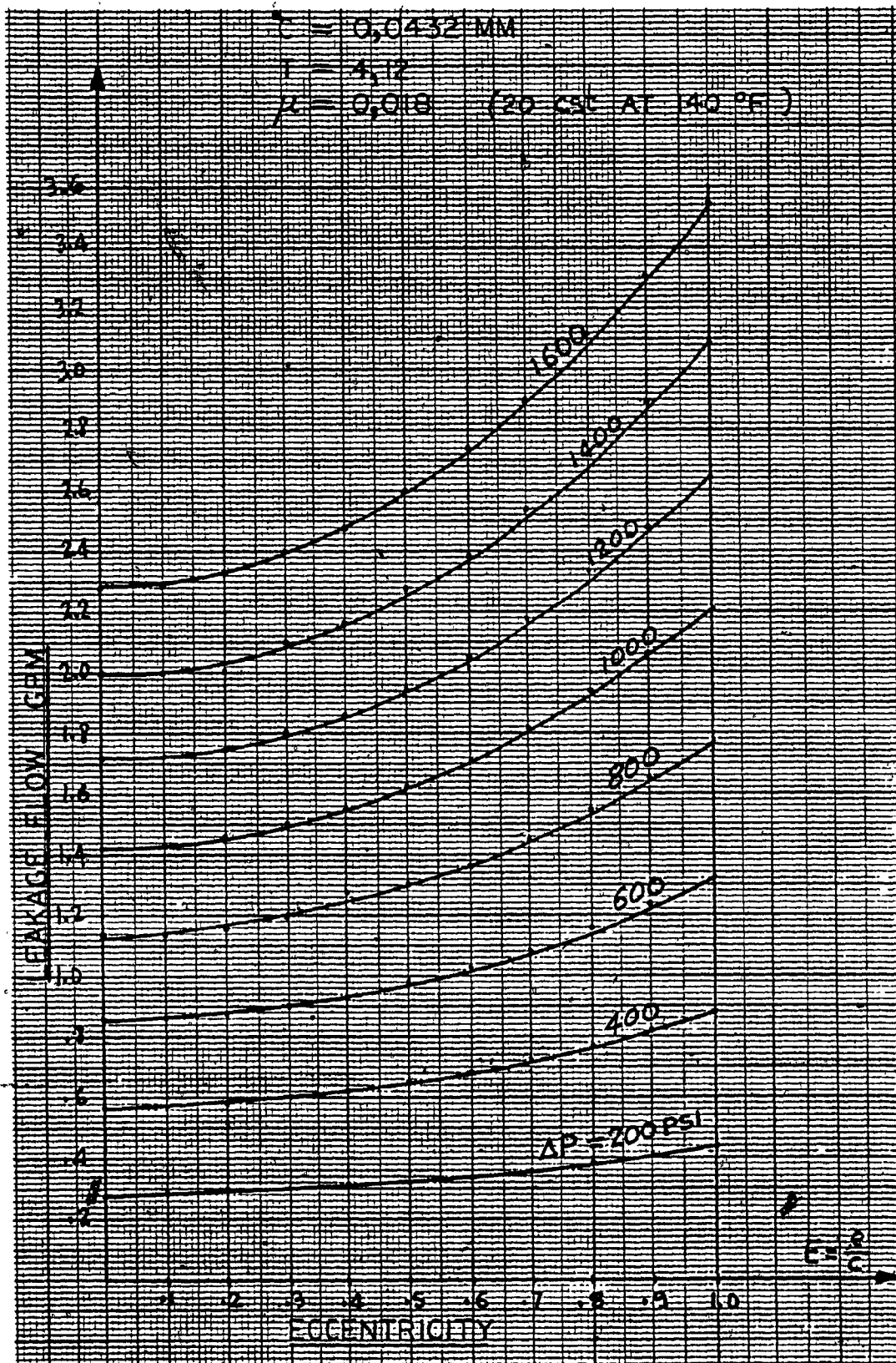


FIGURE 3.5 PISTON BEARING SINGLE

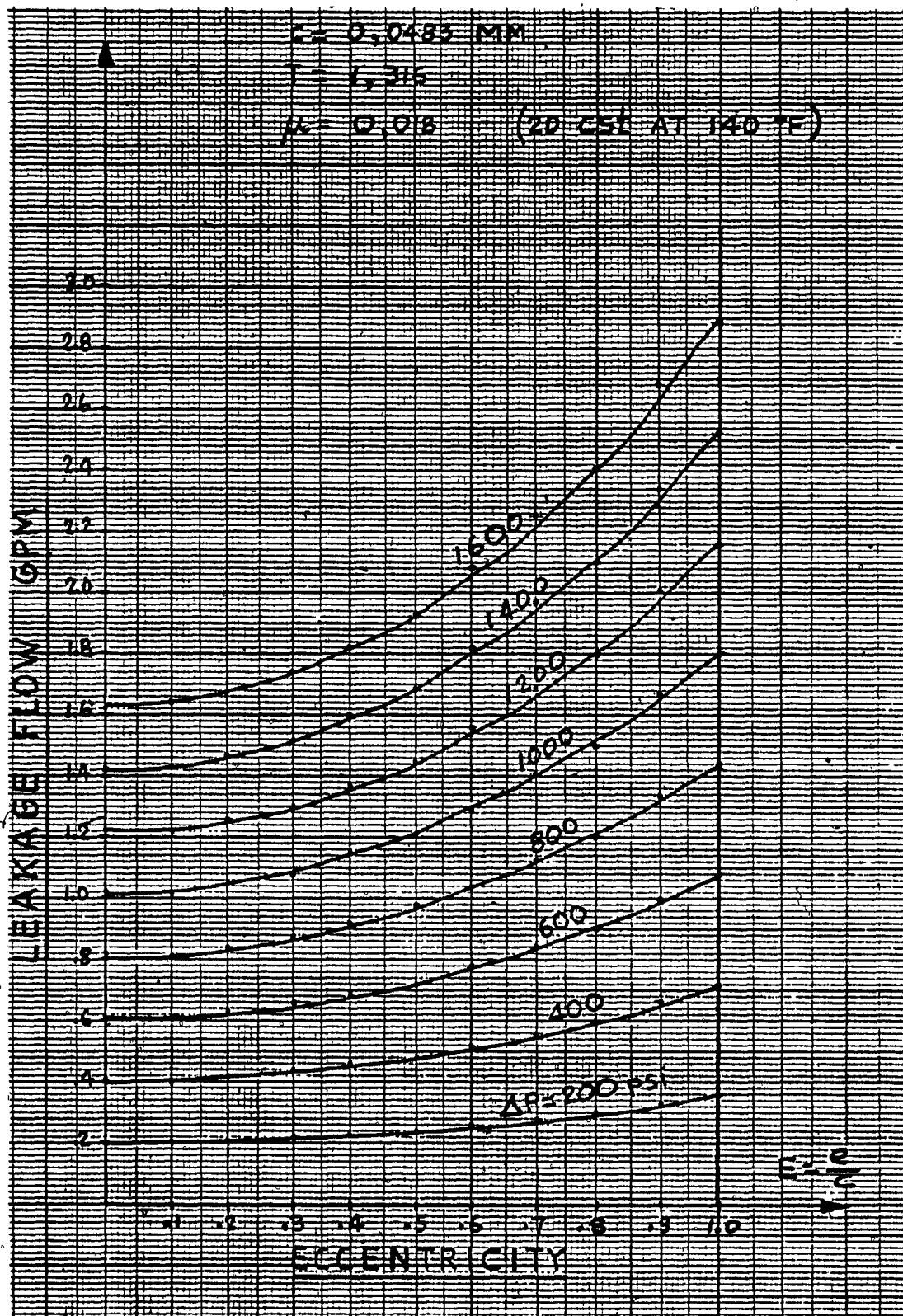


FIGURE 3.6 ROD END BEARING (LOWER)

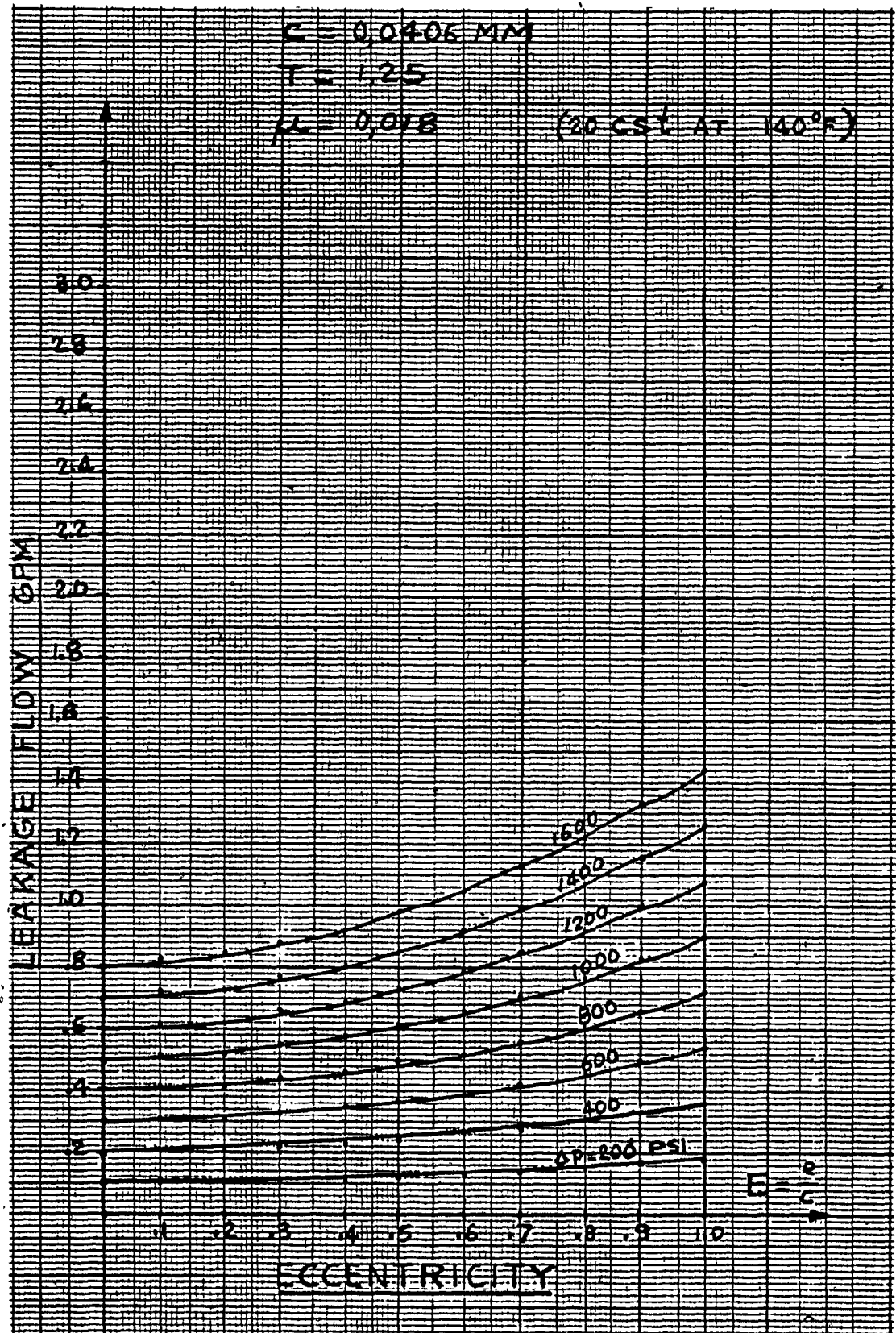


FIGURE 3.7 ROD END BEARING (UPPER)

TABLE 3.2

VISCOSITY VS TEMPERATURE

HYDRAULIC OIL SHELL TELLUS 46

$w = 54.64 \text{ lb/ft}^3$

TEMPERATURE  °F	KINEMATIC VISCOSITY, $\nu$		DYNAMIC VISCOSITY, $\mu$	
	SSU	CENTISTOKES $\frac{\text{mm}^2}{\text{sec}}$	$\frac{\text{lb-sec}}{\text{in}^2} \times 10^{-6}$	$\frac{\text{N-sec}}{\text{m}^2}$
100	220	46	5.83	0.0405
110	170	37	4.69	0.0326
120	140	30	3.79	0.0264
130	115	24	3.04	0.0212
140	98	20.5	2.59	0.0180
150	85	17	2.15	0.0149
160	75	14.5	1.84	0.0128

### 3.2.2 Bearing Centering Force Calculations

Solving Equation 3.3 for single piston bearing (Figure 3.2) the value of bearing force  $F$ , is obtained as a function of eccentricity and piston speed. The results are shown in Figure 3.8. For  $V = 0$  it shows that force  $F$  is continuously increasing with eccentricity  $E$ . According to Equation 3.3 the bearing force  $F$ , is reduced proportionally to the speed  $V$ . For each value of  $V$ , the corresponding curve has a maximum  $F$  at a certain value of eccentricity  $E$ , and for greater values of  $E$ , the stiffness  $dF/dE$  becomes negative. For single bearings the decreasing part of the curves is meaningless, since the corresponding bearing performance is unstable. The locus of the maxima (where  $dF/dE = 0$ ) includes all possible combinations of maximum bearing forces  $F$  and speed  $V$ .

Figures 3.9 and 3.10 show curves obtained solving Equation 3.3 for the rod end bushing bearing (Figure 3.4). This double bearing is not symmetrical. However, Figures 3.9 and 3.10 show the characteristics of single bearing, one dimensional flow and the influence of eccentricity and speed on bearing force.

Comparing the three obtained figures, it can be seen that when the dimensionless parameter  $T$ , is increased the maximum bearing force  $F$ , is increased at zero velocity, but it is decreased as velocity is increased. This proves that smaller taper on the bearing produces higher bearing forces at zero velocity. At higher velocities the bearing force will be maximum at certain value of eccentricity, and then will drop drastically.

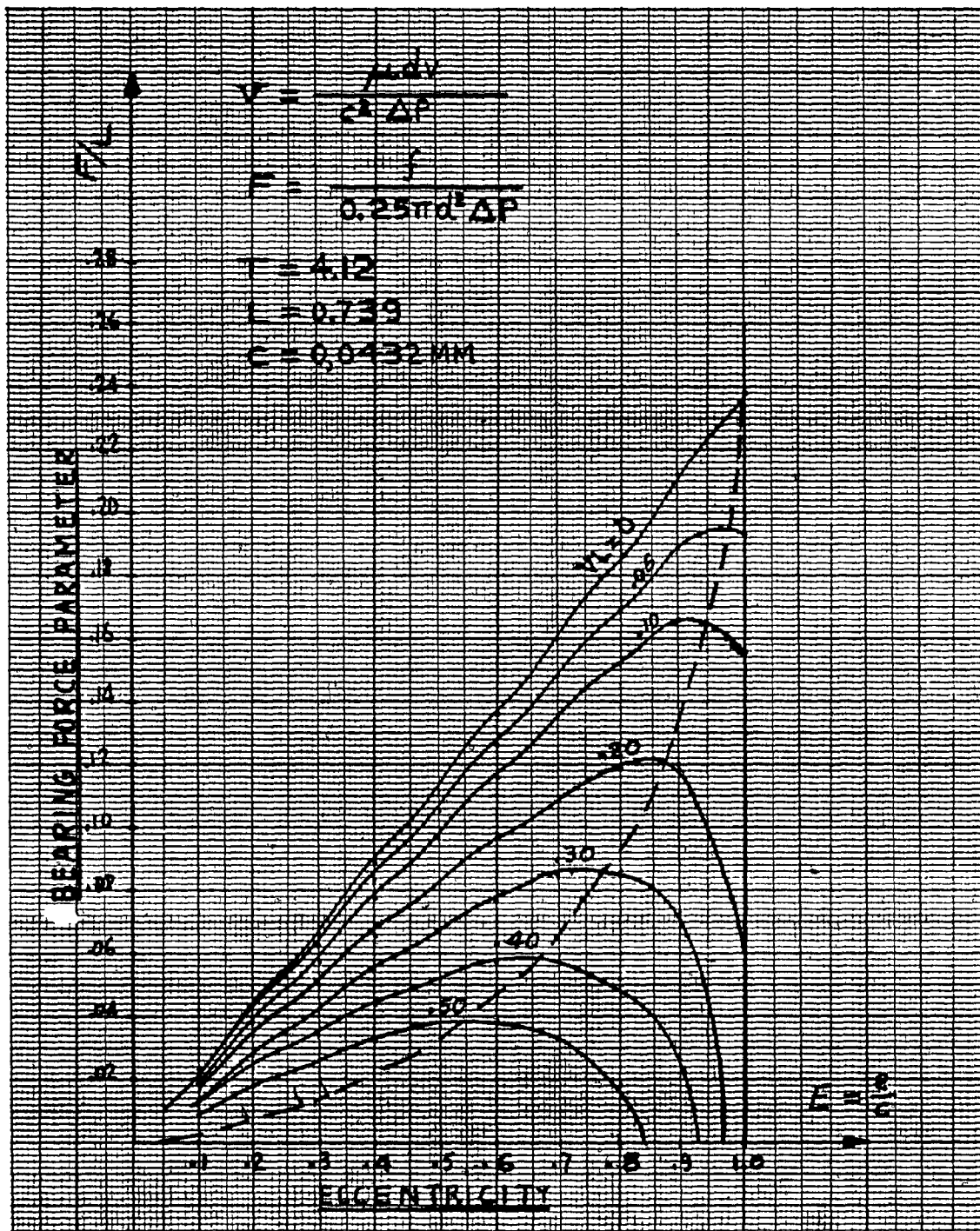


FIGURE 3.8 PISTON BEARING

CHARACTERISTICS OF SINGLE BEARING ONE-DIMENSIONAL FLOW.  
INFLUENCE OF ECCENTRICITY AND SPEED ON BEARING FORCE.

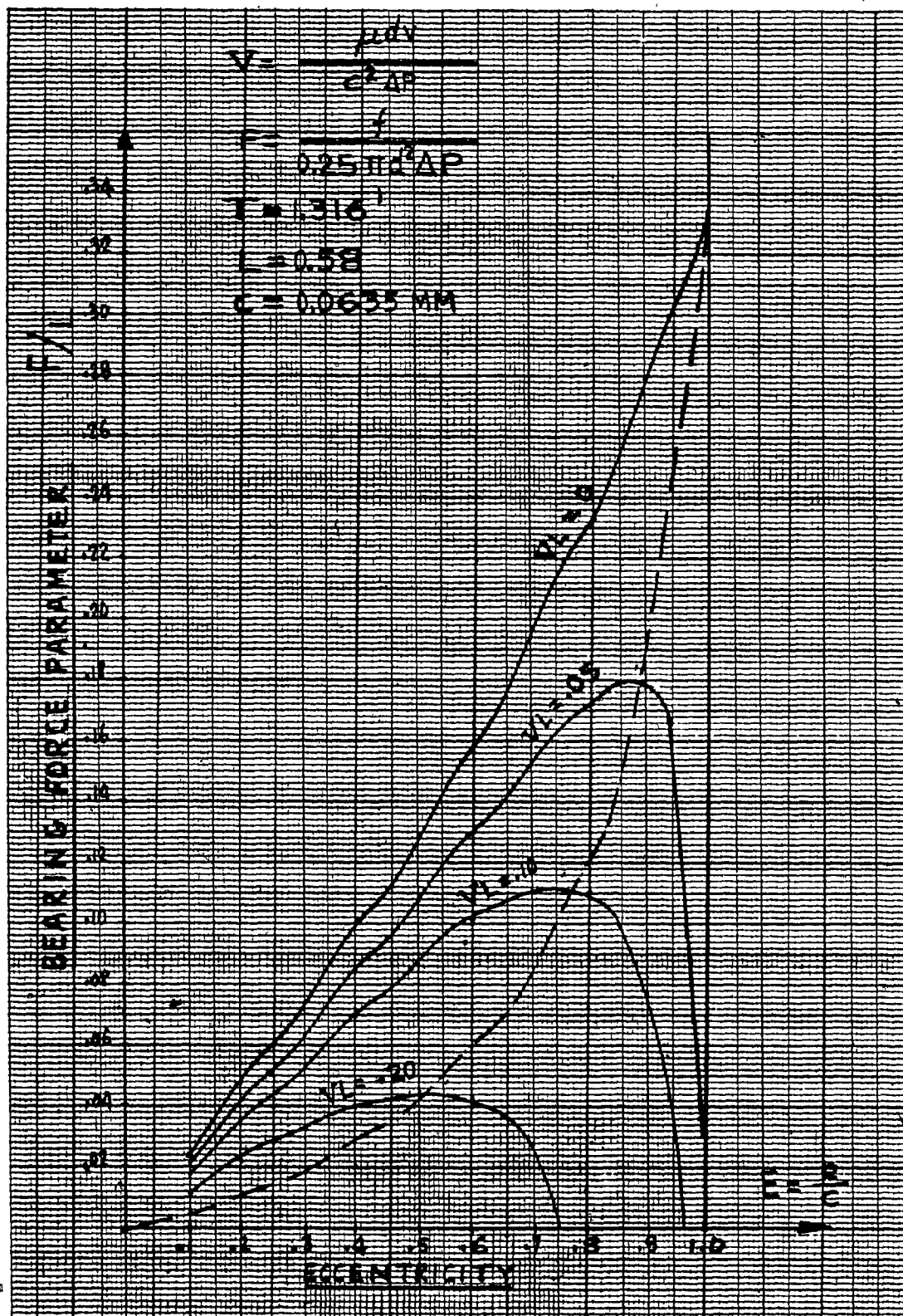


FIGURE 3.9 ROD END BEARING (LOWER)

CHARACTERISTICS OF SINGLE BEARING ONE-DIMENSIONAL FLOW.  
 INFLUENCE OF ECCENTRICITY AND SPEED ON BEARING FORCE.



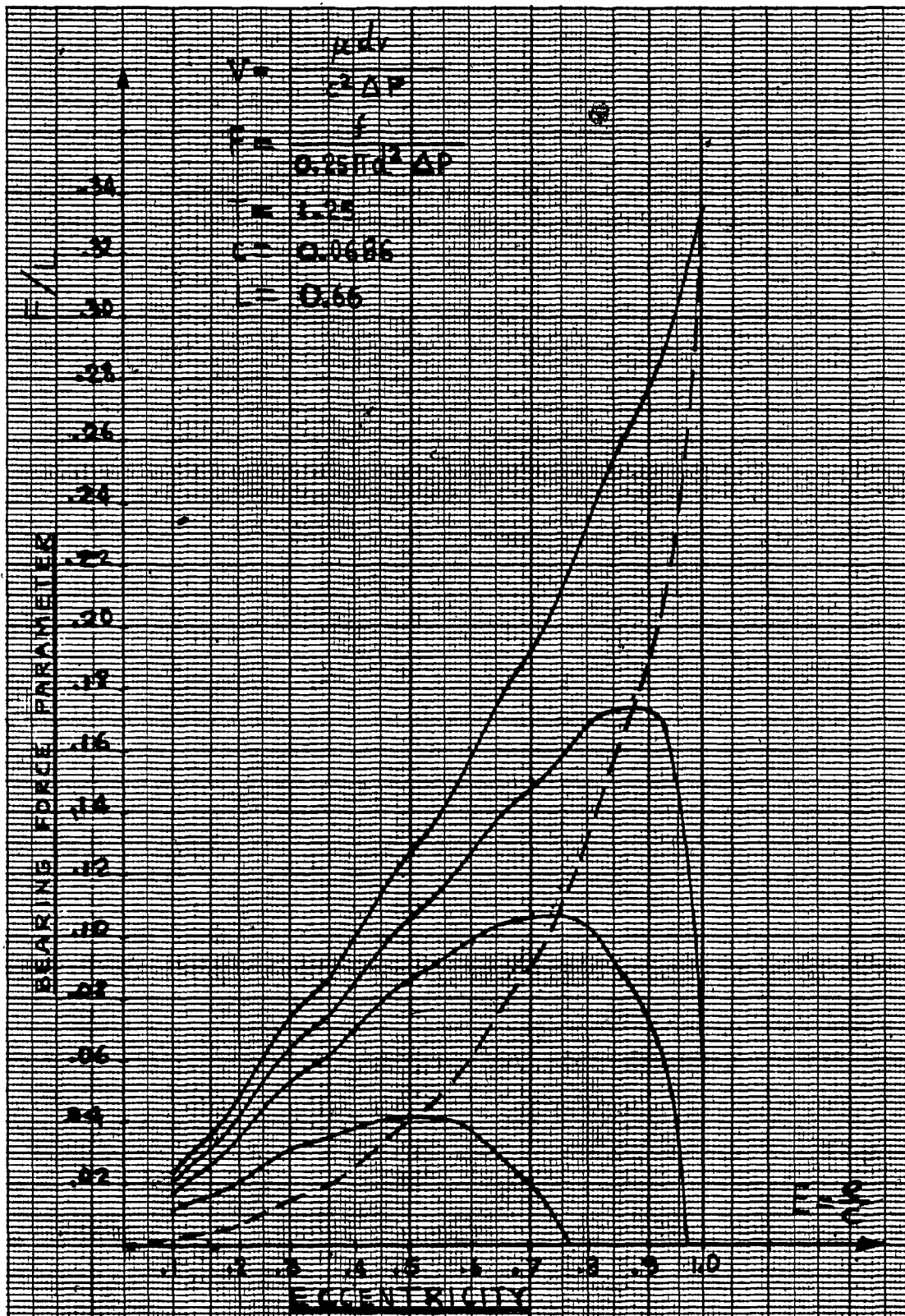


FIGURE 3.10 ROD END BEARING (UPPER)

CHARACTERISTICS OF SINGLE BEARING ONE-DIMENSIONAL FLOW.  
 INFLUENCE OF ECCENTRICITY AND SPEED ON BEARING FORCE.

Even though high velocities imply negative pressure on one side of the piston, with the use of double hydrostatic bearings, the negative pressure is cancelled by the positive pressure on the other side of the piston. Thus, speed influences the maximum bearing force only indirectly.

Table 3.3 shows the dimensions and values of parameters used for calculating bearing forces, and summary of calculated values for  $\bar{F}$ ,  $V^*$ ,  $V_c$  and  $f$ . For calculations of the rod end bearing forces, the dimensions of the upper bearing (Figure 3.4), were used, and were applied using the theory of double symmetrical bearing.

The calculations were done under the condition where the piston is at neutral position, stationary, with balanced forces (650 psi on cap end and 1500 psi on rod end). Under this condition, the total pressure drop at piston bearing is 2150 psi (148 bar). The pressure drop at the rod end bearing under the same conditions is 1500 psi (103 bar).

With piston maximum required velocity  $v = 24$  in/sec, the value of the dimensionless speed parameter  $V^*$  is:

a) For piston bearing

$$V^* = \frac{\mu dv}{c^2(P_2 + P_1)} = \frac{2.59 \times 10^{-6} \times 3.500 \times 24}{(0.0017)^2 \times 1,500} = 0.035$$

$$\text{and } V_c = 0.1 \frac{T}{L} = 0.1 \times \frac{4.12}{0.739} = 0.558$$

Since  $V^* < V_c$ ,  $F = \bar{F} = 0.12$  at  $V = 0$  and  $E = 0.75$

then the piston bearing force is  $f = F \left[ \frac{\pi}{4} d^2 (\Delta P_I + \Delta P_{II}) \right]$

TABLE 3.3

DIMENSION/ PARAMETER	PISTON BEARING DOUBLE	ROD END BEARING DOUBLE	UNITS *
d	3.500 ( 88.90 )	2.500 ( 63.50 )	in. ( mm )
ℓ	2.585 ( 65.66 )	1.60 ( 40.64 )	in. ( mm )
c	0.0017 ( 0.0432 )	0.0016 ( 0.0406 )	in. ( mm )
T = t/c	4.12	1.25	-
L = ℓ/d	0.739	0.660	-
μ	2.59 × 10 <sup>-6</sup> ( 0.018 )	2.59 × 10 <sup>-6</sup> ( 0.018 )	lb-sec/in <sup>2</sup> ( N-sec/m <sup>2</sup> )
P1	650 ( 45 )	0	lb/in <sup>2</sup> ( bar )
P2	1500 ( 103 )	1500 ( 103 )	lb/in <sup>2</sup> ( bar )
F      V = 0 E = .75	.127	.119	-
v	24.0 ( 0.60 )	24.0 ( 0.60 )	in/sec ( m/sec )
$V^* = \frac{\mu dv}{c^2(P_2 + P_1)}$	0.035	0.040	-
V <sub>c</sub> = 0.1 T/L	0.558	0.189	-
f	2,622 ( 11,666 )	886 ( 3,943 )	lbs. ( Newtons )

Dimensions and parameter values for calculating bearing forces.

\* Dimensions in brackets are in metric units.

where  $\Delta P_I = 650 \text{ psi (45 bar)}$

$\Delta P_{II} = 1,500 \text{ psi (103 bar)}$

$$\begin{aligned} \text{and } f &= 0.12 \left[ \frac{\pi}{4} \times (3.500)^2 \times 650 + 1,500 \right] \\ &= 2,622 \text{ lbs. (11,666 Newtons)} \end{aligned}$$

b) Similarly for rod end bearing

$$\begin{aligned} v^* &= \frac{2.59 \times 10^{-6} \times 3.500 \times 24}{(0.0016)^2 \times 1,500} \\ &= 0.04 \end{aligned}$$

Again  $v^* < v_c$ , and  $F = \bar{F} = 0.12$  at  $y = 0$  and  $E = 0.75$

Then the rod end bearing force is

$$\begin{aligned} f &= 0.12 \left[ \frac{\pi}{4} \times (2.500)^2 \times 1,500 \right] \\ &= 886 \text{ lbs (3,943 Newtons)} \end{aligned}$$

### 3.3 Design Critical Parameters

The design of the hydrostatic bearings in a hydraulic cylinder requires very close tolerances. The effects of the cylinder piston bearing clearances were examined in Section 3.2.1, where it was shown that an increase or decrease in clearance will increase or decrease the leakage flow significantly. A large tolerance in piston bearing and cylinder diameters will make it impossible to predict the leakage flow. A recommended clearance is in the range of .0008 to .0025 inches.

The tapers on piston and bushing bearings will affect the centering force depending on the piston velocity. If the dimensionless parameter  $T = t/c$  is increased by increasing the taper  $t$ , the maximum centering force will be decreased at zero velocity by almost the same factor. At higher velocities,  $VL > .15$ , the maximum centering force will be increased.

Reference 6, recommends  $T \approx 2$  for  $L = 0.5$  to  $1.0$ . In the present hydrostatic bearing design the value of  $T$  is  $4.12$  for  $L = .73$  and  $T = 1.25$  for  $L = .66$ .

With the above dimensions the system performs satisfactorily. The centering force is a function of the piston velocity and it is linear up to a certain value of eccentricity as shown in Figure 3.8. The system maximum operating velocity is  $24$  in/sec ( $V^* = .035$ , or  $VL = .026$ ), producing a maximum centering force of  $2,623$  lbs at piston bearing and  $886$  lbs at rod end bearing. Since there are no lateral external forces on the cylinder the above design is satisfactory.

Another critical parameter to be considered in the bearing design is piston bearing and rod end bearing housing materials. By using the same material for the cylinder body and bearing, thermal effects are eliminated. However, in practice, seizing problems may be encountered due to very small clearances.

It is thus recommended that bearing be manufactured of lower strength materials than the cylinder body and piston rod. The materials for the cylinder tube and piston rod are selected to withstand the system pressure, and loading, while the bearings can be made from a softer material, such as bronze bar.

In Section 2.2, the cylinder strength and stresses were analyzed where it was found that eccentricity may be introduced by misalignment of the assembled cylinder parts.

The component parts that are considered to be the causes of misalignment are: piston bearing, piston shaft, cylinder tube and rod end bearing. The errors have been calculated in terms of angular displacement of the piston shaft about the true axis of the servojack, between the piston center and rod end bearing.

The calculated errors due to misalignment of the above mentioned parts when assembled are as follows:

Piston major diameter eccentricity	= 0.027'
Piston mounting diameter clearance	= 0.074'
Piston shaft eccentricity	= 0.027'
Piston shaft straightness	= 0.27'
Cylinder straightness	= 0.40'
Cylinder end squareness	= 0.26'
Cylinder mounting diameter clearance	= 0.27'
Rod end mounting squareness	= 0.76'
Rod end tapers run-out	= <u>0.49'</u>

Total theoretical worst case angular error = 3.08'

The probable worst case angular error is calculated in terms of  
3 - sigma values = 1.30'.

The worst case permissible angular error of the shaft within the  
rod end bearing before metal-to-metal contact occurs is 1.76',  
corresponding to a lateral deflection of approximately 0.030 in.  
when jack is fully extended.

#### 4.0 CUSHION DESIGN

The cushion is required to act as a safety device in the event of loss of control, or runaway of any servojack. The cushion must be capable of safely absorbing the full impact of any servojack reaching the end of its stroke at maximum velocity, driven by full system pressure. The cushion also ensures a smooth return to neutral rest under normal shutdown.

The cushion safety system is aided by programmed deceleration which occurs automatically at the ends of stroke, when the system is under computer control. A limit switch shuts-off the system power when the jack is at fully retracted position.

Conventionally a piston is cushioned by closing off the discharge and by-passing the trapped flow through a fixed or variable orifice. This can be achieved internally with a spear at the end of the piston, mating with a close fitting fluid exhaust passage. A problem exists when the passage initially is blocked, and the pressure build-up is very rapid due to load inertia, velocity and driving force.

A fixed orifice provides a deceleration force which diminishes rapidly as the piston slows down. Consequently, the pressure initially builds up and then reduces rapidly.

A variable orifice can provide a constant deceleration, or constant pressure drop, as the orifice area is varied continuously to compensate for the piston velocity.



The kinetic energy absorbed by any cushion is represented by the area under the performance curve (Figure 4.1a).

For the straight spear cushion, most of the work is concentrated at the beginning of the cushioning and the initial pressure can be extremely high. The remainder of the cushioning stroke absorbs relatively little energy, and therefore, it has little decelerating effect on the piston.

For the variable orifice area cushion (constant deceleration), the same total kinetic energy is absorbed but it is done gradually and smoothly over the entire cushioning stroke. The stresses are lower the process is more effective, and the overall cushioning time is less.

The best way to vary the orifice area, is to have a spear or plunger, that is tapered, slotted or drilled to produce a continuously varying area. The ideal profile of the taper is a concave parabola, where the orifice area is larger in the beginning of the cushion and rapidly reduces at the end. It is impractical, however, to produce a perfect parabola without a tape-controlled machine tool, so it is approximated by cutting a series of straight taper slots along the axis of the spear.

The cushioning design for both lower and upper cushions is similar as shown in Figures 4.2 and 4.3, with the exception of diameter, and the adjustable metering orifice is preset to provide a constant velocity of 0.5 in/sec, once the piston has entered the stop region at point-D.

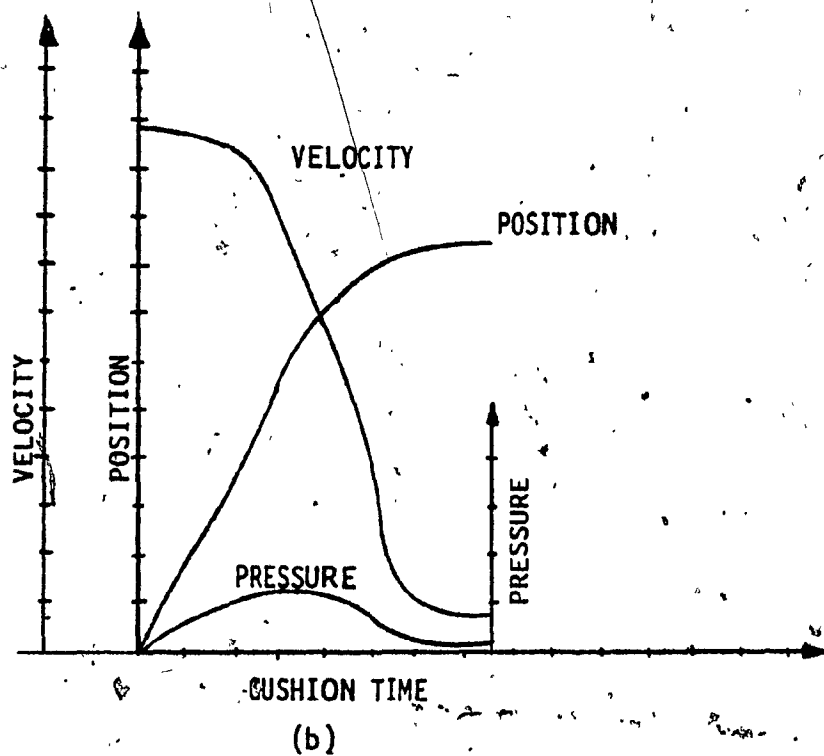
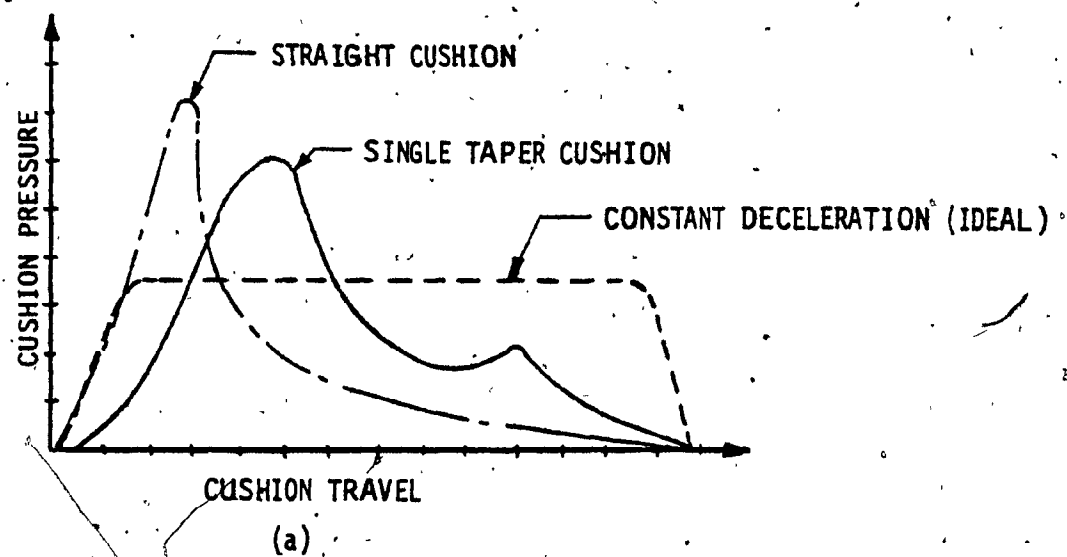


FIGURE 4.1 - CUSHION TYPICAL PERFORMANCE CURVES.

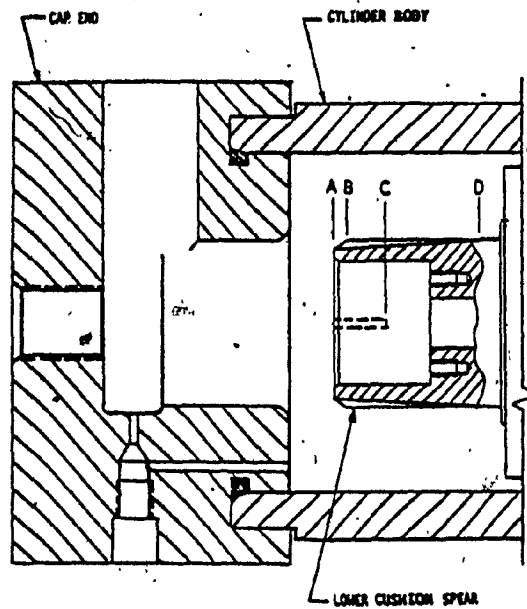


FIGURE 4.2 - LOWER CUSHION

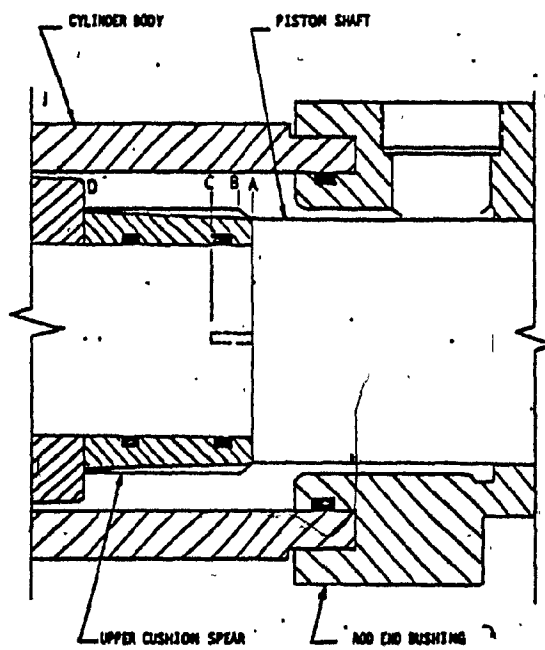


FIGURE 4.3 - UPPER CUSHION

Spears of both cushions are provided with four tapered grooves on the outside diameter, sized such that, the cushion (orifice) area is gradually decreased as cushion enters the cap or rod end cushion bore of the cylinder.

In order to determine the plot of orifice area versus piston position for a constant deceleration (variable orifice) the following basic equations are involved (References 7,8,9)

$$F = M\alpha = \frac{W}{g} \quad \text{Newton's second law of motion} \quad (4.8)$$

$$\frac{P_1 - P_3}{W} = \frac{v_i^2}{2g} \quad \text{Bernoulli's equation} \quad (4.9)$$

$$A_1 v_i = C A_o v_o \quad \text{Law of continuity}$$

$$\text{Work} = E_K - E_P \quad \text{Conservation of energy} \quad (4.11)$$

$$E_K = \int_{v_i}^{v_o} M v dv \quad \text{Kinetic energy equation}$$

$$E_P = \int_0^x F dx \quad \text{Work done equation} \quad (4.13)$$

Referring to Figure 4.4 the following equations can be obtained.

$$Q_2 = A_2 \dot{x} \quad (4.14)$$

$$Q_1 = A_e \dot{x}$$

$$W + P_2 A_2 = f + P_1 A_e + P_3 A_3 + M \ddot{x} \quad (4.15)$$

or 
$$W + P_2 A_2 = f + (P_1 - P_3) A_3 + P_3 (A_e + A_3) + M \ddot{x}$$

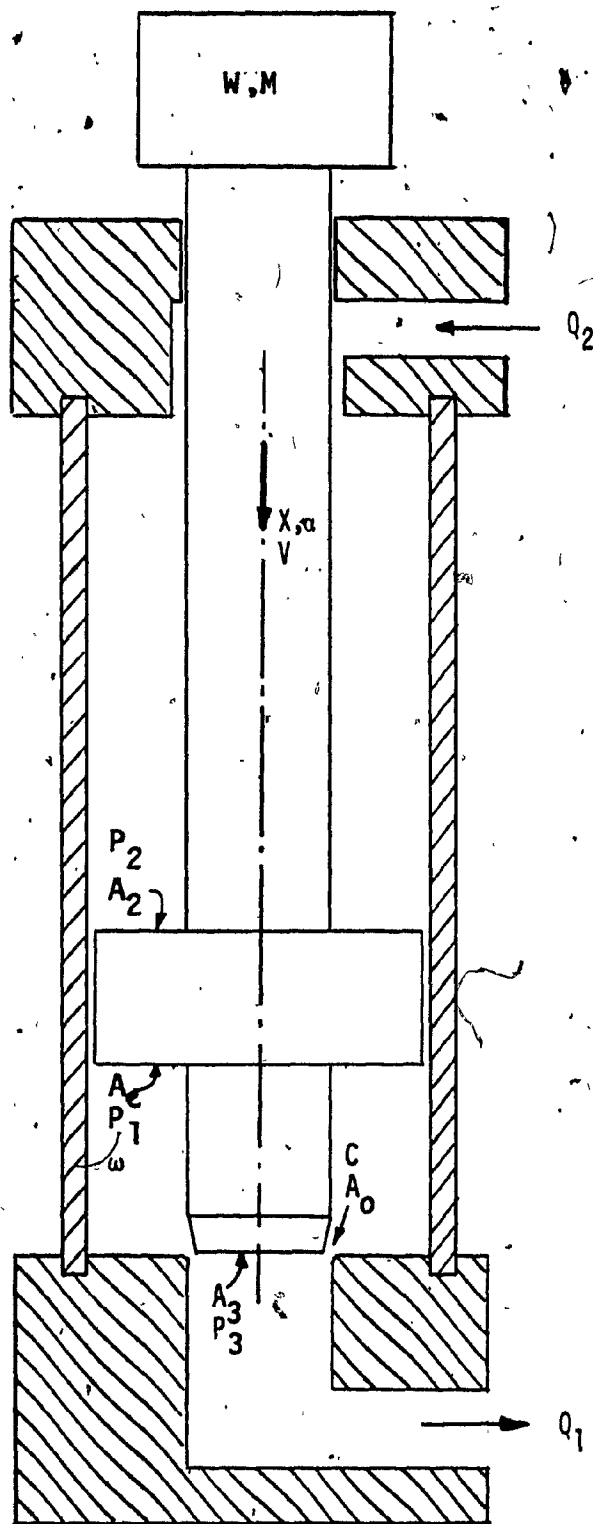


FIGURE 4.4. CYLINDER CUSHION PARAMETERS

where the term  $(P_1 - P_3)$  is the pressure drop across the orifice and  $f$  is the piston friction. As the spear approaches the cavity bore,

$$Q_1 = C A_o \sqrt{\frac{2(P_1 - P_3)}{\rho}} \quad (4.16)$$

where  $\rho$  - fluid density =  $\frac{w}{g}$  lb sec<sup>2</sup>/in<sup>4</sup>

$w$  = fluid specific weight, lb/in<sup>3</sup>

From Equations 4.14 and 4.16 the orifice pressure drop is

$$P_1 - P_3 = \frac{w v_i^2 A_e^2}{2g C^2 A_o^2} \quad (4.17)$$

In order to obtain a constant deceleration, the pressure drop must be constant. This will be obtained by reducing the orifice area  $A_o$  as velocity  $v_i$  is reduced.

The exhaust or return line pressure is assumed to be 100 psi.

From the above equations and considering the case of a vertical drop the orifice area is given by the following composite equation.

$$A_o = \left[ \frac{A^3 (v_i^2 - 2\alpha X)}{2C^2 W(\alpha + g)} \right]^{1/2} \quad (4.18)$$

The only unknown parameter in the above equation is the load acceleration, which is obtained from

$$\alpha = \frac{v_i^2}{2X} \quad (4.19)$$

Where  $X$  is the effective cushion travel (1.57 in.)

#### 4.1 Mathematical Model

In the presently used cushion design (Series 500 motion system) the cushion (orifice) area changes according to the following relationship, as the cushion spear travels by a distance  $X$  into cushion area.

a) Lower (cap end) cushion

$$A_{OCB} = 0.653 - 2.581 X - 1.045 X^2 \quad \text{for } 0 < X < 0.22 \quad (4.20)$$

$$A_{OBC} = 0.054 - 0.043 X \quad \text{for } 0 < X < 0.40 \quad (4.21)$$

$$A_{OCD} = 0.035 - 0.012 X \quad \text{for } 0 < X < 1.00 \quad (4.22)$$

b) Upper (rod end) cushion

$$A_{OAB} = 1.035 - 4.388 X - 1.046 X^2 \quad \text{for } 0.0 < X < 0.22 \quad (4.23)$$

$$A_{OBC} = 0.044 - 0.039 X \quad \text{for } 0.0 < X < 0.40 \quad (4.24)$$

$$A_{OCD} = 0.025 - 0.008 X \quad \text{for } 0.0 < X < 1.30 \quad (4.25)$$

Where the subscript of  $A_O$  denotes area for  $X$  between points A and B, B and C, C and D.

The curves obtained using the above equations are shown in Figure 4.5 .

The mathematical model equations are theoretical and the actual area may vary, depending on the dimensional tolerances of the mating parts.

Note that the effective cushioning will start at  $X = 0.3$  in. at which point the orifice area is approximately  $0.05 \text{ in}^2$ . Figure 4.6 shows cushion orifice area versus travel in linear scale for travel from point B to bottom of stroke.

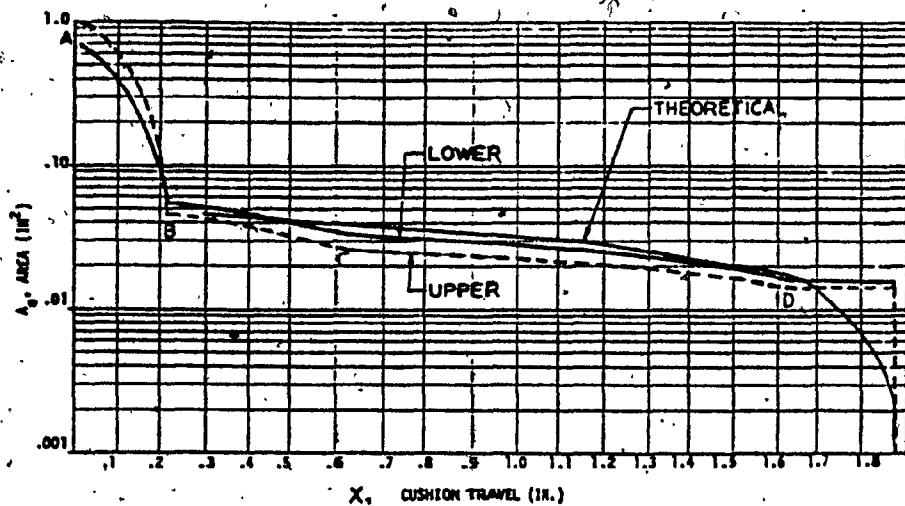


FIGURE 4.5 CUSHION ORIFICE AREA VERSUS TRAVEL

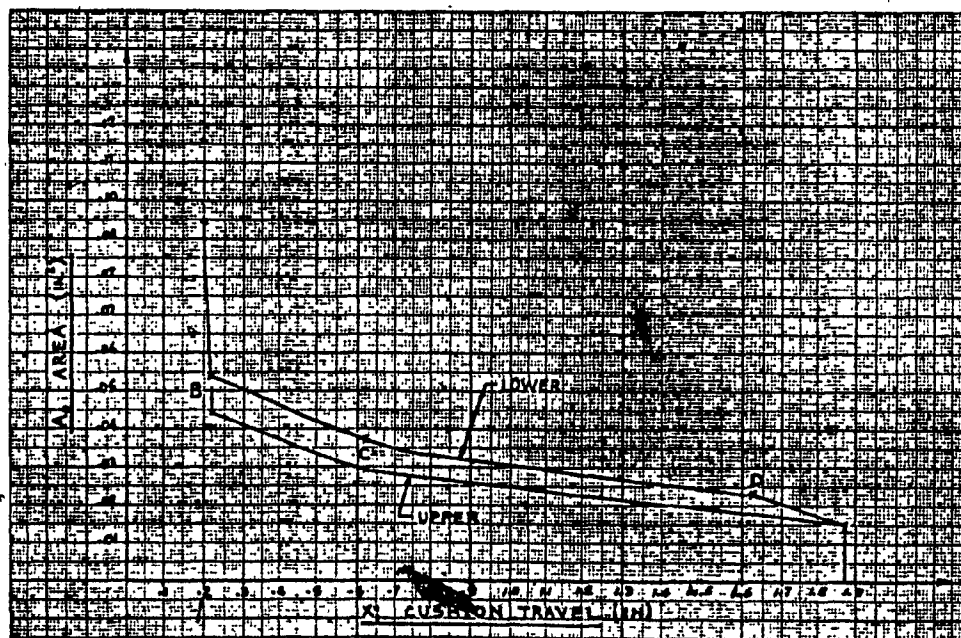


FIGURE 4.6 CUSHION ORIFICE AREA VERSUS TRAVEL



#### 4.2 Calculations of Cushion Pressure and Forces

Equation 4.17 can give an instantaneous pressure generated behind the piston as it enters the cushion area. This pressure depends mainly on the piston velocity, orifice area and orifice constant.

Assuming a hardover failure of the servovalve, the piston accelerates to its maximum velocity,  $v_1$ , and as the piston spear enters the cushion region, the cushion pressure will start to build up.

The maximum cushion pressure can be calculated at the beginning of the effective cushioning where all parameters in equation 4.17 are known. For

$$\omega = 0.0316 \text{ lb/in}^3$$

$$v_1 = 24 \text{ in/sec}$$

$$A_e = 7.21 \text{ in}^2$$

$$A_o = 0.045 \text{ in}^2$$

$$C = 0.8$$

$$g = 386 \text{ in/sec}^2$$

$$P_3 = 100 \text{ psi}$$

then

$$P_1 = \frac{0.0316 \times (24)^2 \times (7.21)^2}{2 \times 386 \times (0.8)^2 \times (0.045)^2} + 100$$
$$= 1,046 \text{ psi}$$

This cushion pressure will generate a resistive load of

$$F_r = P_1 A_e = 1,046 \times 7.21$$
$$= 7,542 \text{ lbs.}$$

In order that the piston velocity can be decreased to zero over the 1.57 in. cushion length, the theoretical deceleration constant is

$$\alpha = \frac{v_i^2}{2X} = \frac{24^2}{2(1.57)} = 183 \text{ in/sec}^2$$

and the duration time is

$$t_c = \frac{v_i}{\alpha} = \frac{24}{183} = 0.13 \text{ sec.}$$

Assuming now a constant deceleration of  $183 \text{ in/sec}^2$ , a constant orifice constant, and a vertical load of 4,000 lbs, equation 4.18 will give the orifice area as a function of cushion travel  $X$  with an initial velocity  $v_i$

$$A_o = \left[ \frac{0.0316(7.21) [24^2 - 2(183X)]}{2(0.8)^2(4,660)(183 + 386)} \right]^{1/2}$$

$$= [0.0020 - 0.0013X]^{1/2}$$

The maximum cushion area will be  $A_o = 0.045 \text{ in}^2$  at the beginning of effective cushioning where  $X = 0$ .

The curve obtained by solving the above equation is shown in Figure 4.5 as theoretical curve, and it is compared to the actual curve obtained by the actual piston-cushion dimensions.

During an actual servojack cushion testing the acceleration and velocity profiles were recorded as shown in Figure 4.7 for a vertically installed jack with a dead weight of 3,600 lbs. The cylinder piston was driven into the lower cushion with a 20.5 in/sec velocity.

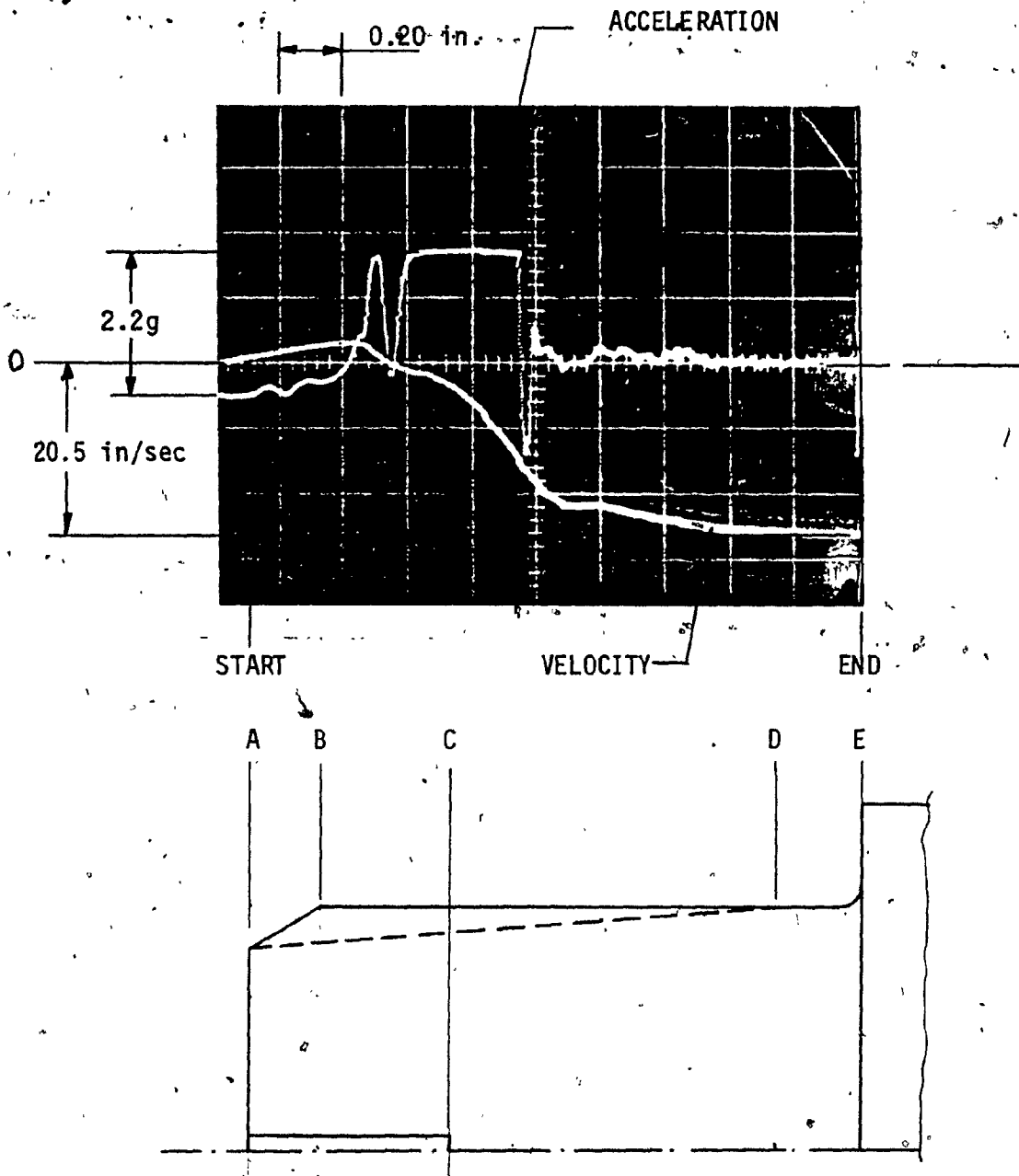


FIGURE 4.7

LOWER CUSHION ACCELERATION AND VELOCITY VS DISPLACEMENT  
AND CUSHION SPEAR PROFILE  
(3600 lbs load)

To obtain the above velocity the piston was accelerated downwards at 0.5g, and as it enters the cushion region after point B the acceleration changes to upwards for a total change of 2.2g. Most of the deceleration, thus velocity drop, occurred during approximately 1.00 in. travel.

The cushion force developed during deceleration can be calculated for a decelerated load of 3,950 lbs (which includes 350 lbs for piston assembly weight and oil column) at 2.2 g.

$$F_r = 3,950 \times 2.2 = 8,690 \text{ lbs} \quad (\text{theoretical } 7,542 \text{ lbs})$$

The cushion pressure is then

$$P_1 = \frac{F_r}{A_e} = \frac{8,690}{7.21} = 1,203 \text{ psi} \quad (\text{theoretical } 1,046 \text{ psi})$$

The actual cushioning time was measured to be 0.05 seconds compared to theoretical 0.13 seconds.

All recorded values for acceleration, pressure and force were higher than the expected ones, probably because of the actual shaping profile of the cushion orifice, and change in the value of the orifice constant coefficient.

The results showed the cushion pressure is still far below the system pressure of 1,500 psi and does not create any problems. However, it could be decreased by increasing the orifice area at the beginning of the stroke, thus providing a better distribution of the kinetic energy to be absorbed.

Examining the orifice area curves in Figure 4.5 it can be seen that

the theoretical and actual curves are quite close, however; the results showed much higher deceleration than the calculated one. The difference caused is most likely due to different loading, velocity, change in the orifice constant value and the actual cushion length.

The cushion must also be designed for a terminal velocity, so that sufficient flow area is available to come out of the cushion.

## 5. SERVO-VALVE CHARACTERISTICS

### 5.1 Introduction (References 10,11,12)

Specification and selection of a servo valve is one of the most important and difficult tasks in system design. It is the component that links the electrical and the hydraulic components of a system. The servovalve controls the dynamic response, rate capability and accuracy of the system. The type of servovalve to be discussed is the two stage type shown in Figure 5.1 .

The first stage is double nozzle flapper valve controlled by an electrical torque motor. The second stage is a 4-way spool valve whose output flow at a fixed valve pressure drop is proportional to spool displacement from null. Feedback of the second stage spool position is through a cantilevered feedback spring wire attached to the armature.

The servovalve is connected to system supply and return by ports on the mounting face of the servovalve. Supply pressure fluid is ported to the output spool where it is metered to the control ports and also applied through two fixed inlet orifices to the arrangement. The fluid pressure developed between the fixed and variable orifices exerts a force on both ends of the second stage spool. Depending on the differential pressure created by the variable orifices of the nozzle-flapper the second stage spool is displaced thus connecting the supply and return to the control ports.

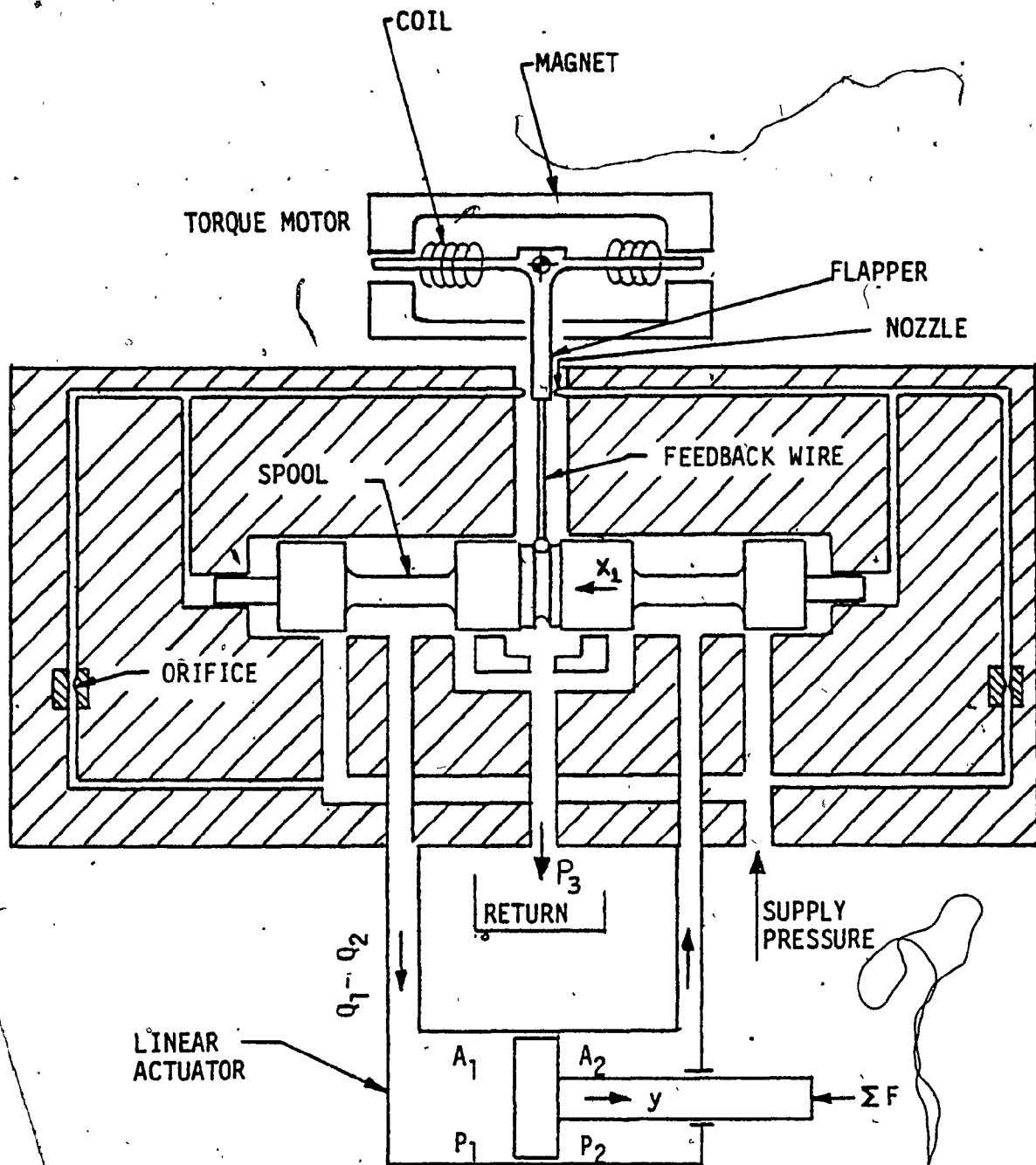


FIGURE 5.1 - TWO STAGE ELECTROHYDRAULIC SERVO VALVE

The output flow from the servovalve is proportional to the 2nd stage spool displacement and is expressed by

$$Q = C A_v \sqrt{2 \Delta P / \rho} \quad (5.1)$$

where  $Q$  = Output flow

$C$  = Discharge coefficient (.611)

$A_v$  = Uncovered slot area

$\Delta P$  = Valve pressure drop

$$= P_S - P_L - P_3 \quad (5.2)$$

$\rho$  = Mass density

Thus, servovalve control flow is proportional to the square root of the pressure drop across the valve. Since the first stage controls the second stage spool positions and since the flapper position is proportional to input current and control flow is expressed as

$$Q = K_v i \sqrt{\Delta P} \quad (5.3)$$

where  $Q$  = Output flow

$K_v$  = Valve sizing constant

$i$  = Input current

The plotted graph in Figure 5.2 shows the control flow versus input current relationship. The ideal or normal curve should be a straight line at zero load pressure. The normal curve consisting of two slopes are in the null region and the other in the normal flow region. The null region is that area of low input current where flow is affected by the relative spacing of spool edges and sleeve openings. Because of spool lap effects,



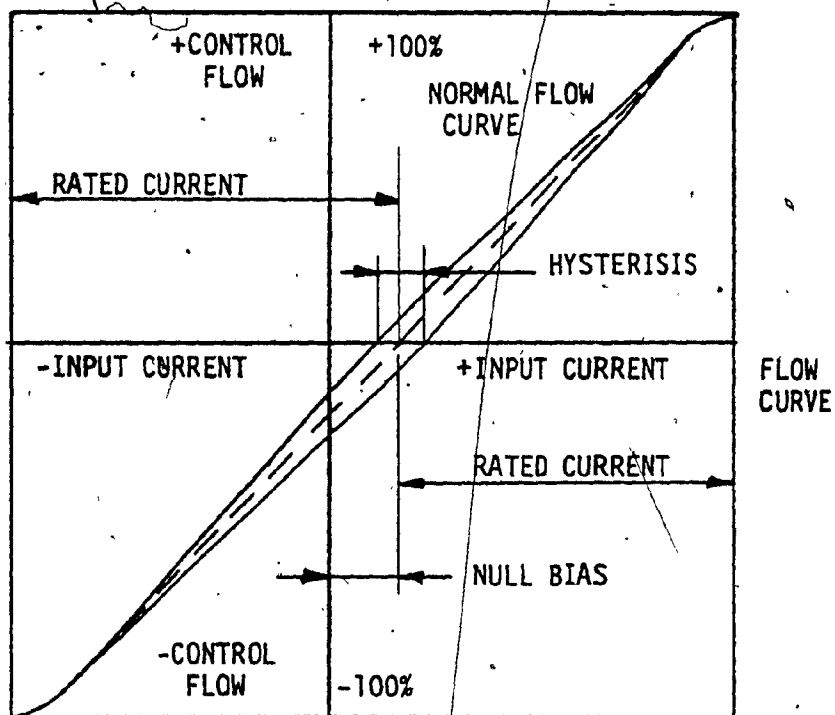


FIGURE 5.2 - SERVOVALVE FLOW-INPUT CURRENT RELATIONSHIP

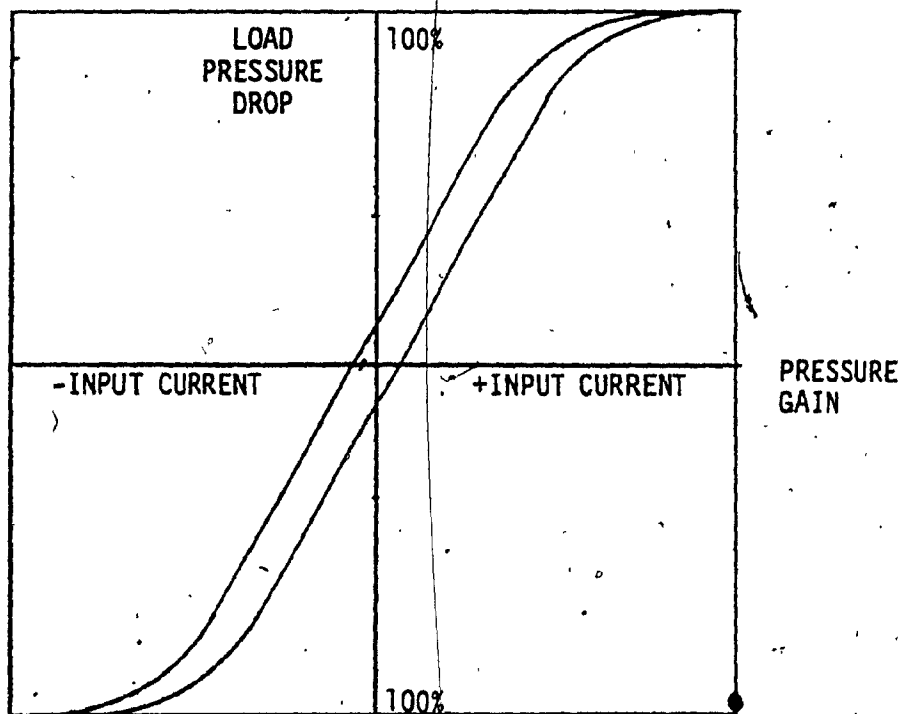


FIGURE 5.3 - SERVOVALVE PRESSURE-INPUT CURRENT RELATIONSHIP

flow gains in the two regions are not equal and can vary up to 200% of the normal flow gain.

The graph in Figure 5.3 shows the output pressure versus input current relationship. The curve is non-linear and the pressure gain slope is given between  $\pm 40\%$  of maximum pressure drop.

## 5.2 Types of Lap and Their Characteristics

The lap type of the second stage in a servovalve greatly influences the servovalve performance. Figure 5.4 presents a schematic diagram of a spool in relation to the output ports in the valve sleeve. There are three possible conditions:

- a) Zero Lap. In the null position the spool lands are exactly the same size and coincide with the supply and return pressure ports on the valve bushing. In this case, at null position, the flow is completely blocked. Any movement of the spool will result in instantaneous flow in the control ports. The flow gain in the null region is the same as in the normal region resulting in a linear flow curve.
- b) Overlap. Here the spool land width is greater than the bushing slot width. The result again is zero flow at null position. However, in this case, a finite amount of spool motion must occur before the bushing slots are uncovered and there is flow to the control port. Flow gain in null region is less than normal flow gain. The pressure gain in the overlap valve can be as high as in the zero-lap once the dead zone is traversed.

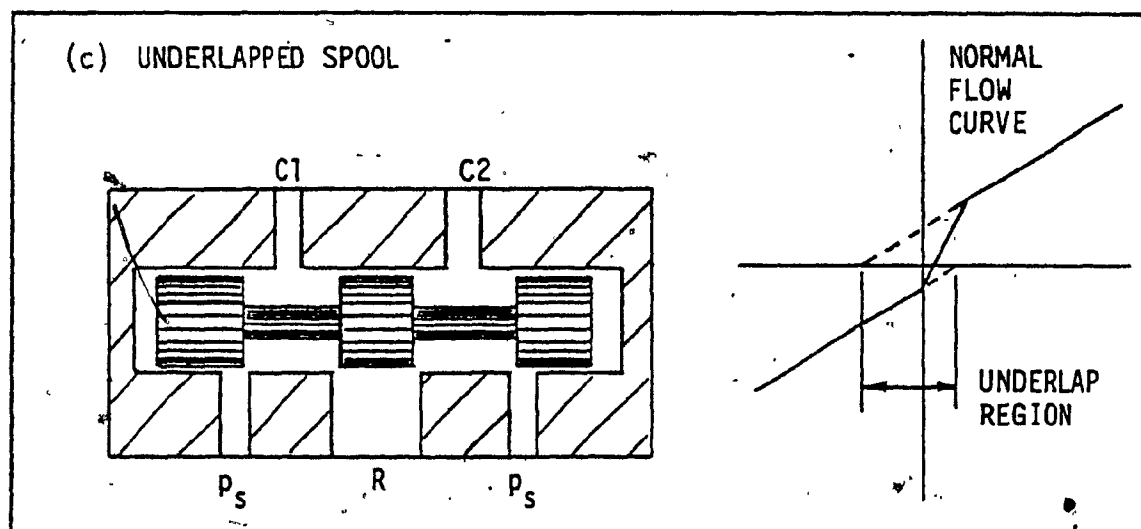
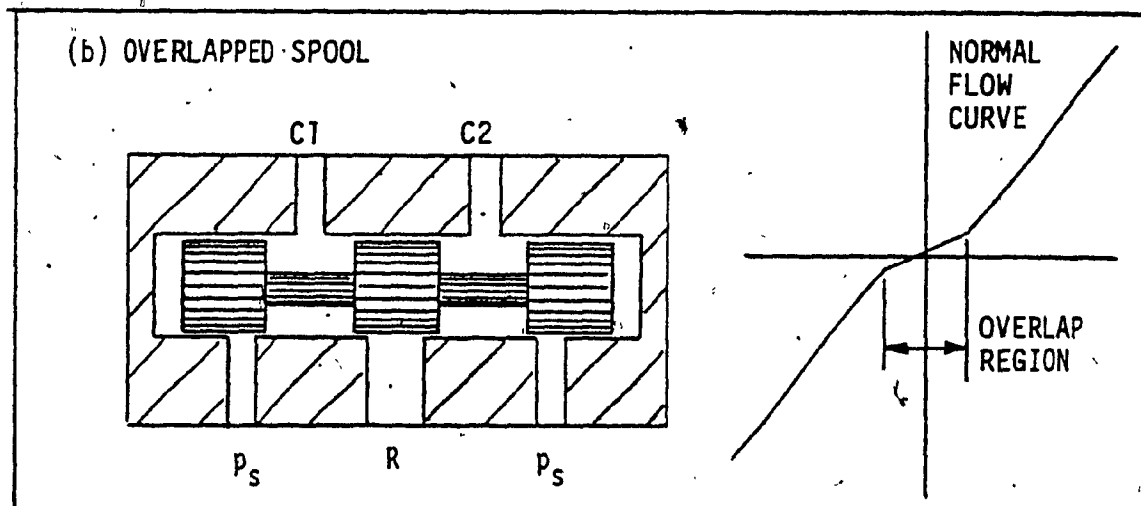
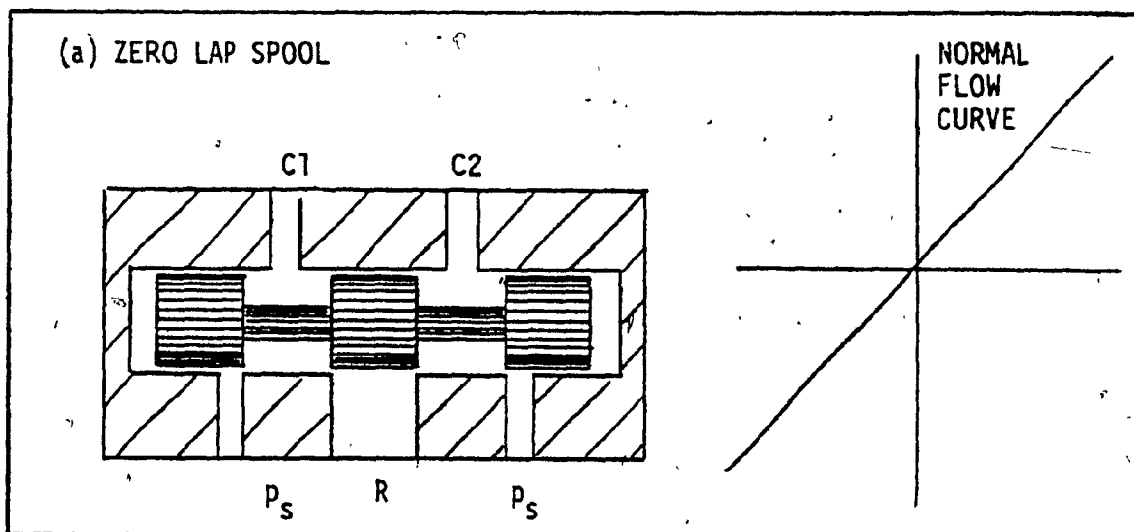


FIGURE 5.4 - TYPES OF SERVO VALVE SPOOLS AND FLOW CURVES.

- c) Underlap. In this case the spool land width is less than the bushing slot width. Under this condition, control, return and pressure ports are interconnected at null position acting as an open center valve. In an underlapped valve null, null flow gain is greater than the normal flow gain. The pressure gain in the null region is lower than the zero-lap valve, because the underlap produces intermediate pressure to the cylinder ports at null. Full system pressure is not developed in the control port until the leakage path to the return port is completely blocked.

### 5.3 Position Accuracy

Since in the most applications, one of the prime reasons for using an electro-hydraulic position servo is the ability to position a load precisely, position accuracy is an important characteristic to be considered. In the case of motion simulation position accuracy is not critical; however, the following parameters affect the position accuracy of a servovalve.

- a) Null Flow Gain. A servovalve operates most of the time around null position, where the error signal is close to zero. Thus, null flow gain affects position accuracy. A slightly underlapped valve with high flow gain is the most desirable from the standpoint of reducing positioning error. However, any disturbance (caused by shock vibration, acceleration electromagnetic disturbance of torque motor or noise in the command input) will generate a large flow increase to the actuator.

From a standpoint of accuracy the "ideal" valve has zero lap with linear flow throughout the null and normal region. Depending on the application, any of the three lap types can be used. An overlapped valve will have a dead zone in the null region which may not be acceptable in certain applications since it increases the steady state error of the system.

- b) Hysteresis. Hysteresis decreases position accuracy and is affected by temperature, fluid contamination, and electro-magnetic effects. For example a 50% drop in temperature may increase hysteresis by 25%. Contamination which increases internal friction also increases hysteresis. Magnetic effects can increase valve hysteresis and system position error.
- c) Null Bias. Null bias will directly introduce system error, and an error signal will be required to null out the valve. Null bias is affected by pressure fluctuation in supply pressure, and temperature fluctuations which cause differential expansion in the first stage torque motor.
- d) Threshold. Threshold contributes to increase in system position error and it is affected by fluid contamination, supply pressure, temperature and output spool lap. Due to very small clearances in the spool-bushing assembly, the presence of small particles will cause spool friction.

In a two stage valve, threshold depends on the force available to drive the second stage spool. For this reason supply pressure

affects threshold because the force available to drive the spool depends on the fluid pressure acting on the ends of the spool. Any significant decrease in supply fluid pressure will increase valve threshold. A change in temperature will change oil viscosity, which will increase threshold at lower temperatures. Spool lap can influence valve threshold. In an overlapped valve the presence of fluid contamination creates spool friction at null and the valve has a tendency to silt. An underlapped valve is more favourable since it has larger leak paths resulting in constant flow through the metering edges, thus avoiding increases in threshold. One way to improve servovalve threshold without altering the valve is to add dither to the input signal. Dither is low amplitude, high frequency signal superimposed on the input signal. The effect of dither is to move the output spool at low amplitude, high frequency. Thus apparent spool friction is decreased from breakaway friction to sliding friction.

- e) Pressure Gain. When a hydraulic system must position a load, load fluctuations or disturbances tend to alter the position of the load. Because the fluid is somewhat incompressible a valve with high pressure gain can cause the system to respond rapidly to such load disturbances and thus improve position accuracy under load fluctuations or disturbances. Pressure gain is affected by temperature, contamination and spool lap. Age is another factor which causes rounded edges of the spool and sleeves slots resulting in a decrease in pressure gain.

Pressure gain is higher for zero lap spools, but because of the difficulties involved in producing zero lap valve, the best practical condition for pressure gain is a minimum overlap servovalve. The underlap valve has lower pressure gain than the overlap and zero lap valves. But, since the flow gain at null position is an important criterion in determining system frequency response and stability, underlapped valve may be more desirable.

#### Trade Offs

In specifying servovalve characteristics it is understood that certain tradeoffs are involved according to the application. Overlap improves valve life because of lower wear and reduces energy demand by reducing valve null leakage. Moderate overlap also results in pressure gain higher than that of an underlapped valve, thus improving the frequency response and stability due to load fluctuations. However, overlap can increase positioning error due to dead zone. Valve susceptibility to contamination is increased in an overlapped valve since it causes silting and results in system instability. Underlap on the other hand, improves dynamic response at small amplitudes and decreases contamination sensitivity of a valve, because fluid is continually permitted to flush the leakage paths. Valve underlap increases leakage flow, which is undesirable when energy supply is limited.

In addition, system performance is degraded at large amplitudes. For stability system gain must be set at null, where the valve's contribution to damping is low and gain is high. As a result, system gain decreases and performance suffers. High leakage flow is desirable from the standpoint of frequency response and contamination. High leakage permits the use of looser tolerances and manufacturing costs decrease. However, the disadvantages of high leakage in a valve are: shorter life, performance degradation due to erosion wear, reduced pressure gain and increased energy consumption.



#### 5.4 Servo valve Important Parameters

Some of the most important parameters which have to be considered after specifying the valve size are:

- a) Frequency Response. The servo valve dynamic response can be expressed for comparative purposes by the frequency at which the servo valve phase is  $90^{\circ}$ . The dynamic response in the frequency range to the  $90^{\circ}$  phase lag and below can be approximated by a second order transfer function with a damping ratio between 0.5 to 0.7. The frequency response of a typical servo valve is shown in Figure 5.5. The servo valve frequency response will vary with the input signal amplitude, supply pressure, temperature and internal valve parameters. Response measured with  $\pm 20\%$  peak-to-peak sinusoidal input signal and 1,000 psi supply pressure is used as a standard for comparative purposes. Servo valve response will improve with higher supply pressure. For closed loop control, in order to have high performance the servo valve  $90^{\circ}$  phase point should exceed the load resonant frequency by at least a factor of two. The load resonant frequency is usually determined by the load mass and the fluid compliance. The average load resonant frequency of the hydrostatic actuator is approximately 9 Hz at neutral position.
- b) Stability. The stability of a linear system depends on the characteristics of the system. The degree of stability can be determined from an analysis of either the transient behaviour or the response to sinusoidal inputs.

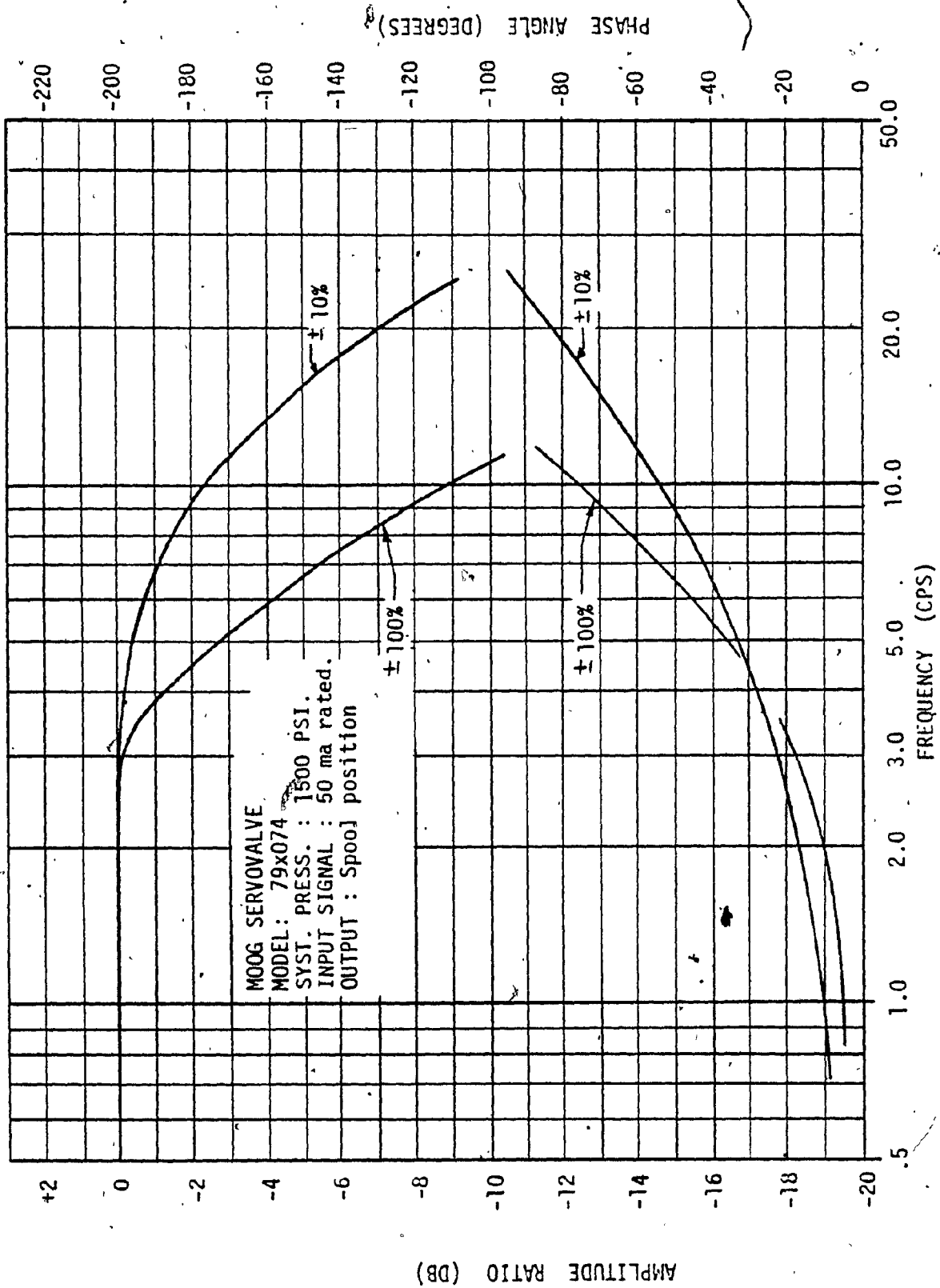


FIGURE 5.5 SERVOVALVE DYNAMIC RESPONSE

Since the servovalve is approximated by a second order system, its stability depends on the system damping ratio. The damping ratio depends on the fluid viscosity, which is also affected by the fluid temperature.

The system stability can also be affected by the servovalve spool configuration, since flow gain at null position is an important criterion in determining frequency response and stability.

- c) Reversal Bump. Reversal bump in many motion systems when the platform slows down, stops, and changes direction. Previous studies have shown that the causes of reversal bump or turn-around are friction in the jack, overlap in the servovalve and mismatched flow in the servovalve due to differential piston areas. All the above causes can be reduced or eliminated by introducing the hydrostatic bearing servojack with asymmetrically ported critically lapped servovalve.
- d) Noise. Coulomb friction in servovalve spool produces acceleration noise. The level of acceleration noise indicates the motion system smoothness and it is different in each degree of freedom.
- e) Audible Noise. It is important that there should be no audible noise in the simulator cockpit, produced by the hydraulic fluid throttling in the servovalve during operation at the required acceleration movements.

### 5.5 Servo Valve Asymmetry

Symmetric cylinders controlled by symmetrically ported valves do not cause complications. But in the case of a hydraulic servojack where an asymmetric cylinder is used, a symmetric valve is not ideal. Problems will be noticed, even at no load condition, around any zero velocity point. As the direction of velocity changes, pressure jumps are caused due to the differential piston area.

For accurate and smooth control the incompatibility of a symmetric valve and an asymmetric cylinder has been proven by test. In order to avoid discontinuities and ensure smooth operation, an asymmetric servovalve should be used, having port-openings proportional to the corresponding piston areas.

Figure 5.6 shows an asymmetrical cylinder controlled by a 4-way valve. The implication of an asymmetrical 4-way zero lap valve is

$$\frac{a_1}{A_1} = \frac{a_3}{A_2} \quad \text{and} \quad \frac{a_2}{A_1} = \frac{a_4}{A_2}$$

With a piston area ratio of 2.04 the valve orifice area rating will be  $a_1 = 1$   $a_3 = \frac{1}{2.04} = 0.49$

with  $a_1 = a_2$   $a_3 = a_4$

More detailed study on the valve-cylinder symmetry is found in Reference 6.

The standard rating of a servovalve is given for a symmetrical valve. The relative rating for an asymmetric valve is given as a percentage of the symmetric valve rating.

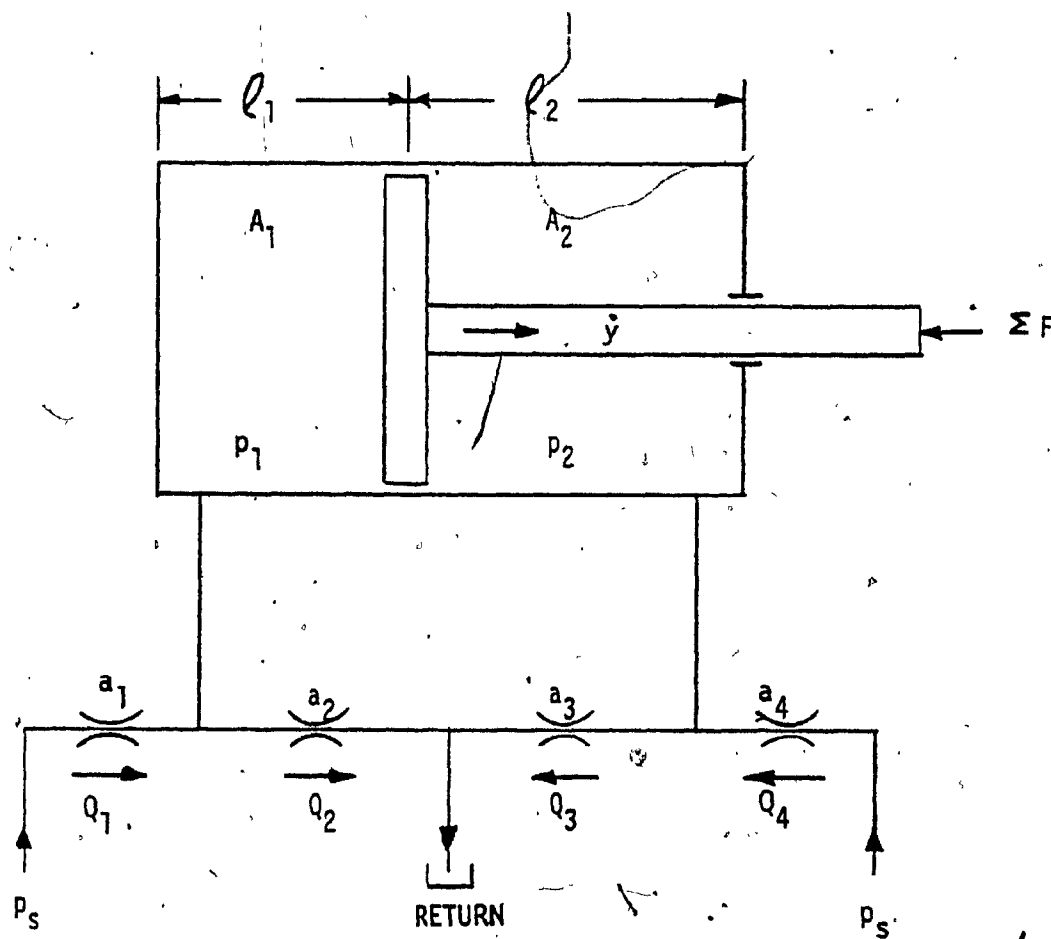


FIGURE 5.6 - ASYMMETRIC CYLINDER WITH 4-WAY VALVE

For a symmetric valve  $a_1 = a_2 = a_3 = a_4 = 1$ ,  
and considering that orifices  $a_1$  and  $a_3$  are in series, the net  
orifice area coefficient is given by

$$A_{\text{net-sym.}} = \sqrt{\frac{a_1^2 a_3^2}{a_1^2 + a_3^2}} = \sqrt{\frac{1}{1+1}} = 0.71$$

For an asymmetrical servovalve  $a_1 = a_2 = 1$  and  $a_3 = a_4 = 0.49$ .  
Considering again that orifices  $a_1$  and  $a_3$  are in series the net  
area coefficient is:

$$A_{\text{net-assym.}} = \sqrt{\frac{a_1^2 a_3^2}{a_1^2 + a_3^2}} = \sqrt{\frac{1 \times 0.24}{1 + 0.24}} = 0.44$$

Then the rated flow of the asymmetric valve is

$$Q_{\text{rated}} = \frac{0.44}{0.71} = 0.62 \text{ or } 62\% \text{ of the symmetric valve flow.}$$

## 5.6 Servo Valve Evaluation

Due to the system design requirements, standard servo valves were not satisfactory and custom made valves were required.

A number of servo valves by two manufacturers were compared on the test stand and on the motion system.

All valves were asymmetric, and matched to the jack area ratio. Slight variations in underlap and valve dynamics were compared with 60, 80 and 100 GPM valves. The valves were compared on the basis of open loop frequency response, and acceleration noise level at constant velocity, for a range of velocities from a very low to maximum. Finally, two valves, one Moog 100 GPM and one Pegasus 80 GPM have been selected for comparison on a complete motion system.

Considering the parameters discussed in Section 5.4, the specifications and comparison of the two selected valves are shown in Table 5.1.

The Model 1282 Pegasus valve provides good dynamic response, negligible threshold and good turnaround bump performance. Actuator velocity versus servo valve current was quite linear up to 80 GPM, with slight increase in gain at the extremes. Threshold was significant (3 to 4%) and it was apparent on small amplitude operation. Noise level was considered acceptable.

The model 79-074 Moog valve originally provided non-linear actuator velocity versus servo valve input current and poorer dynamic response than the Pegasus valve. Threshold was negligible and noise was higher. Later improvements by Moog brought its

performance to equal that of the Pegasus valve.

Figure 5.5 shows the dynamic response of the 79-074 Moog valve. Dynamic response of the Pegasus valve is similar with slightly higher gain.

Comparison for acceleration noise is shown in Figure 5.7 for both valves. Noise on Moog valve at maximum velocity is double of that of Pegasus valve. Reversal bump noise is not included in this graph.

The actuator velocity versus servovalve input current relationships for both valves are shown in Figs. 5.8 and 5.9. These figures were obtained from a valve static test with a maximum input current of 4 mA which is 10% of the full range current. The actuator velocity is proportional to the hydraulic fluid flow, and 0.10 m/sec is proportional to 10 gpm. Figures 5.8 and 5.9 are thus, similar to Figure 5.2.

This servovalve evaluation has shown that both valves perform equally, and they are interchangeable with the difference of an adaptor plate required for Moog valve (due to larger port size) and driving circuit (due to electrical specifications as shown in Table 5.1).

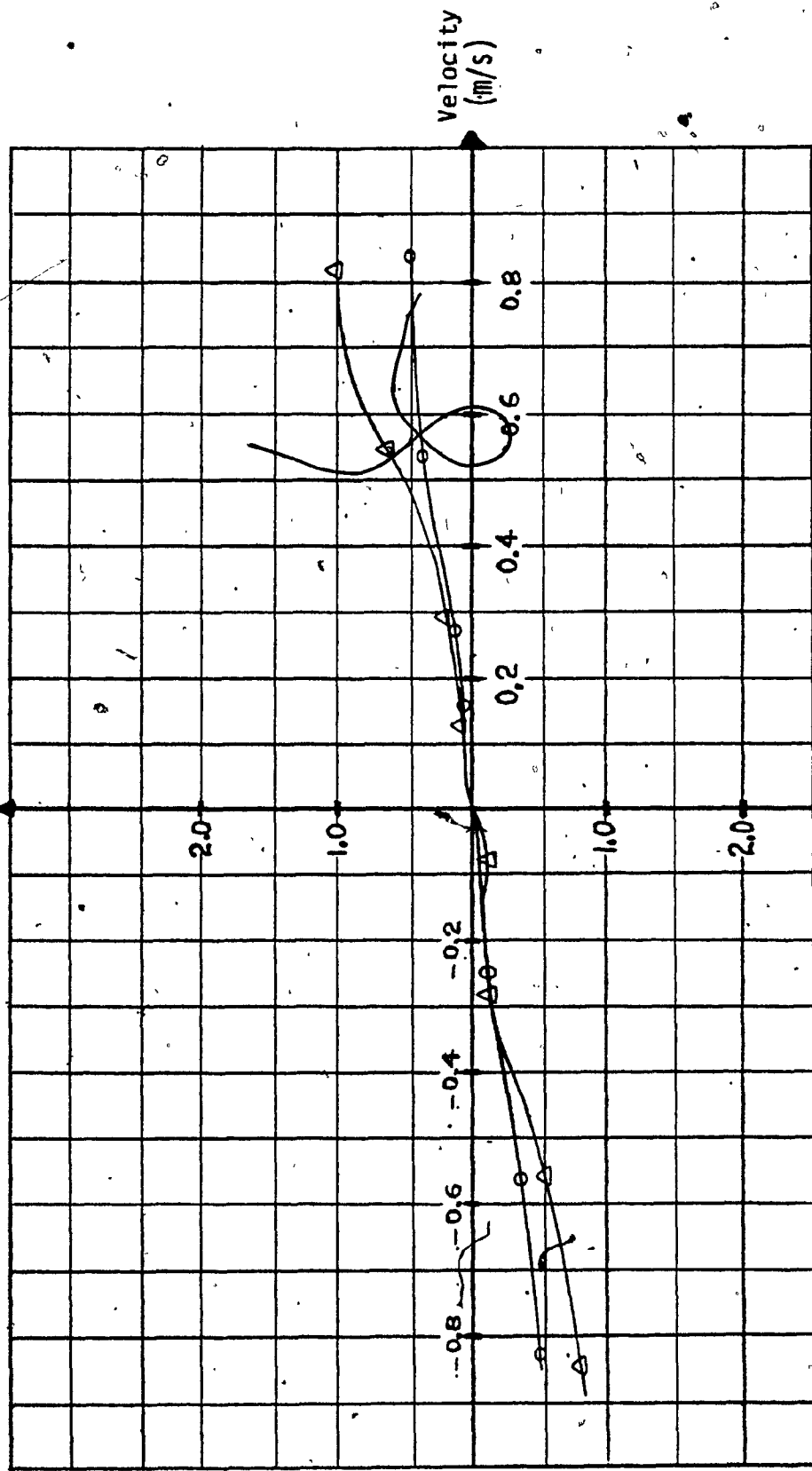


TABLE 5.1

SERVOVALVE SPECIFICATION COMPARISON

<u>PERFORMANCE PARAMETER</u>	<u>MOOG 79-074</u>	<u>PEGASUS 1282 A</u>
Actuator Area Ratio	2.04:1	2.04:1
Spool Lap	0 - 0.2% U.L.	0.1 - 0.4% U.L.
Hysteresis	3%	3%
Resolution	1%	0.5%
Rated Flow @ 1000 psid	63 gpm $\pm$ 10%	84 gpm $\pm$ 5%
Rated Current	50 ma	40 ma
Coil Resistance	320 ohms	285 ohms
Coil Inductance	20 Henries	20 Henries

Noise Acceleration  
Peak to Peak (m/s<sup>2</sup>)



△ Moog 79-074  
○ Pegasus 1282A

FIGURE 5.7- NOISE ACCELERATION

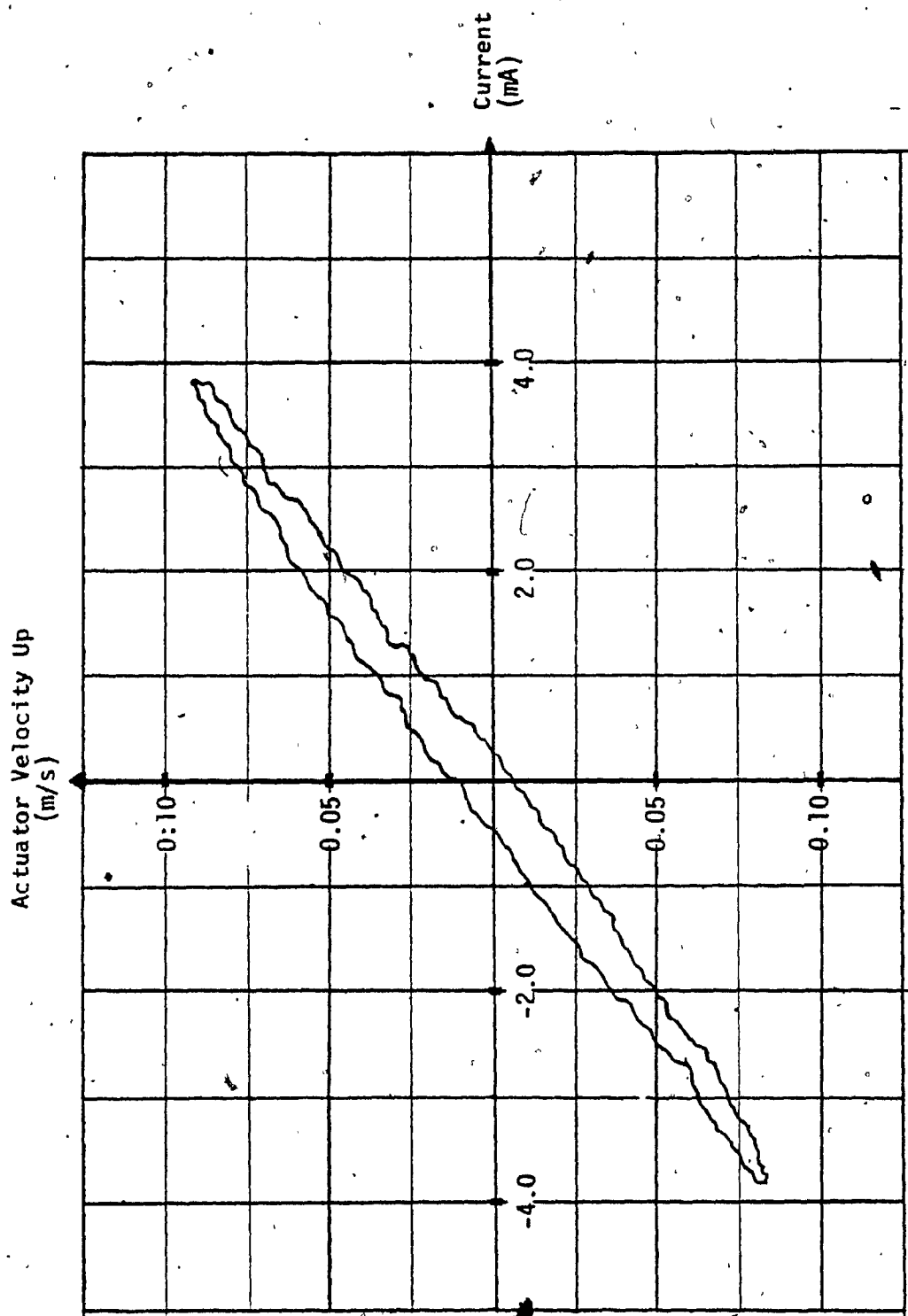


FIGURE 5.8

ACTUATOR VELOCITY-SERVOVALVE INPUT CURRENT RELATIONSHIP  
STATIC TEST AT 10% OF FULL RANGE (MOOG 79-074)

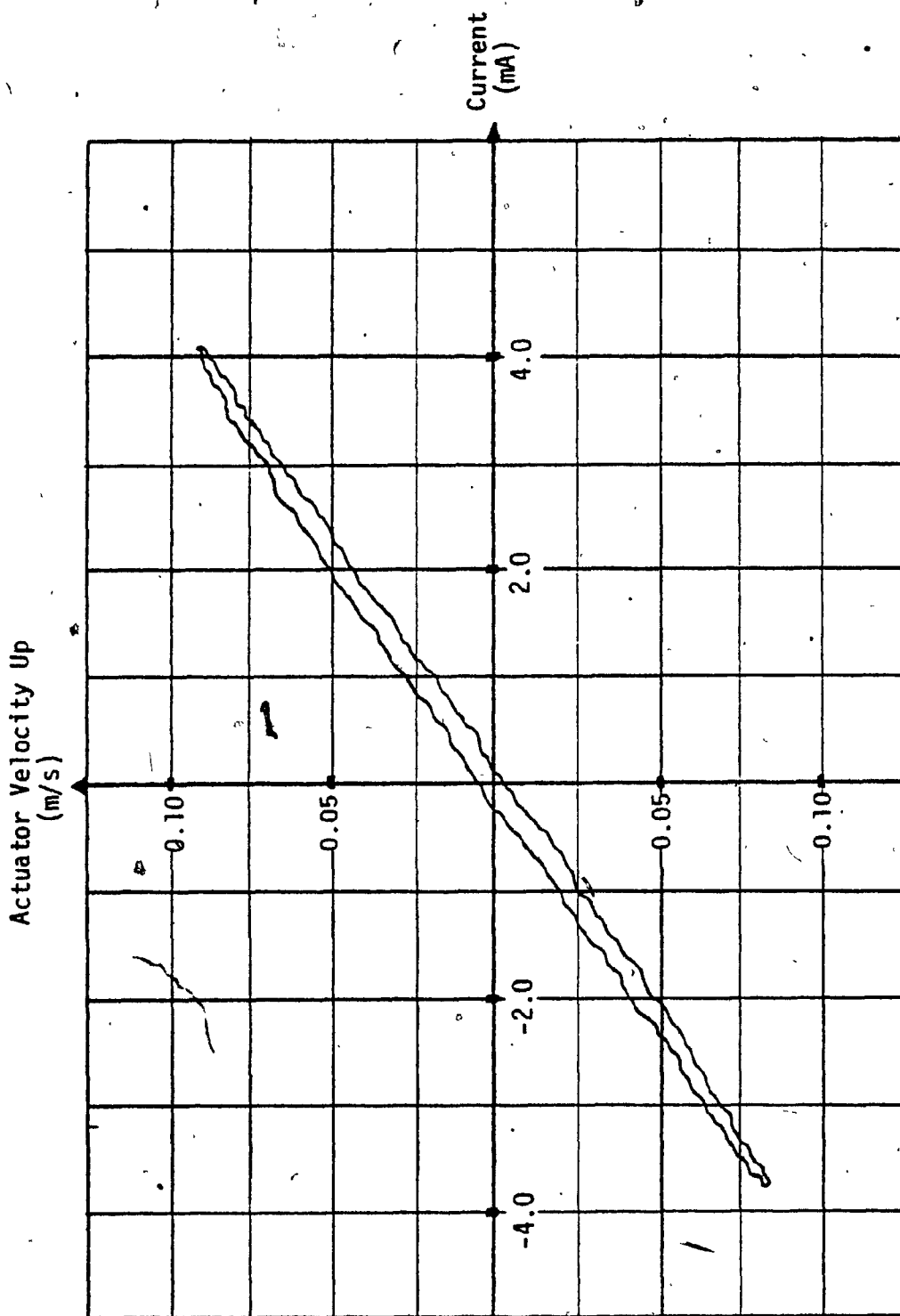


FIGURE 5.9

ACTUATOR VELOCITY-SERVOVALVE INPUT CURRENT RELATIONSHIP  
STATIC TEST AT 10% OF FULL RANGE (PEGASUS 1282A)

## 6. SERVO JACK CONTROL

### 6.1 Mathematical Model

Considering a hydraulic asymmetric actuator controlled by an asymmetric 4-way zero-lapped valve (Fig. 5.6), and using the theory in Ref. 6, the following relationships are obtained:

$$P_1 A_1 - P_2 A_2 = \Sigma F = F_e + M \ddot{y} + B \dot{y} \quad (6.1)$$

$$\dot{y} = \frac{a_1}{A_1} C \sqrt{2 \frac{P_s - P_1}{\rho}} - \frac{a_2}{A_1} C \sqrt{2 \frac{P_1}{\rho}} - \frac{\ell_1}{\beta} \dot{P}_1 \quad (6.2)$$

$$\dot{y} = \frac{a_3}{A_2} C \sqrt{2 \frac{P_2}{\rho}} - \frac{a_4}{A_2} C \sqrt{2 \frac{P_s - P_2}{\rho}} + \frac{\ell_2}{\beta} \dot{P}_2 \quad (6.3)$$

where the symbols are defined in Nomenclature and in Figure 5.6.

The above equations can be rearranged as follows:

$$\dot{y} = \frac{b_1}{A_1} C \sqrt{\frac{P_s}{\rho}} \left[ x_1 \sqrt{1 - \frac{|x_1|}{x_1} \cdot \frac{P_L}{P_s}} \right] - \frac{\ell}{2\beta} \dot{P}_L \quad (6.4)$$

$$\text{or } \dot{y} \approx \frac{b_1}{A_1} C \sqrt{\frac{P_s}{\rho}} \left[ x_1 - \frac{x_1}{2P_s} \cdot P_L \right] - \frac{\ell}{2\beta} \dot{P}_L \quad (6.5)$$

By introducing parameters  $K_v$ ,  $c_h$ , and  $c_o$ , for velocity gain, hydraulic stiffness and oil stiffness,

$$K_v = \frac{b_1}{A_1} C \sqrt{\frac{P_s}{\rho}} \quad (6.6)$$

$$c_h = \frac{A_1 + A_2}{|x_1|} P_s \quad (6.7)$$

$$c_o = \frac{A_1^2 \beta}{A_1 \ell_1 + V_1} + \frac{A_2^2 \beta}{A_2 \ell_2 + V_2} \quad (6.8)$$

Equation 6.5 becomes

$$\dot{y} = K_v \left[ x_1 - \frac{\Sigma F'}{c_h} \right] - \frac{\Sigma \dot{F}}{c_o} \quad (6.9)$$

where  $\Sigma F' = \Sigma F - 0.5(A_1 - A_2) P_s$

Equation 6.9 is represented by the block diagram in Figure 6.1 where the servovalve transfer function is

$$\frac{x_1}{\epsilon} = K_s G_s(s) \quad (6.11)$$

Substituting Equation 6.11 into 6.9 and after laborious calculations the following differential equation is formed:

$$\frac{\ddot{y}}{w_o^2} + 2 \frac{\dot{y}}{w_o} + y = K'_v \left( G_s \epsilon - \frac{\Sigma F}{C_h} \right) - \frac{\Sigma F}{C_o} \quad (6.12)$$

$$\text{where } w_o = \sqrt{\frac{C_o}{M}} = \text{Undamped natural frequency} \quad (6.13)$$

$$\zeta = \frac{K'_v C_o}{2 w_o C_h} = \text{Relative damping} \quad (6.14)$$

$$K'_v = K_s K_v = \text{Velocity gain} \quad (6.15)$$

$$C_o = c_o = \text{Oil spring stiffness} \quad (6.16)$$

$$C_h = K_s c_h = \text{Hydraulic stiffness} \quad (6.17)$$

Equation 6.12 is represented by the block diagram in Figure 6.2.

The systems shown in Figures 6.1 and 6.2 are theoretically linear, according to the linear differential equations. However, in reality they are not, because none of the parameters is truly constant.

For example, oil spring stiffness,  $C_o$ , varies considerably with piston position as indicated by Equation 6.8 and Section 2.3.3.

Thus analysis on a linear model holds only for small perturbations about one position.

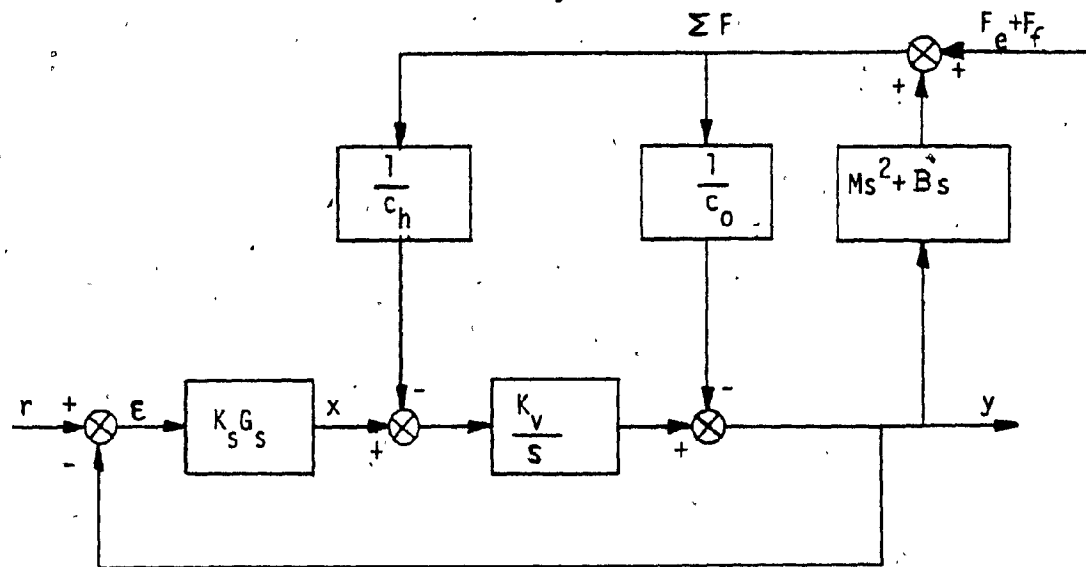


FIGURE 6.1 BLOCK DIAGRAM OF HYDRAULIC SERVO "PHYSICAL MODEL"

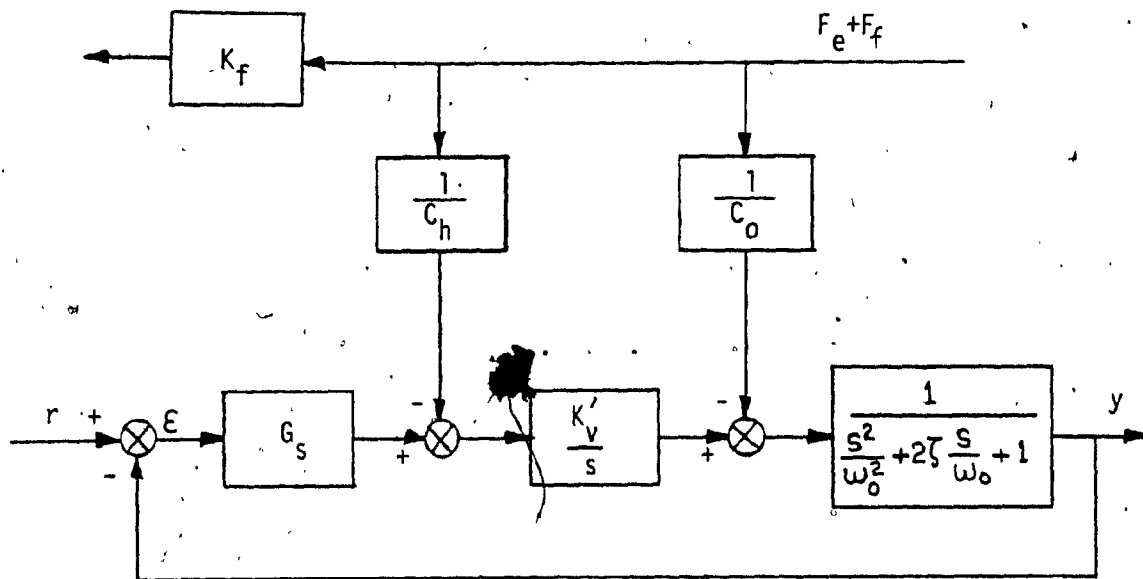


FIGURE 6.2 BLOCK DIGRAM OF HYDRAULIC SERVO "CONTROL MODEL"

Hydraulic stiffness,  $C_h$ , also, changes drastically from an underlapped valve ( $|x_1| < U$ ), to a zero lap where

$$C_h = \infty \quad x_1 = 0.$$

In the application of the hydrostatic servojack the Coulomb friction  $F_f$ , and the viscous friction  $B\dot{y}$  will be neglected, since the design of hydrostatic bearings have almost eliminated friction (to less than 1.0% of load capacity).

Velocity gain  $K'_V$  is frequency dependent, since the servovalve is also frequency dependent, and the valve-actuator system can be represented by the following transfer function

$$\frac{K'_V}{s} = \frac{K_V}{s \left[ \frac{1}{\frac{s^2}{\omega_{OV}^2} + 2\zeta_V \frac{s}{\omega_{OV}} + 1} \right]} \quad (6.18)$$

where  $K_V$  = Velocity gain of servovalve and actuator, and from servovalve data the typical values for

$$\omega_{OV} \text{ and } \zeta_V \text{ are } \omega_{OV} = 35 \text{ Hz and } \zeta_V = 0.9$$

In order to have a system that will act as a pure integrator with a large load variation and large frequency domain, compensation is required for the load effects from the mass and external forces, as well as the servovalve lag.

Figure 6.3 shows a modified block diagram that includes compensation for oil stiffness, hydraulic stiffness and servovalve lag.

The compensating functions are defined as follows:



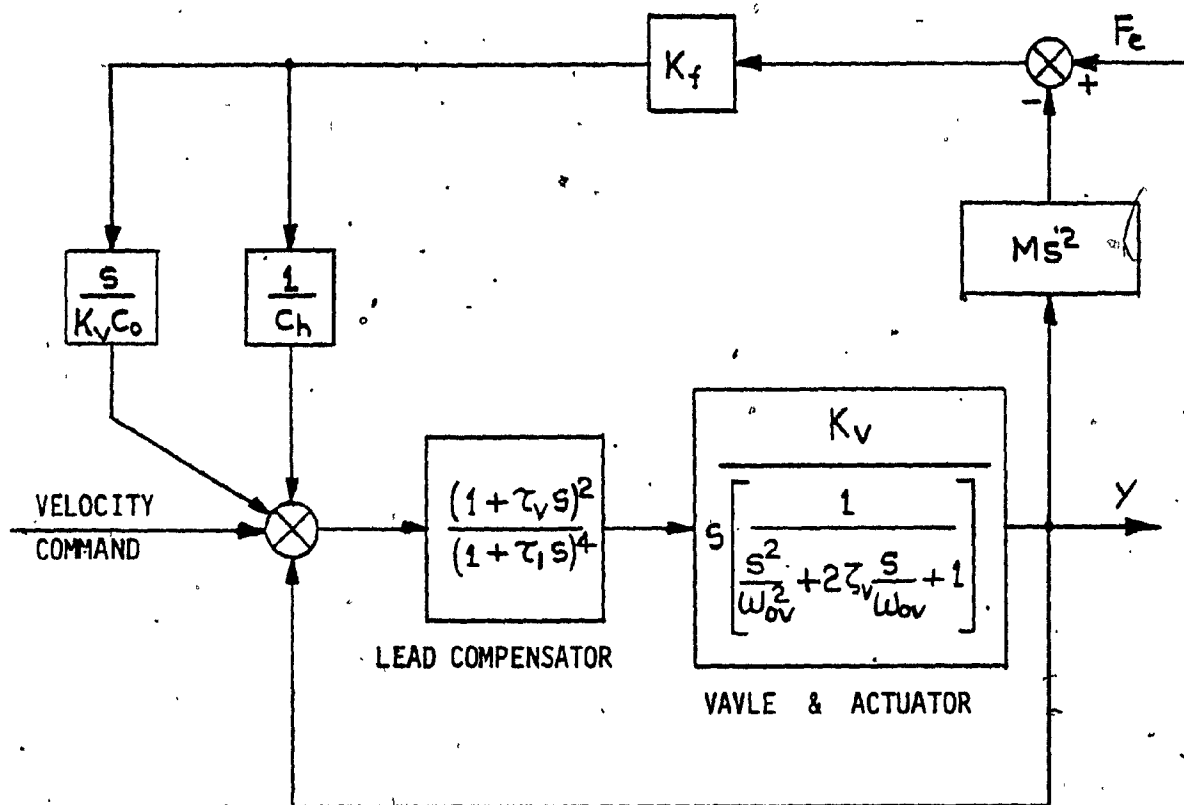


**FIGURE 6.3 MODIFIED BLOCK DIAGRAM OF SERVO-LOOP**

$$H_{C1} = \frac{s}{K_V C_0} \quad (6.19)$$

$$H_{C2} = \frac{1}{C_h} \quad (6.20)$$

$$H_{C3} = \frac{(1 + \tau_v s)^2}{(1 + \tau_l s)^4} \quad (6.21)$$

Where  $\tau_v = 5 \text{ ms}$  and  $\tau_l = 0.5 \text{ ms}$ .

## 6.2 Damping Methods

The Relative damping coefficient  $\zeta$  in Equation 6.14 is

$$\zeta = \frac{K_v C_o}{2\omega_o C_h} \text{ and including the viscous friction becomes}$$
$$\zeta = \left[ \frac{K_v}{2\omega_o} \cdot \frac{C_o}{C_h} \right] + \frac{B}{2M\omega_o} \quad (6.22)$$

The desirable value of  $\zeta$  is 0.3 to 0.7. As the two components of  $\zeta$  are proportional to the ratio of oil spring stiffness to hydraulic stiffness  $C_o/C_h$ , and the viscous friction coefficient  $B$  respectively, one of the factors or both must be present.

However, it is desirable to have a low  $C_o/C_h$  to produce a small load sensitivity at low frequencies. Thus, an excellent damping method depends almost completely on the viscous friction coefficient  $B$ .

The damping coefficient in the hydrostatic bearing design (where Coulomb friction is eliminated) can be as low as

$\zeta = 0.05$ . If insufficient viscous friction is present,

Equation 6.22 suggests increasing the ratio  $C_o/C_h$  in order to obtain sufficient damping, but this will decrease the load stiffness and valve gain. The oil stiffness  $C_o$ , which is proportional to the piston area, has to ensure both load capacity and bandwidth. The hydraulic stiffness  $C_h$ , which is proportional to  $P_s \cdot A/U$ , then has to be decreased in order to increase damping.

A direct method to increase damping is to introduce an under-lapped valve, at the expense of larger fluid flow required.

Pressure feedback is another important damping method, which provides an extra servovalve spool displacement  $x$ , proportional to the load pressure. Pressure feedback has the disadvantage of increased load sensitivity, but this could be avoided by introducing dynamic pressure feedback which has a transfer function

$$H_m = K_p \left[ \frac{\tau s}{\tau s + 1} \right] \quad (6.23)$$

At low frequencies  $H_m = 0$  and the load stiffness is not affected. At higher frequencies  $B, w_0, C_o/C_h$  has no effect, and  $H_m = K_p$  providing adequate damping if  $1/\tau \ll w_0$  or  $w_0 \gg 1$ .

A very elegant damping method and most attractive for electro-hydraulic systems is the use of acceleration feedback. Simple feedbacks can be achieved using transient velocity feedback and shaping networks in conjunction with the servo amplifier. This method has the disadvantage of being less sensitive to structural noise which might be picked up by the accelerometer.

Feedback shaping can be used to greater effect, especially in closing the loop around the valve, torque motor and amplifier. This gives much greater control of the valve position which is effectively equivalent to output velocity.

In the present hydrostatic servojack motion system in order to increase damping  $\zeta$ , the viscous damping  $B$ , was increased by using higher viscosity hydraulic fluid. The viscosity of the oil used is 46 centistokes at 40°C.

### 6.3 Load compensation

The valve-actuator system shown in Figure 5.6 acts as an integrator with a velocity (flow) input and a displacement output. The flow input is a function of the servovalve spool displacement  $x$  (see Figure 5.1), producing an actuator piston displacement  $y$ .

If an external force  $\Sigma F$  is applied in the opposite direction of piston displacement  $y$ , the pressure  $P_1$  will be increased. Consequently, the pressure drop  $P_s - P_1$  will be decreased and the flow into cylinder  $Q_1 - Q_2$  will also be decreased. This effect is introducing a load error  $\Sigma F/c_h$ , where,  $c_h$  (Hydraulic Stiffness) changes drastically from an open center valve to a closed center valve ( $c_h = \infty$  at  $x = 0$ ).

On the other hand, the load  $\Sigma F$  applied on the piston will compress the oil column by a small deflection depending on the fluid compressibility. This effect now introduces another load error  $\Sigma F/c_o$ , where  $c_o$  (Oil Spring Stiffness) depends on piston position and the bulk modulus of fluid,  $\beta$ .

Both of the above load errors are shown in block diagram in Figure 6.1. The piston velocity is given by the equation

$$\dot{y} = K_v \left[ \dot{x}_1 - \frac{\Sigma F}{c_h} \right] - \frac{\Sigma F}{c_o} \quad (6.24)$$

where  $c_h = \frac{A_1 + A_2}{|x_1|} p_s$

$$c_o = \frac{A_1^2 \beta}{A_1 l_1 + V_1} + \frac{A_2^2 \beta}{A_2 l_2 + V_2}$$

$$K_v = \frac{b_1}{A_1} c \sqrt{\frac{p_s}{\rho}}$$

The objective is to have a system that will act as a pure integrator

$$y = K_v x_1$$

with a constant velocity gain,  $K_v = \frac{\partial y}{\partial x}$

In order to have a pure integrating system, compensation is required to eliminate the terms  $\Sigma F/c_h$  and  $\Sigma F/c_o$ . The ideal system implies infinite hydraulic and oil stiffness, but since these terms are dependent on the cylinder dimensions, increasing the cylinder diameter and reducing its stroke is almost impractical in most cases, when performance motions have to be met.

#### 6.4 Effects of Coulomb Friction and Damping.

Dynamic analysis and the adjustment of control action is based mainly on frequency response. A non-linear analysis is required due to the presence of the Coulomb friction, but, practice has shown that Coulomb friction only slightly affects the adjustment of the control gain and the stability of the system in some applications. However, even though Coulomb friction can be neglected in some applications, in other cases it may deteriorate the system completely with respect to special specifications such as accuracy (due to dead zone) bandwidth (due to dynamic dead zone) or slip stick motion (due to acceleration disturbances caused by irregular friction behaviour (Ref. 6).

Besides load compensation the only other remedy to overcome these effects is the elimination of Coulomb friction completely by introducing hydrostatic bearings.

From frequency response analysis of a hydraulic servo system it is known that velocity gain is limited by the system natural frequency and the damping ratio. Satisfactory responses are obtained with a damping ratio of 0.3 to 0.7. Low damping results in a nervous step response while higher damping slows down step response and the bandwidth decreases rapidly. A hydraulic control system with an adequate damping coefficient between 0.3 and 0.7 and a well adjusted velocity gain shows a bandwidth limited by the valve natural frequency.

Damping on the other hand depends completely on the viscous friction coefficient which is almost impossible to predict beforehand. In most cases, viscous friction is neglected, but is present all the time along with Coulomb friction.

In the hydrostatic bearing design where the Coulomb friction is eliminated the damping coefficient is very low (as low as .05). In this case, in order to increase damping the hydraulic stiffness must be reduced. This can be obtained by the introduction of open center or underlapped valves. Another method to reduce hydraulic stiffness is to introduce a leakage flow with a cross port bleed.



## 6.5 Preliminary Design Performance

The design of linear servo actuator deals with the determination of the piston area  $A_1$ , stroke  $S$ , valve capacity  $Q_{\max}$  and supply pressure  $P_s$  for actuating of mass  $M$ . Certain specifications such as maximum speed  $\dot{y}_{\max}$ , maximum acceleration  $\ddot{y}_{\max}$  and required bandwidth or speed of response are determined to meet the system requirements.

This section will show the relations between the specification and design data for a sinusoidally actuated linear actuator, loaded by inertia forces and a constant preload. A performance diagram will show some fundamental relations in a frequency diagram.

Performance calculations will be obtained for an asymmetric actuator controlled by an asymmetric 4-way zero-lapped valve.

Specifications of the system to be designed are:

Load mass,  $M = 7.81 \text{ lb-sec}^2/\text{in}$  (3,000 lbs load)

Piston cap end area  $A_1 = 9.62 \text{ in}^2$

Piston rod end area  $A_2 = 4.71 \text{ in}^2$

Asymmetric servovalve flow  $Q_{\max} = 60 \text{ U.S. GPM} = 231 \text{ in}^3/\text{sec}$

Supply pressure  $P_s = 1,500 \text{ psi}$

Maximum actuator stroke  $S = 52.0 \text{ in.}$  (1.32 m)

Calculations: (Ref. 6)

a) Maximum actuator velocity upward.

$$\dot{y}_{\max} = \frac{Q_{\max}}{A_1} = \frac{231}{9.62} = 24.0 \text{ in/sec} \quad (0.60 \text{ m/sec})$$

$$\hat{y}_{\max} = \frac{S}{2} = \frac{52}{2} = 26 \text{ in.} \quad (0.65 \text{ m})$$

In order to remain within the linear behaviour of the valve, it will be assumed that only 66.6 % of the supplied pressure  $P_s$  is available for dynamic generation.

- b) Relation between valve capacity and maximum speed  $\dot{y}_{\max}$  for full amplitude sinusoidal movements.

$$\begin{aligned} Q_{\max} &= A_1 \dot{y}_{\max} = A_1 \hat{y}_{\max} \gg A_1 \omega y \\ \omega_1 &= \frac{Q_{\max}}{A_1 y_{\max}} = \frac{\hat{y}_{\max}}{\hat{y}_{\max}} \\ &= \frac{24.0}{26.0} = 0.93 \text{ rad/sec} = 0.15 \text{ Hz} \end{aligned} \quad (6.25)$$

- c) Relation between cavitation boundary and maximum acceleration  $\ddot{y}_{\max}$ . The load pressure is given by

$$P_L = \frac{\sum F}{A_1} = \frac{M \ddot{y} + F_{st}}{A_1} \quad (6.26)$$

To avoid cavitation  $P_L \leq 0.66 P_s$ , then at sinusoidal movements with  $F_{st} = 0$

$$\begin{aligned} P_L &= \frac{M \ddot{y}_{\max} + F_{st}}{A_1} = \frac{M \omega^2 \hat{y}}{A_1} \leq 0.66 P_s \\ \text{or } \omega_2 &= \frac{0.66 P_s A_1^2}{M Q_{\max}} \\ &= \frac{0.66 \times 1,500 \times (9.62)^2}{7.81 \times 231} = 50.8 \text{ rad/sec} = 8.1 \text{ Hz} \end{aligned} \quad (6.27)$$

- d) Relation between maximum stroke and bandwidth.

For a well designed servo system the obtainable bandwidth  $\omega_b$  roughly equals the natural frequency  $\omega_0$  caused by the oil spring with stiffness  $C_0$  and the moving mass  $M$ .

For an open loop transfer function

$$H(s) = \frac{K_v}{s \left[ \frac{s^2}{w_0^2} + 2\zeta \frac{s}{w_0} + 1 \right]} \quad (6.28)$$

where proper choice of  $K_v$  enables  $w_b = w_0$ , with values of  $\zeta$  between 0.3 and 0.7, and

$$\begin{aligned} w_0 &= \sqrt{\frac{C_0}{M}} \\ C_0 &\gg \frac{4A_1\beta}{s} = \frac{2A_1}{\hat{y}_{\max}} \\ w_3 = w_0 &\approx w_b = \sqrt{\frac{2A_1\beta}{M \hat{y}_{\max}}} \end{aligned} \quad (6.29)$$

with Oil Bulk Modulus of  $\beta = 145,000$  psi

$$w_3 = \left[ \frac{2 \times 9.62 \times 145,000}{7.81 \times 26} \right]^{1/2} = 116.3 \text{ rad/sec} = 18.5 \text{ Hz}$$

e) The maximum acceleration is given by

$$\hat{\ddot{y}}_{\max} = \frac{0.66 P_s A_1}{M} \quad (6.30)$$

$$= \frac{0.66 \times 1,500 \times 9.62}{7.81}$$

$$= 1,220 \text{ in/sec}^2 \quad (31 \text{ m/sec}^2) = 3.16g's$$

with the jack vertically installed

$$\hat{\ddot{y}}_{\max} = 1,220 - 384 = 836 \text{ in/sec}^2 \quad (21 \text{ m/sec}^2)$$

f) Actuator force

$$\begin{aligned}\text{Maximum upward } F_{up} &= P_s A_1 \\ &= 1,500 \times 9.62 \\ &= 14,430 \text{ lbs}\end{aligned}$$

$$\begin{aligned}\text{Maximum downward } F_d &= P_s A_2 \\ &= 1,500 \times 4.71 \\ &= 7,065 \text{ lbs}\end{aligned}$$

g) Preliminary Performance Diagram.

Figure 6.4 shows the performance of the servo-actuator when excited by a sinusoidal signal. The diagram shows the maximum displacement, maximum velocity, maximum acceleration, and the bandwidth values, obtained by the preceding calculations.

The units used in the diagram of Figure 6.4 are in MKS system.

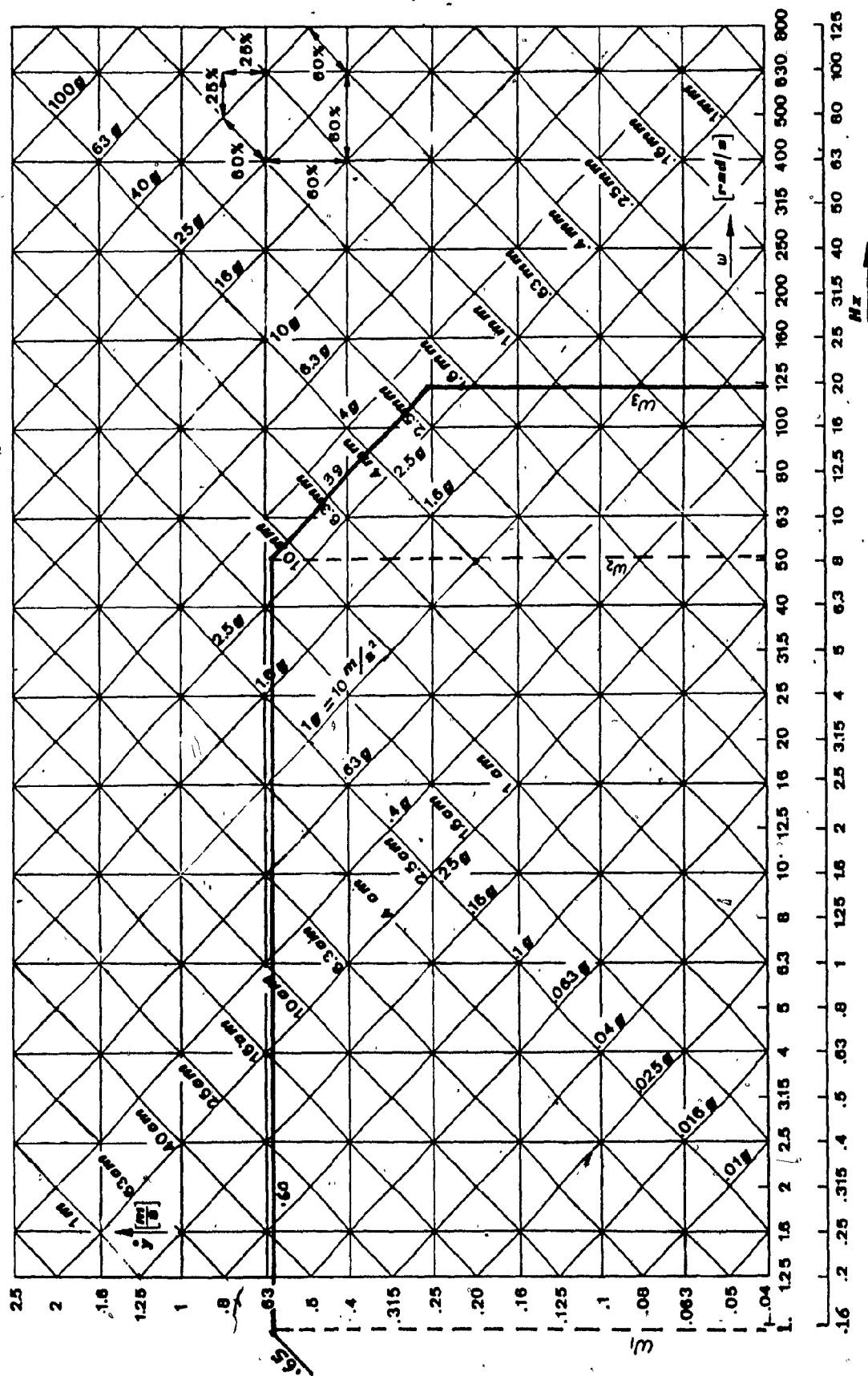


FIGURE 6.4 - PERFORMANCE DIAGRAM

## 6.6 Cue Generation and Wash-out

The basis for wash-out acceleration is a constant wash-out acceleration based upon available and allowable velocity as a function of position. In this way, it is possible to have an efficient use of the available stroke. Assuming that the series 500 actuator will have

$$\dot{y}_{\max} = 23.6, 31.5, 39.4 \text{ in/sec } (0.6, 0.8, 1.0 \text{ m/sec})$$

(depending on the servovalve used)

$$y_{\max} = \pm 23.6 \text{ in. } (0.6 \text{ m})$$

$$a_w = 7.9, 19.7 \text{ in/sec}^2 (0.2, 0.5 \text{ m/sec}^2)$$

Several conditions can be determined, i.e.:

- a) Given  $a_w$ , what is the maximum velocity at a given position to permit the actuator to come to a standstill at maximum stroke with a constant wash-out acceleration  $a_w$ ?

The maximum velocity as a function of acceleration and distance is given by:

$$\dot{y}_{\max} = \sqrt{2 a_w y} \quad (6.30)$$

The graph obtained from above equation is shown in Figure 6.5.

If assumed that the wash-out should be possible with  $a_w = 19.7 \text{ in/sec}^2 (0.5 \text{ m/sec}^2)$ , without a system velocity restriction over at least half the total stroke it can be concluded that  $\dot{y}_{\max} \geq 30.7 \text{ in/sec } (0.78 \text{ m/sec})$

- b) Starting at mid position with a positive (up) step acceleration cue, what is the maximum permissible duration of that cue to obtain  $\dot{y}_{\max}$ ? The maximum velocity is given as a function of acceleration and time, by

$$\dot{y}_{\max} = a \cdot t_a \quad (6.31)$$

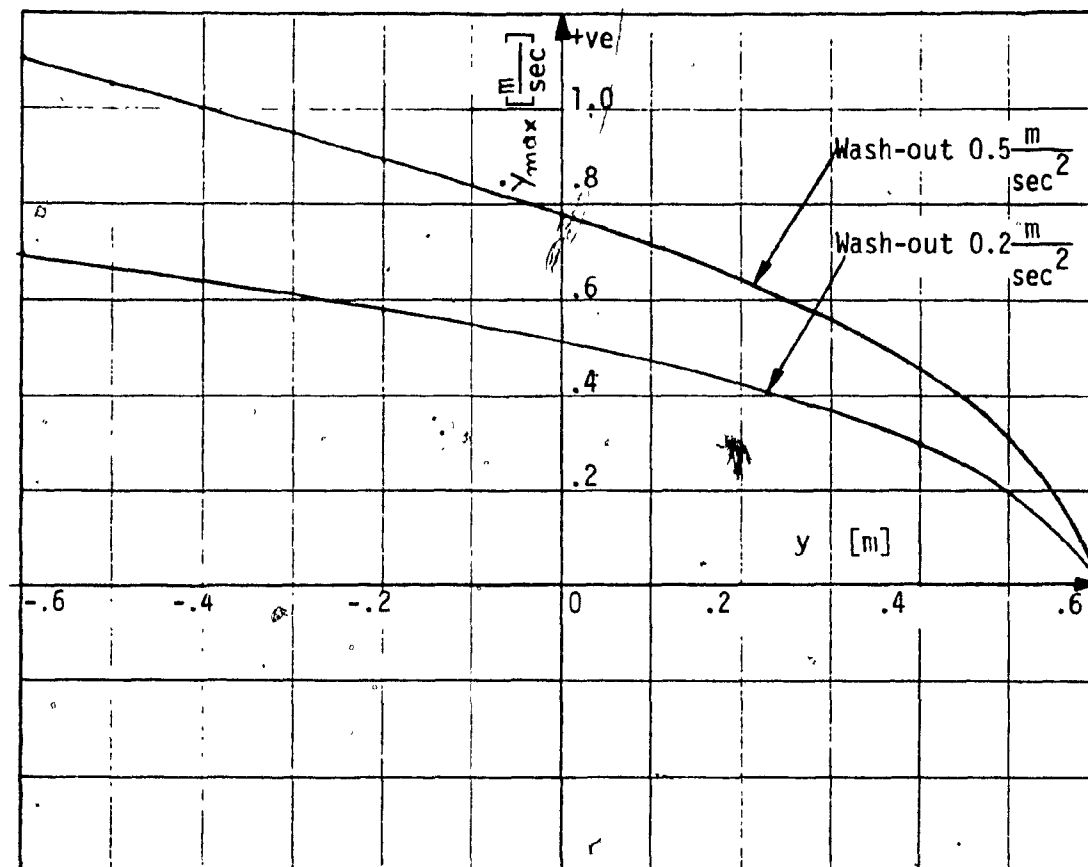


FIGURE 6.5 RELATIONSHIP BETWEEN VELOCITY, DISPLACEMENT AND WASH-OUT

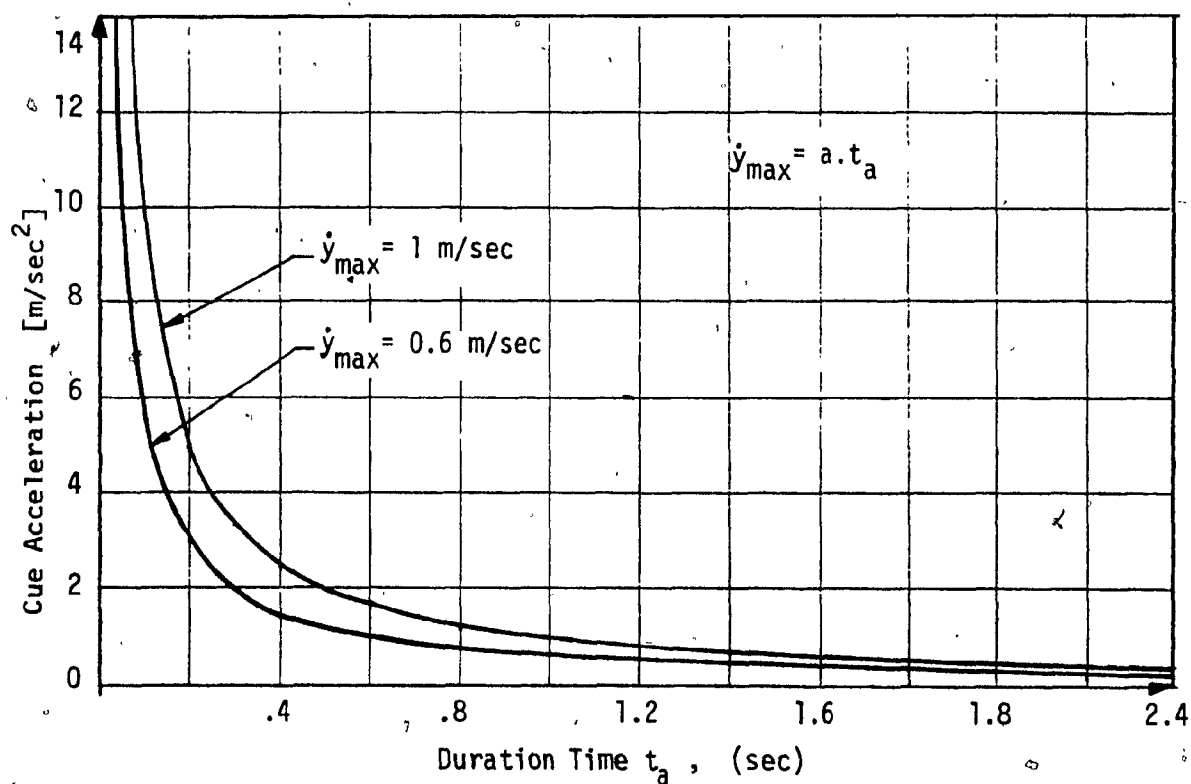


FIGURE 6.6 RELATIONSHIP BETWEEN VELOCITY, CUE ACCELERATION AND DURATION TIME

Figure 6.6, obtained by Equation 6.31 shows the combination of acceleration and duration time to obtain maximum actuator velocity.

- c) Given  $a_w = 19.7 \text{ in/sec}^2$  ( $0.5 \text{ m/sec}^2$ ). Starting at mid-position with a positive step acceleration cue, what is the maximum permissible duration of that cue to obtain by means of the wash-out acceleration?

The cue duration time is given by

$$t_a^2 = \frac{2 a_w y}{a^2 + a \cdot a_w} \quad (6.32)$$

where  $t_a$  = Maximum cue duration time, sec

$a_w$  = Wash-out acceleration,  $\text{in/sec}^2$ , ( $\text{m/sec}^2$ )

$a$  = Cue acceleration,  $\text{in/sec}^2$ , ( $\text{m/sec}^2$ )

$y$  = Total actuator stroke, in., (m)

Given in Figure 6.7 is the cue duration time versus cue amplitude.

If velocity is limited to  $23.6 \text{ in/sec}$  ( $0.6 \text{ m/sec}$ ) this limit will enter before acceleration cue takes over. Figure 6.8 shows the relationship between cue acceleration and travel during cue acceleration.

To summarize the results from the obtained graphs, the following example may be used:

Assume: A step input acceleration cue,  $a = 236.0 \text{ in/sec}^2$  ( $8.0 \text{ m/sec}^2$ )

A wash-out acceleration,  $a_w = 19.7 \text{ in/sec}^2$  ( $0.5 \text{ m/sec}^2$ )

Maximum actuator velocity,  $\dot{y}_{\max} = 23.6 \text{ in/sec}$  ( $0.6 \text{ m/sec}$ )

Maximum actuator travel,  $y_{\max} = \pm 23.6 \text{ in.}$  ( $0.6 \text{ m}$ )

From Figures 6.7 and 6.8 we obtain

Acceleration cue duration time,  $t_a = 0.1 \text{ sec}$

Displacement duration cue,  $y = 1.56 \text{ in.}$  ( $0.04 \text{ m}$ )



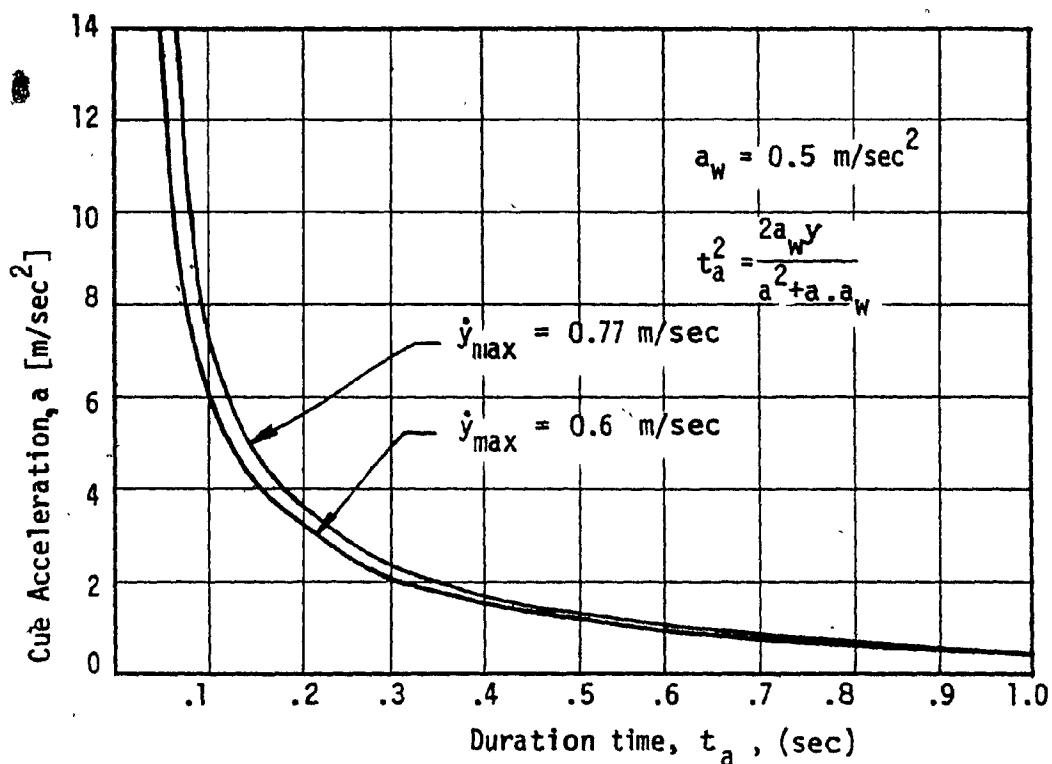


FIGURE 6.7 RELATIONSHIP BETWEEN VELOCITY, CUE ACCELERATION, DURATION TIME AND WASHOUT ACCELERATION

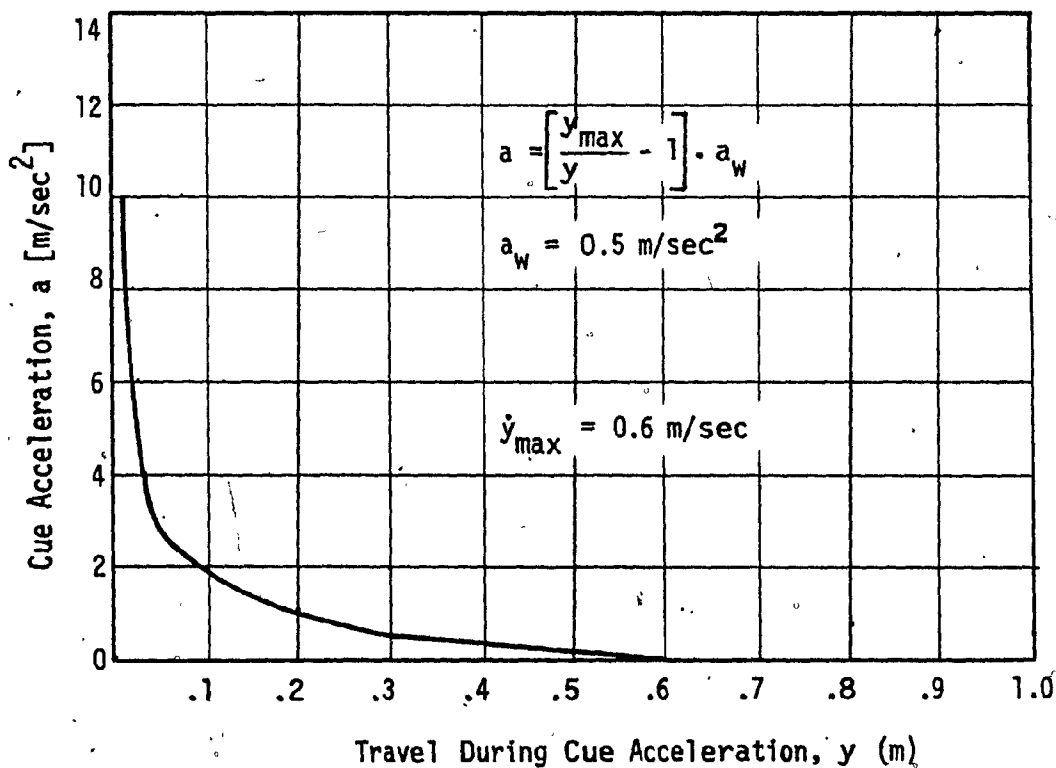


FIGURE 6.8 RELATIONSHIP BETWEEN VELOCITY, CUE ACCELERATION, AND TRAVEL DURING CUE ACCELERATION

## 6.7 Servo Jack Control Block Diagram

A simplified block diagram of the servo jack control is shown in Figure 6.9. This diagram shows only the major components, which are directly related to this study. In order to eliminate digital noise at velocities above 20 Hz, 5th order elliptical filters are installed in the analog computer outputs.

### Forward Path

The command signal is an acceleration or position input. The required velocity obtained after integrating the required velocity is added to the forward acceleration compensation. The need for the forward acceleration is to compensate for frequencies higher than 1 Hz. The sum of the above signals, through a lead compensator, is fed into the current amplifier, and then into the servo valve torque motor. The servovalve output is flow into either end of the hydraulic cylinder. The lead compensator is required to compensate for the servo valve lag. The output of the cylinder is position, velocity, and acceleration, as required.

### Feedback Paths

Feedback paths are required in a closed loop system because they provide:

- a) Increased accuracy, the ability to faithfully reproduce the input signal.
- b) Reduced sensitivity of the ratio of output to input to variations of system characteristics.
- c) Reduced effects of non-linearities and distortion.
- d) Increased bandwidth, for the range of frequencies (of the input) over which the system will respond satisfactorily.



The feedback paths and their functions from block diagram in Figure 6.9 are the following:

- a) Velocity Feedback. The actual velocity is compared to the required velocity and the difference (error) is fed back through a velocity error compensator. Velocity feedback is a form of damping, but its effect on the natural frequency harmonic of the load and actuator is limited. A signal which is strong enough to reduce the harmonics will give too much lag at lower frequencies. However, if another feature is introduced to deal with the harmonic, e.g. orifice bleed, then velocity feedback will enable the gain to be increased and a decrease in dead zone will be achieved. Actual velocity is obtained through differentiation of the actual position measured from the position transducer in the servojack.
- b) Force Feedback. The force feedback is used to compensate for load errors due to external loads, the oil compressibility, and hydraulic stiffness. The computed force is measured by two pressure transducers on each side of the piston and it is compared with the actual force measured from a force transducer (mounted between the piston rod and the load). The difference between the computed and actual forces is the friction. The force feedback is composed of two paths. One path is used for compensation of the oil compressibility  $C_o$ , and it has a minus sign. The other path is used for compensation of the hydraulic stiffness  $C_h$ . The actual force on this path is compared to the valve design load and the error is multiplied with the required velocity at the specified design load.

- c) Position feedback. The actual position measured by the position transducer is compared to the required position and the error is processed to provide a valve command signal. Another path that is added to the position is the required velocity feedback through a velocity damping potentiometer. This setting counts for the second order system damping ratio.
- d) Current feedback. This feedback is used in the servovalve inner loop to provide stability.

#### Drive System

The control parameter for a motion system is the acceleration of the actuator, thus an Acceleration Servo System (ASS) should be used.

The command signal may be either acceleration or position. In Figure 6.9 the actuator is considered as a pure integrator, the input of which is a velocity command and the output is position.

The acceleration servo implements low position gain for steady state stability and a wide bandwidth for acceleration cues. The position servo system has a bandwidth limited to 0.5 Hz. The acceleration noise resulting from the digital-to-analog conversion must be kept below the assumed human perception level of 0.02 g.

In recent study (Reference 13) it was shown that a position servo system with a 1 Hz bandwidth is suitable for motion simulation.

The acceleration transfer function beyond that frequency is greatly deteriorated, if only the position loop is used.

This can be improved by adding an acceleration signal. However,

adding only an acceleration to the acceleration summing point gives an undesirable notch at 0.95 Hz. This is shown in Fig. 6.10, which was produced for a second order system, whose transfer function is:

$$H(s) = \frac{\text{Pos. out.}}{\text{Pos. in.}} = \frac{1}{\left[ \frac{s^2}{10K_2} + K_1s + 1 \right]} \quad (6.33)$$

The transfer function is derived from the block diagram in Figure 6.9. The acceleration transfer function is identical to position transfer function.

A 2nd-order position system has the following normalized transfer function

$$H(s) = \frac{1}{\left[ \frac{s^2}{\omega_0^2} + 2\zeta \frac{s}{\omega_0} + 1 \right]} \quad (6.34)$$

where Natural frequency,  $\omega_0 = 10K_2$

$$\text{Relative damping, } \zeta = \frac{K_1 \cdot 10 K_2}{2}$$

The position servo system has three adjustable constants:

$K_1$  = Position loop damping

$K_2$  = Position loop gain

$K_3$  = Feed forward velocity correction term

Figure 6.10 was produced from software with term  $K_3 = 0$  (see block diagram in Figure 6.9). To compensate for this notch, a velocity term has to be added and therefore the constant  $K_3$  was set to the same value as  $K_1$ . With no elliptic filters at the computer signal output, the acceleration output over acceleration input is forced to unity for the full frequency range, with frequency limitations only in the computer programming.

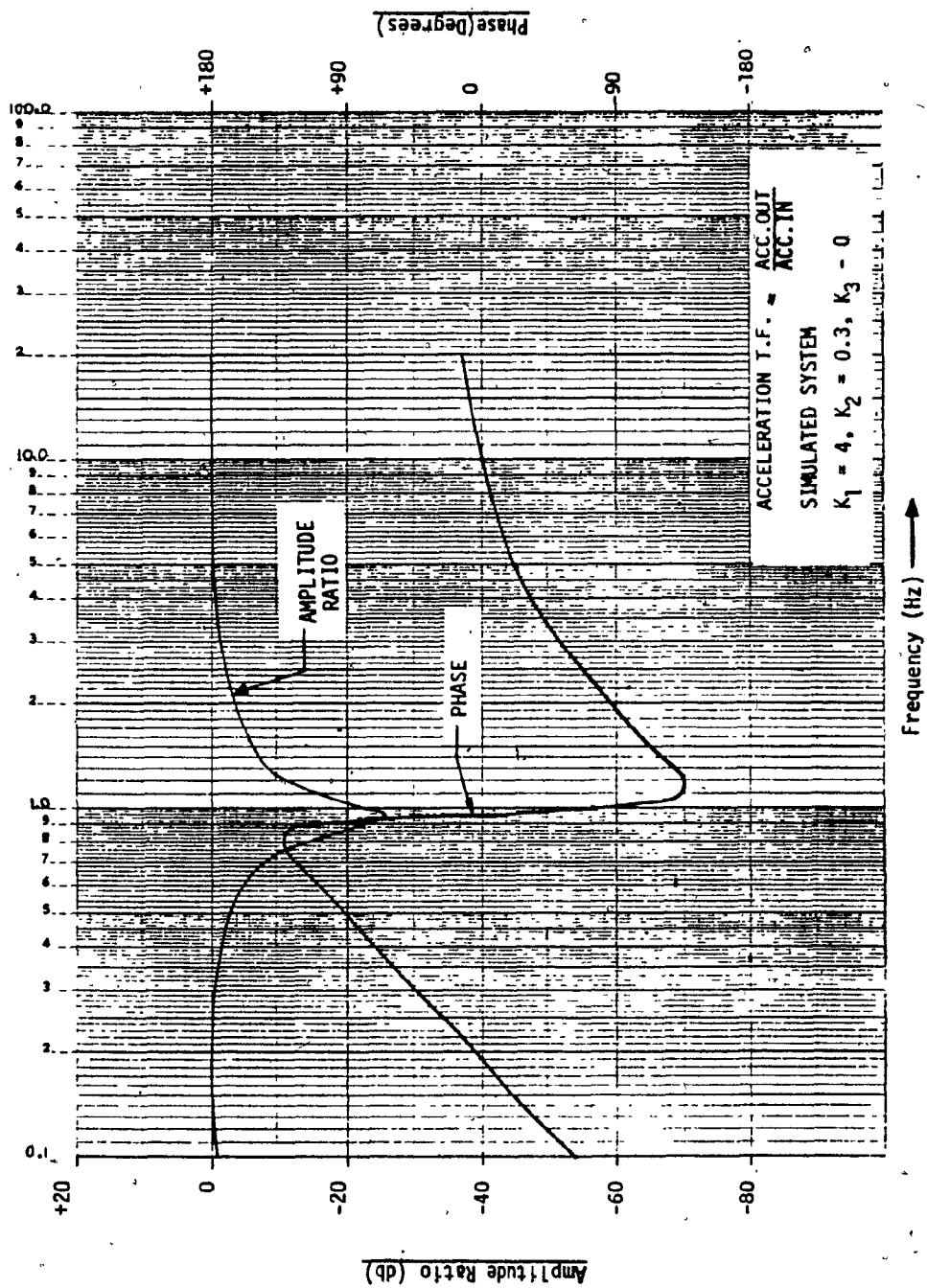


FIGURE 6.10 SIMULATED SYSTEM FREQUENCY RESPONSE

The effect of the velocity term with constant,  $K_3$ , is shown in Figure 6.11 for a simulated system. Also shown in the same figure are:

- a) The total transfer function ACC output to ACC input.  
This is indeed almost a straight line. The actual hardware system will drop off beyond 20 Hz, according to actual measurements.
- b) The acceleration transfer function with only position input connected.
- c) The acceleration transfer function with only acceleration input connected.

In practice, a fifth order elliptic filter tuned to 20 Hz, is used to eliminate the standard iteration rate of 20 Hz. The elliptic filter which is in series with the command input is the limiting factor in the motion system response.

Figure 6.12 shows the response of the 2nd order transfer function with direct acceleration input measured on an actual actuator. The position loop bandwidth in this case was 0.5 Hz. This shows that controlled and linear acceleration are possible from  $\omega_0 = 0$  up to approximately 20 Hz.

Note that load compensation has not been included in any of these groups.



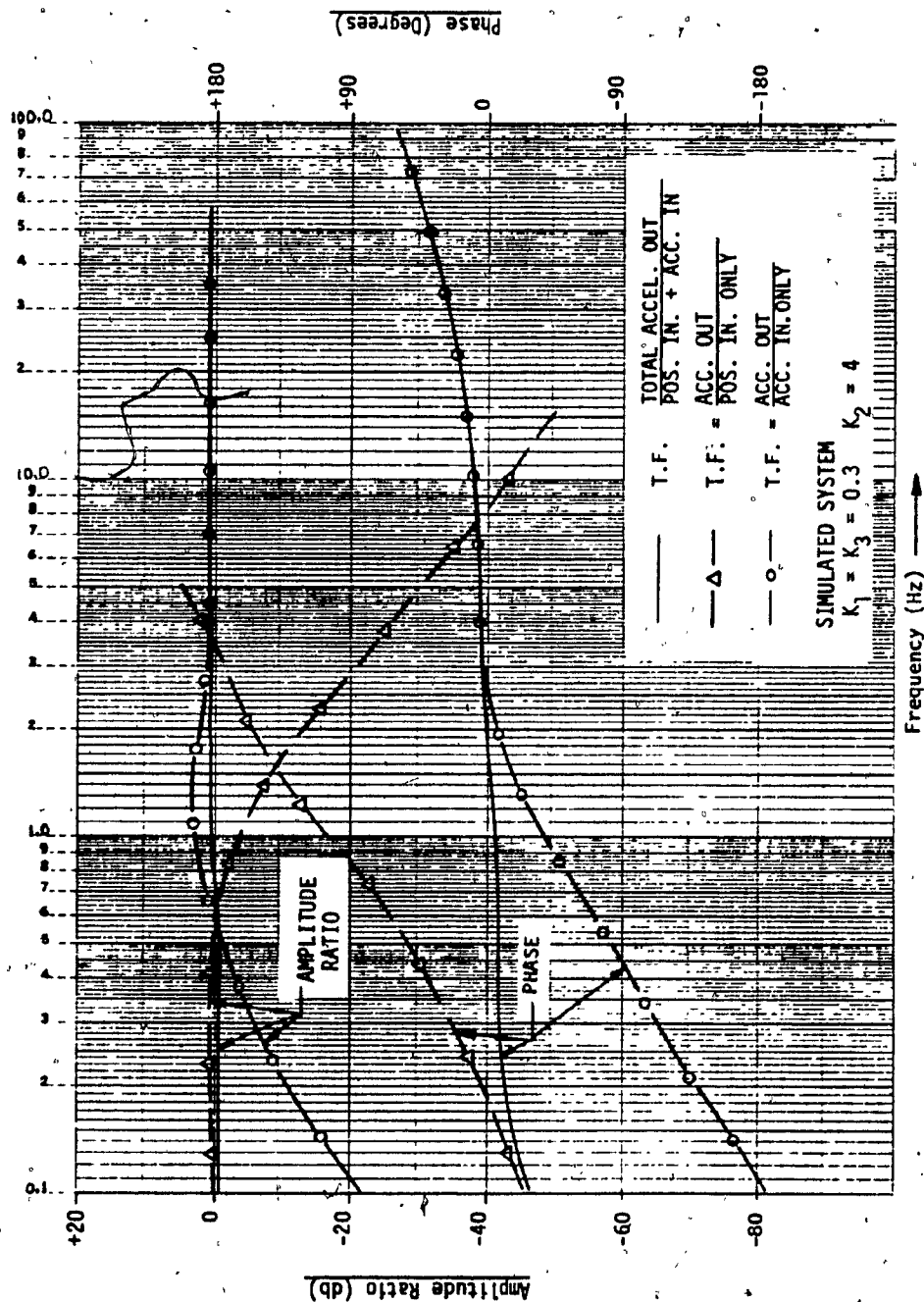


FIGURE 6.11 SIMULATED SYSTEM FREQUENCY RESPONSE

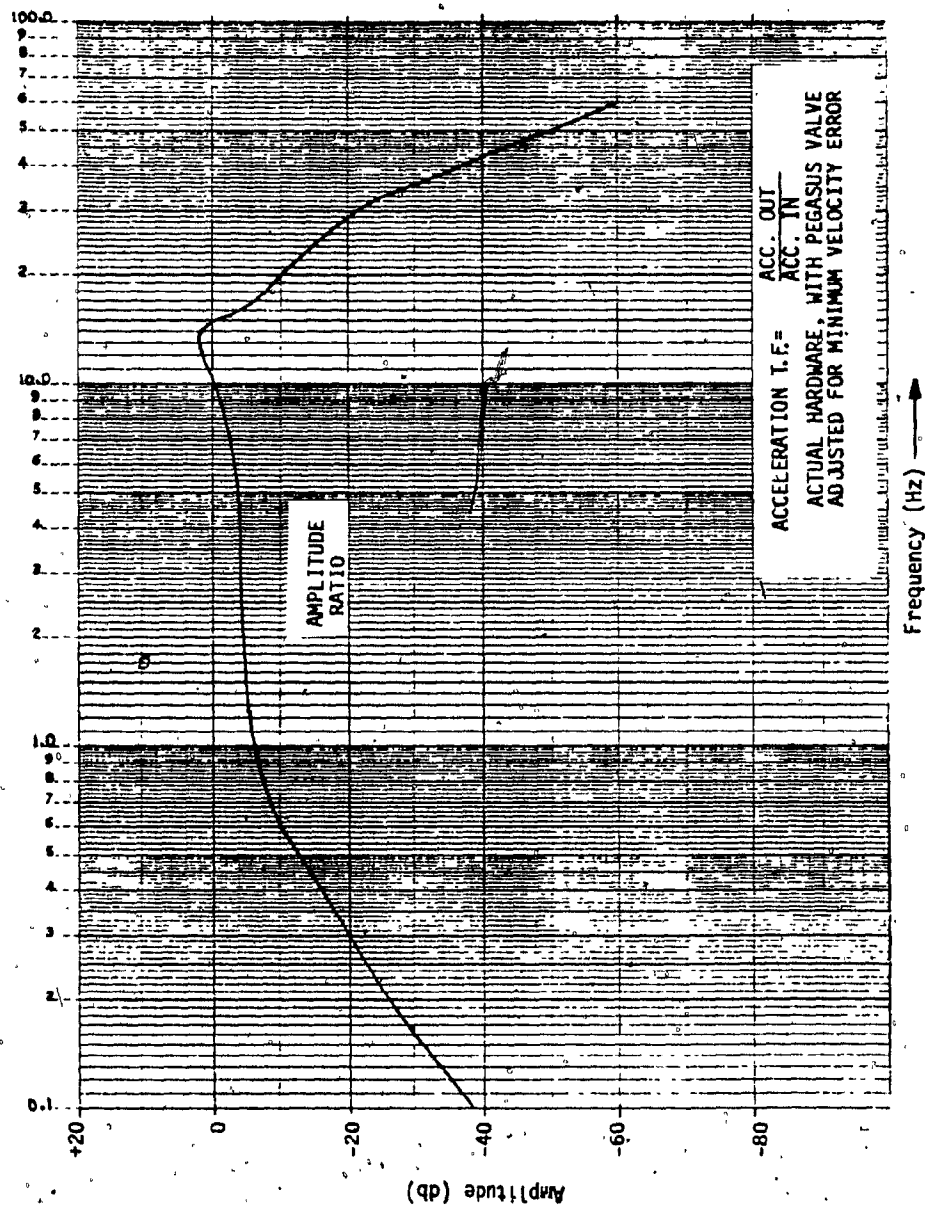


FIGURE 6.12 ACTUAL ACTUATOR FREQUENCY RESPONSE

## 7.0 SERVO JACK PERFORMANCE

Following the design and construction of the first production motion system, a vigorous series of tests was carried out to establish the performance capabilities of the system.

The tests were based on recommendations of AGARD Report 144 (Ref. 14) which defines measures of performance and purposes testing methods for flight simulator motion systems. The tests included measurement of system limits in travel, velocity and acceleration in all six degrees of freedom, measurement of frequency response in all six degrees of freedom, and delay time for pulse or step inputs.

The most exhaustive tests, and the most significant, were those of acceleration noise. Peak-to-peak and rms noise levels were measured in all six degrees of freedom for command inputs in all axes. Further, noise was plotted as function of velocity and commanded acceleration.

The purpose of these tests were to measure the smoothness of motion which, more than any other parameter, determines the quality of the motion simulation. As a reference, the threshold of human perception varies between .02 and .04g, depending on the level of activity and the amount of background acceleration. That is, an active pilot would not detect a pulse .04g if he were accelerating. If one is concentrating on detecting a disturbance in straight and level flight, however, a .02g pulse can be felt.

Figures 7.1, 7.2 and 7.3 show the hydraulic schematic of the tested servo jack, the six DOF motion system and the test equipment set-up.

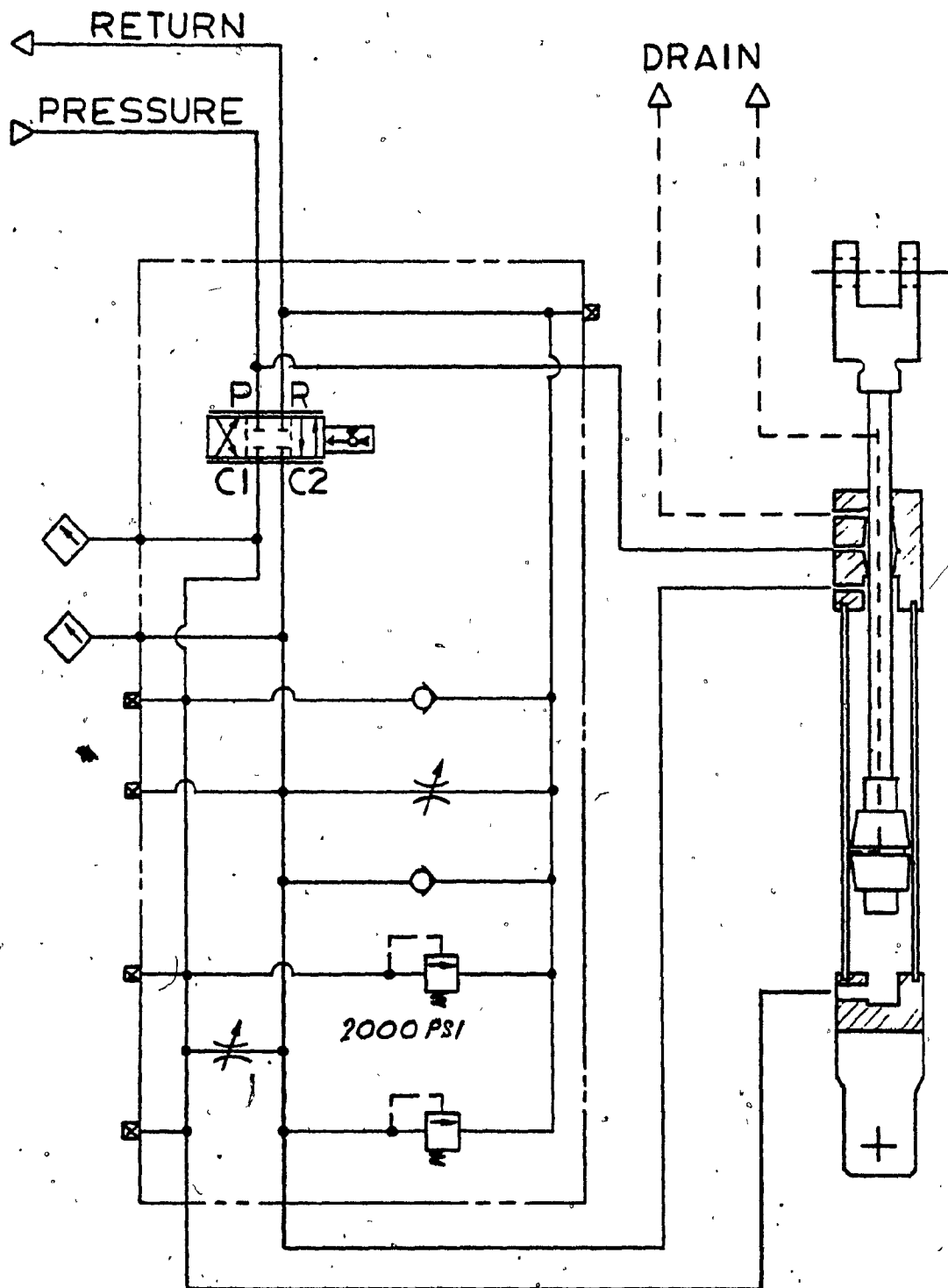


**FIGURE 7.1**

**HYDRAULIC SCHEMATIC DIAGRAM OF SERIES 500 SERVO JACK**

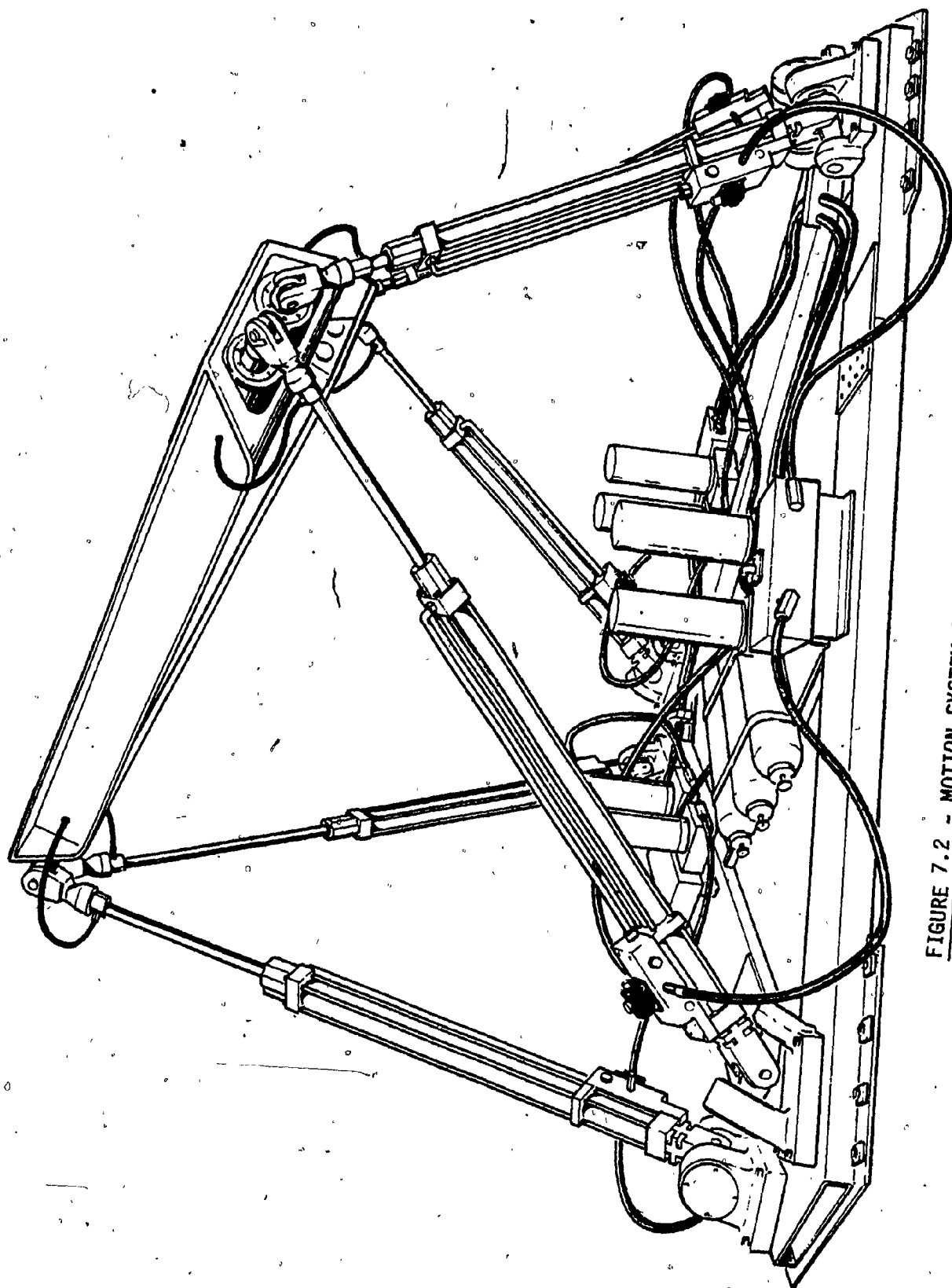


FIGURE 7.2 - MOTION SYSTEM SIX DEGREES OF FREEDOM

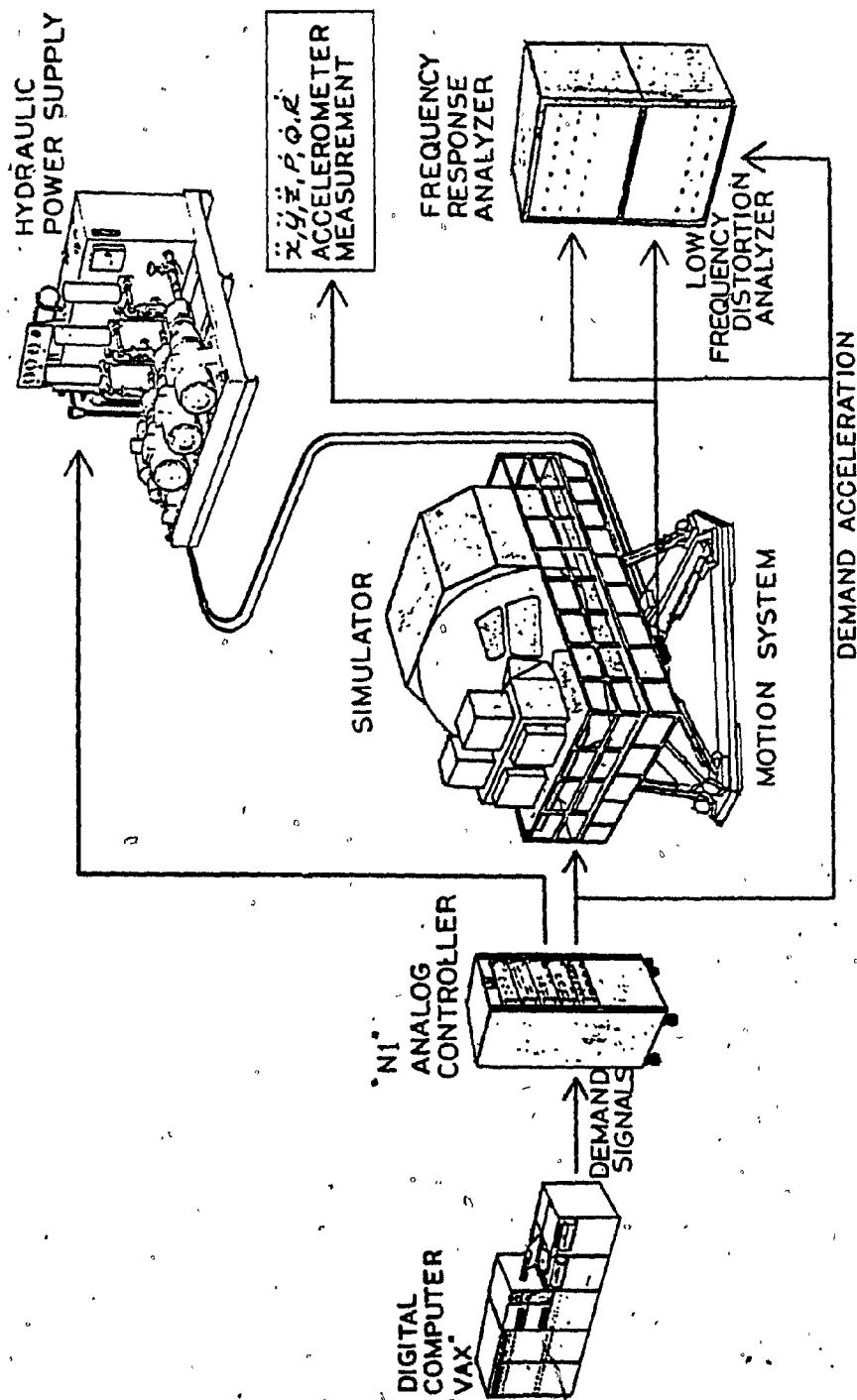


FIGURE 7.3 TEST EQUIPMENT SET UP

## 7.1 Results

The motion system frequency responses in the six axes are shown in Figures 7.4 through 7.9.

These responses were generated using computer generated sine wave inputs to sweep over the required range. The payload was 20,000 lbs and the output acceleration was determined using high precision accelerometers mounted on the upper bearings.

The bandwidth of 10 Hz is well in excess of other commercially available systems.

Figure 7.10 shows the frequency response without the elliptic filter and Figure 7.11 shows the frequency response of the electronic fifth order filter used to provide a cut-off at 10 Hz, to eliminate computer iteration noise. Clearly this filter is the limiting factor on the system response.

Typical acceleration noise versus velocity plots are shown in Figures 7.12 and 7.13. In this case the motion system is driven with 0.5 Hz sinusoidal input in one axes, roll in the case of Figure 7.12. The peak acceleration noise is measured at a variety of velocities in both the driven axes and the five non-driven axis. Peak noise includes the effects of reversal bump.

Figures 7.14 through 7.19 show the noise to signal ratio, (acceleration noise/commanded acceleration) for the six axes modes of excitation. Isolated points are plotted on a composite grid of amplitude versus frequency for a sinusoidal input.

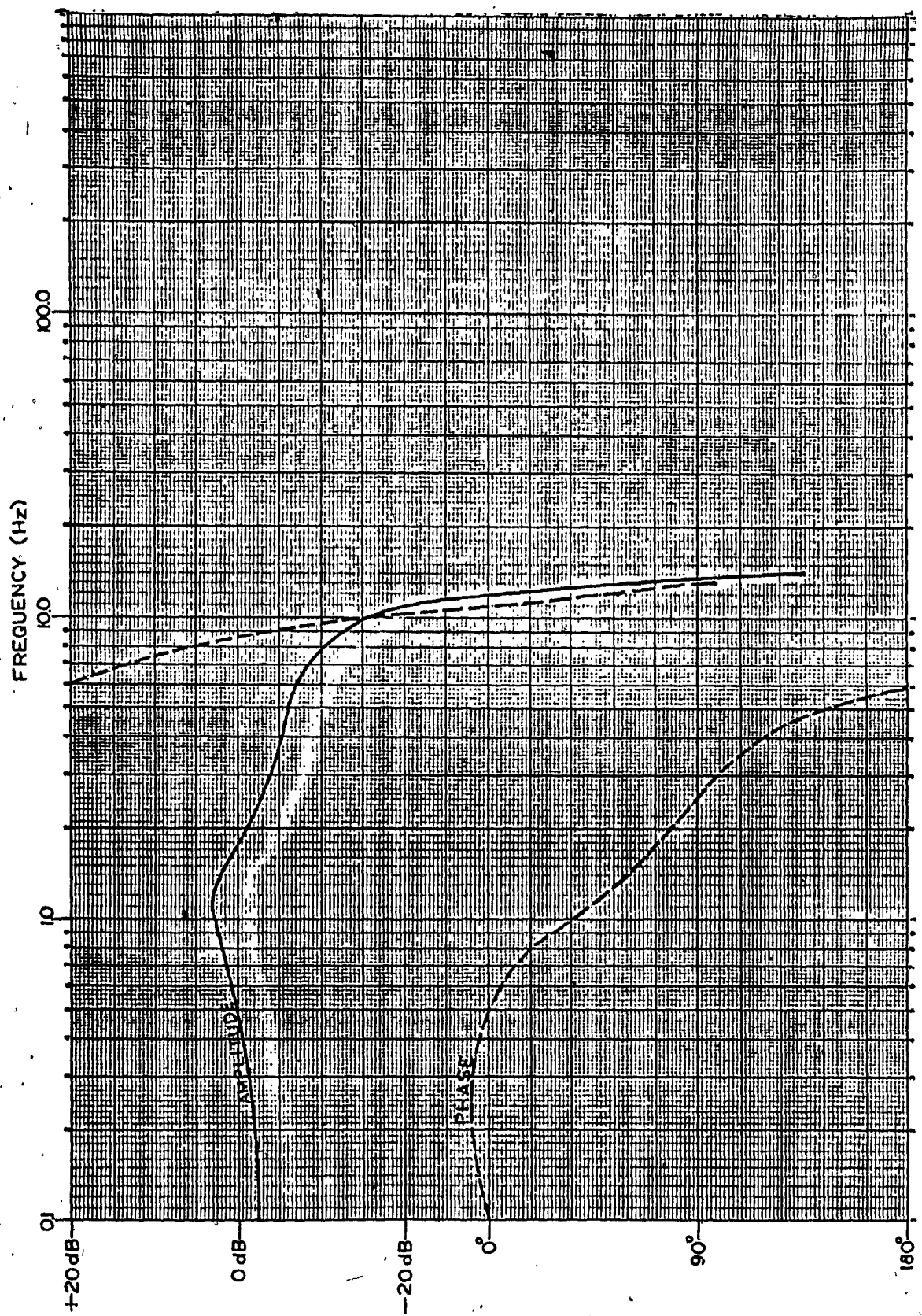


FIGURE 7.4 FREQUENCY RESPONSE - PITCH MODE



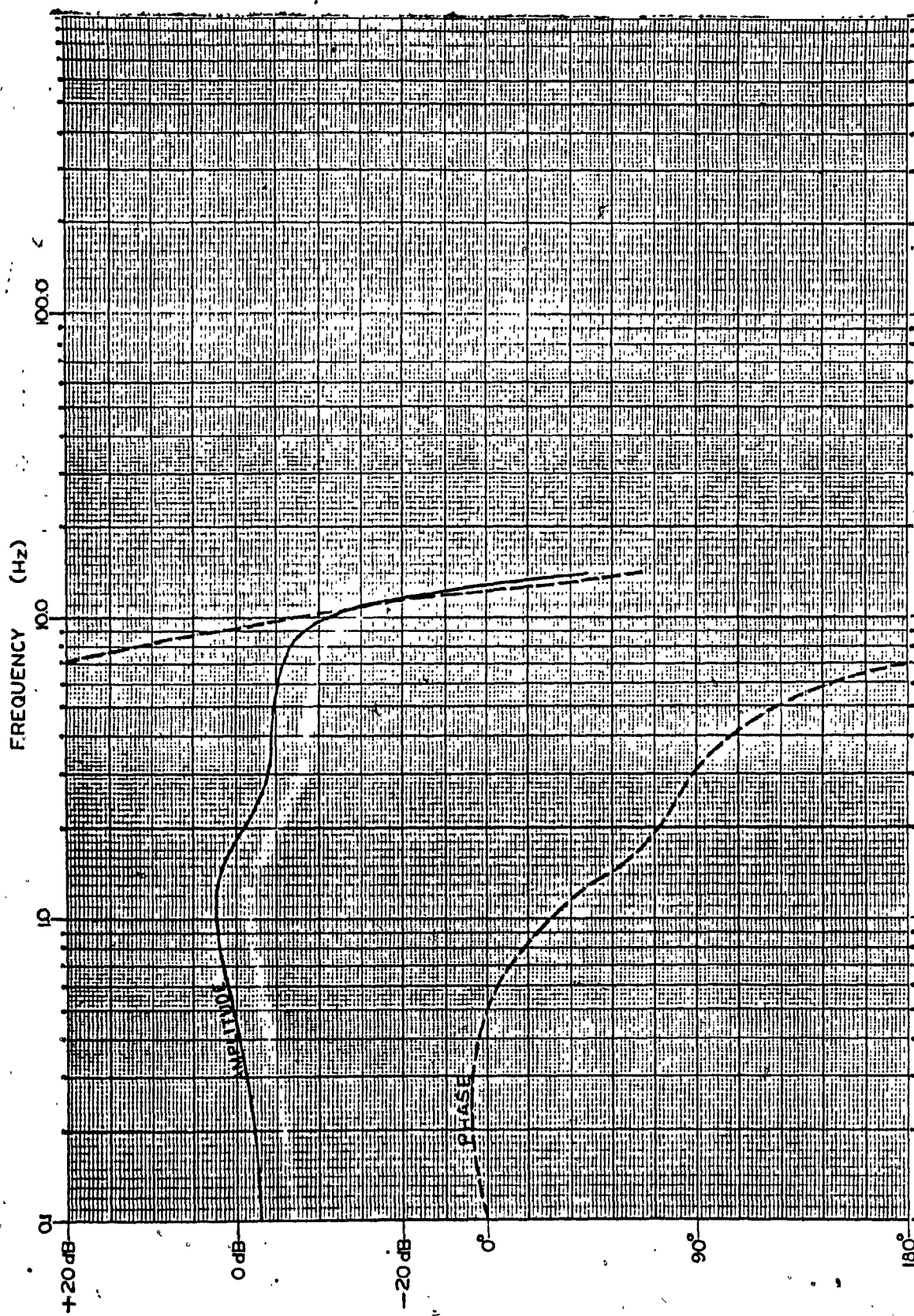


FIGURE 7.5 FREQUENCY RESPONSE, ROLL MODE

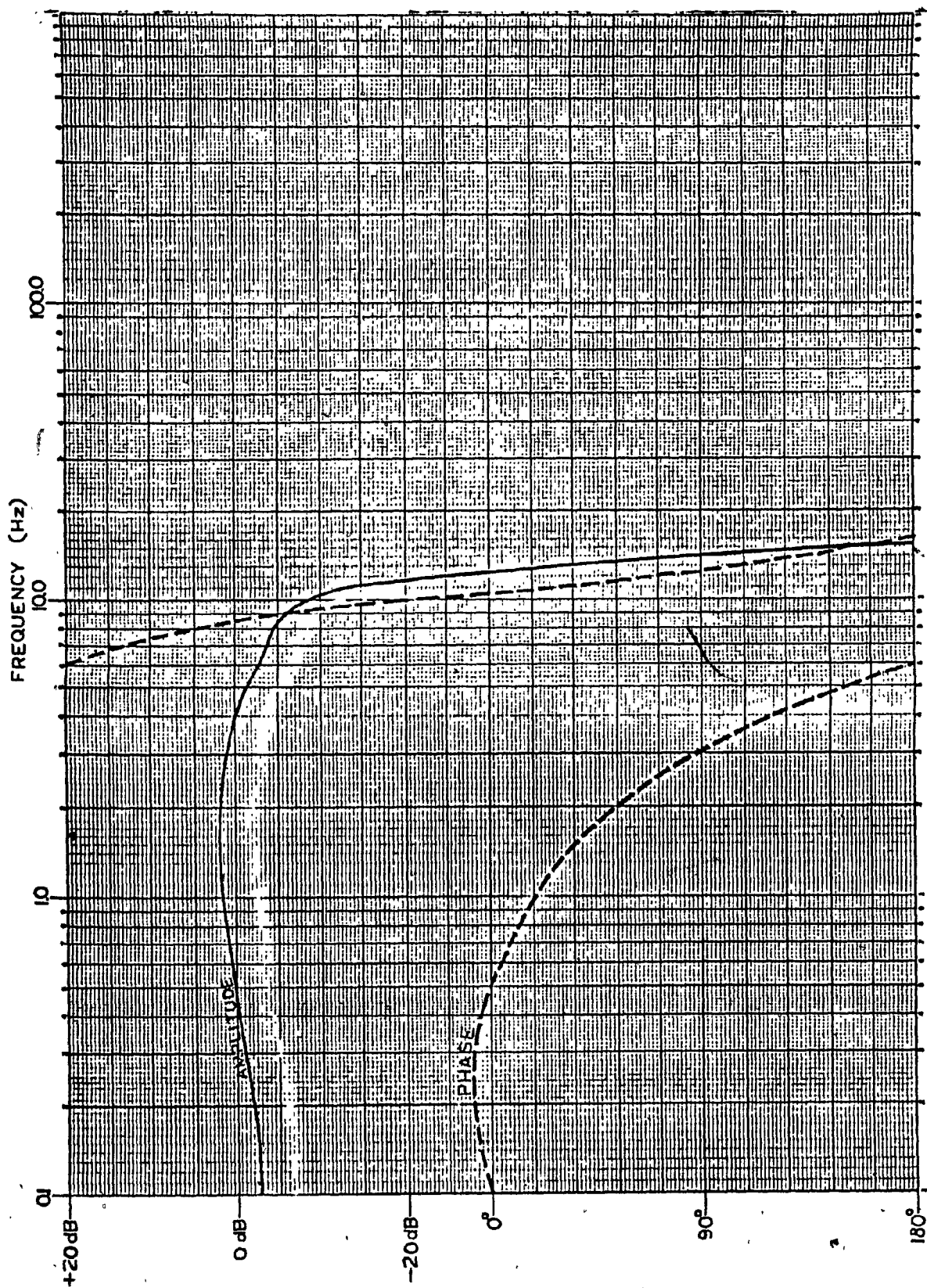


FIGURE 7.6 FREQUENCY RESPONSE, YAW MODE

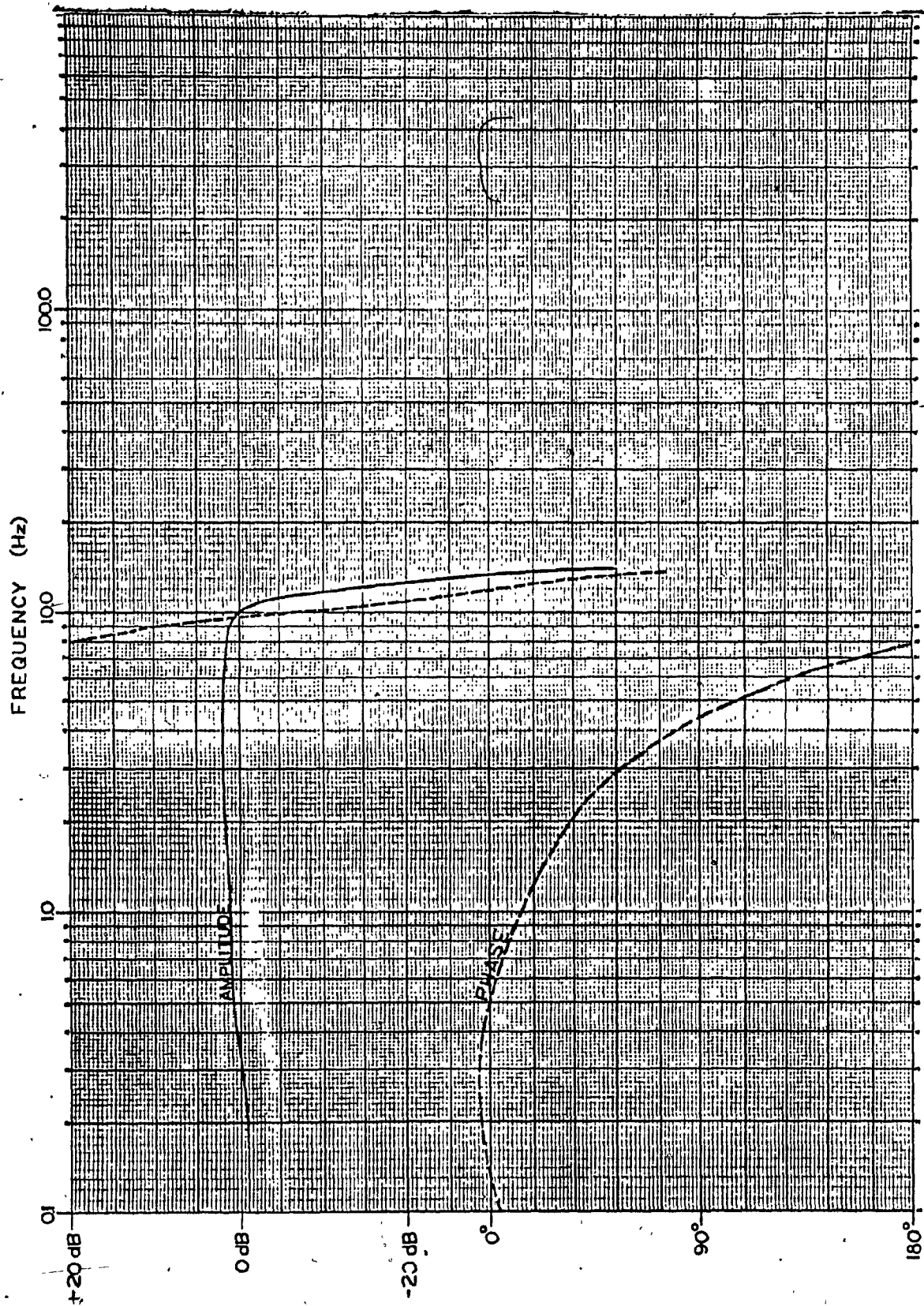


FIGURE 7.7 AMPLITUDE AND PHASE RESPONSE OF MOTION SYSTEM-HEAVE MODE

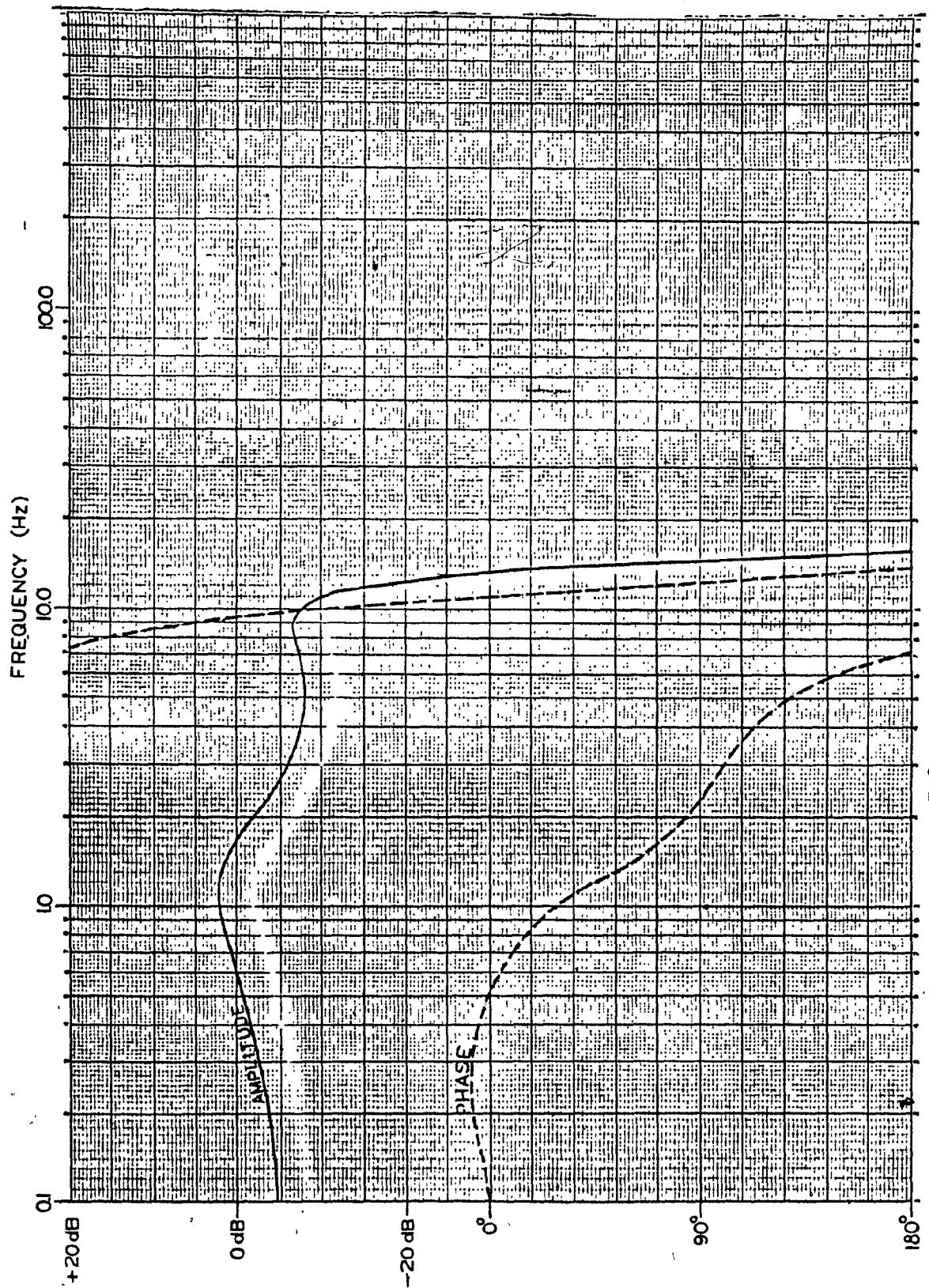


FIGURE 7.8 FREQUENCY RESPONSE, LATERAL MODE

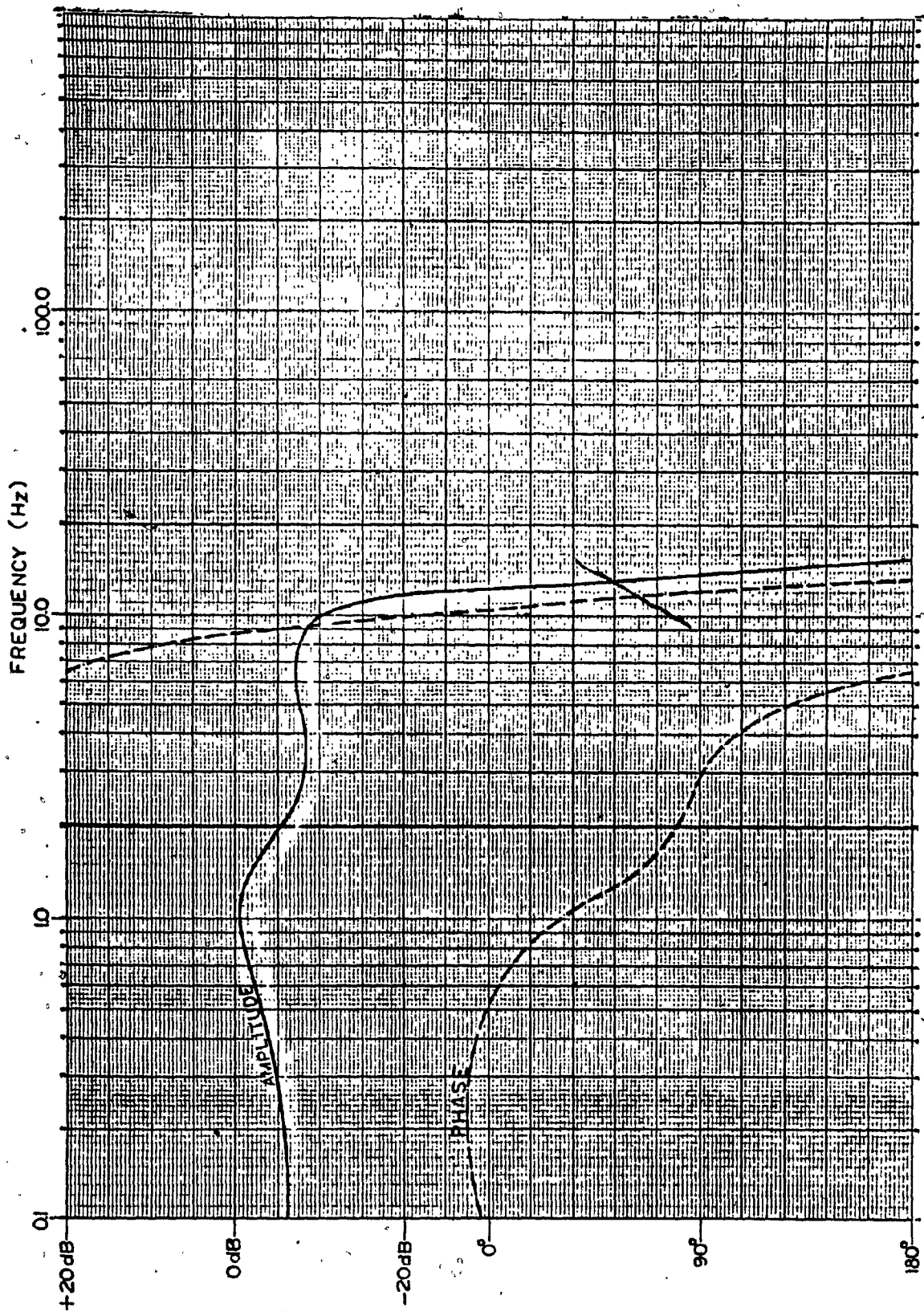


FIGURE 7.9 FREQUENCY RESPONSE, LONGITUDINAL MODE

POOR COPY  
COPIE DE QUALITEE INFERIEURE



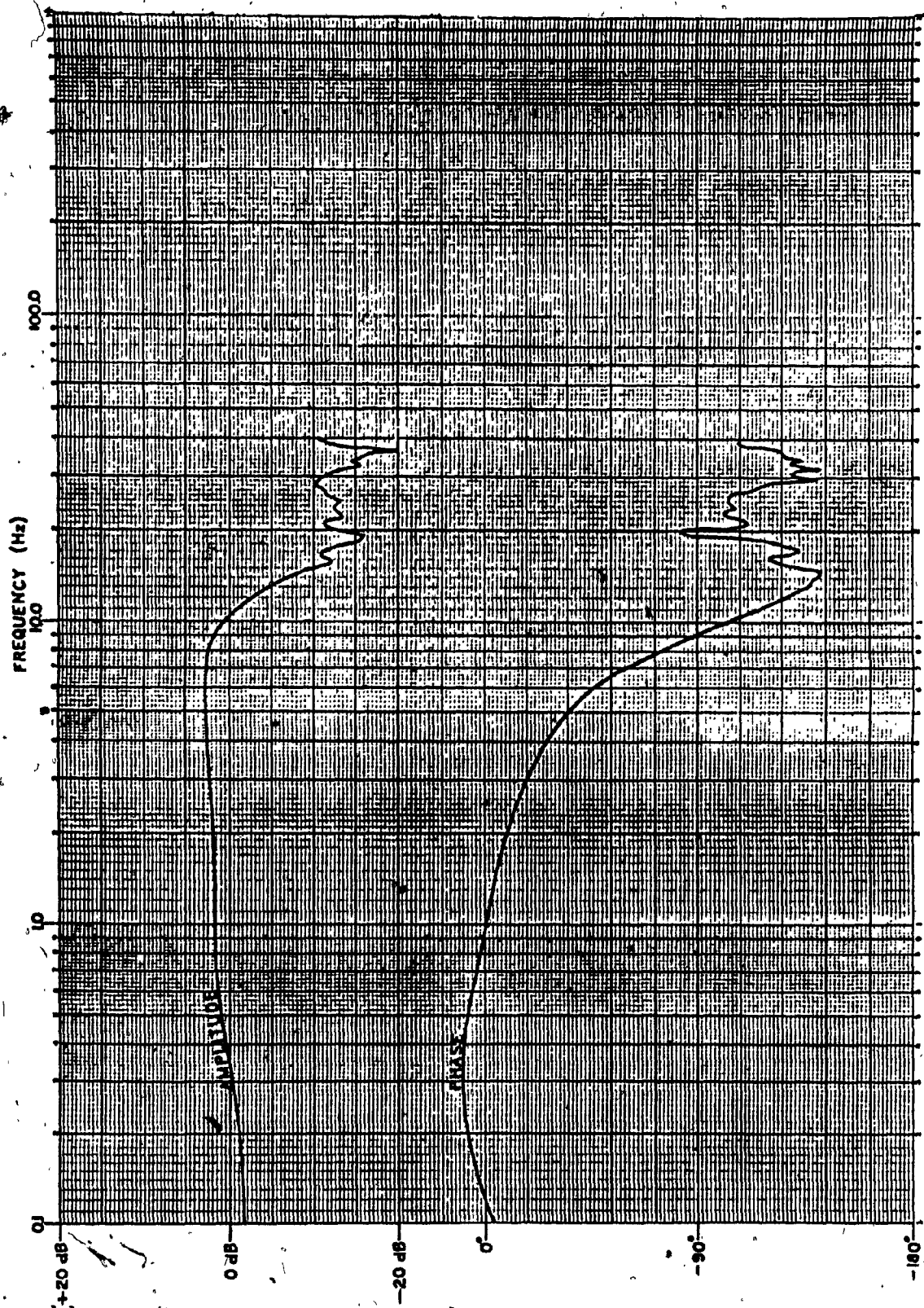


FIGURE 7.10 AMPLITUDE AND PHASE RESPONSE OF MOTION SYSTEM-HEAVE MODE, WITHOUT ELLIPTIC FILTER

POOR COPY  
COPIE DE QUALITEE INFERIEURE

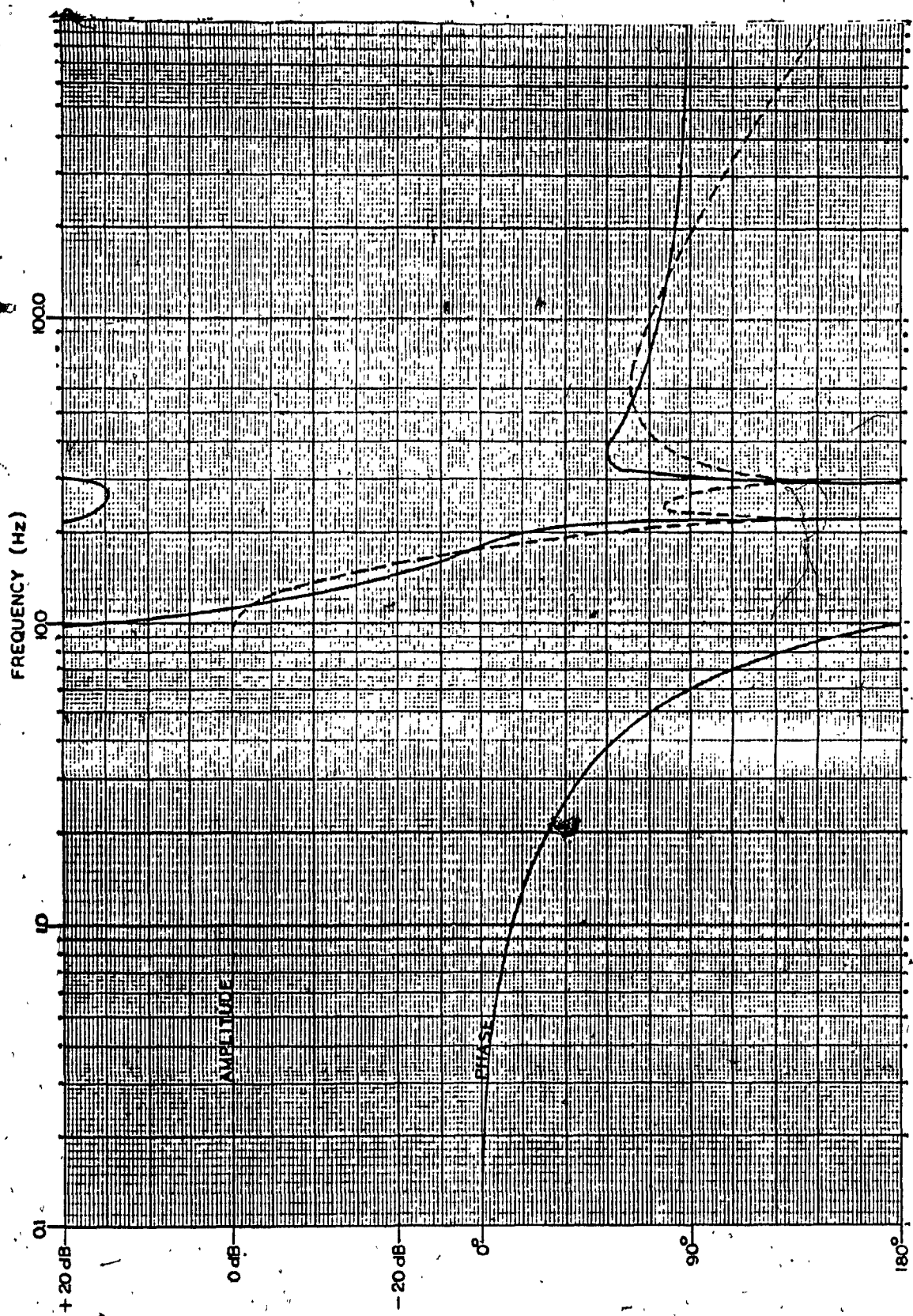
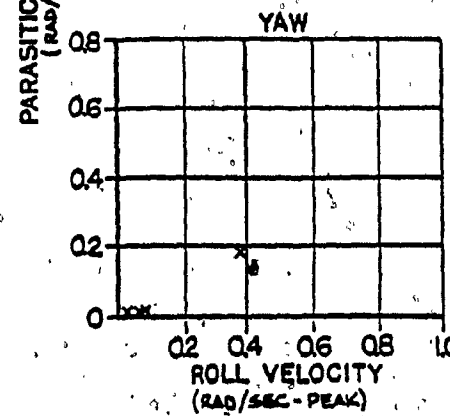
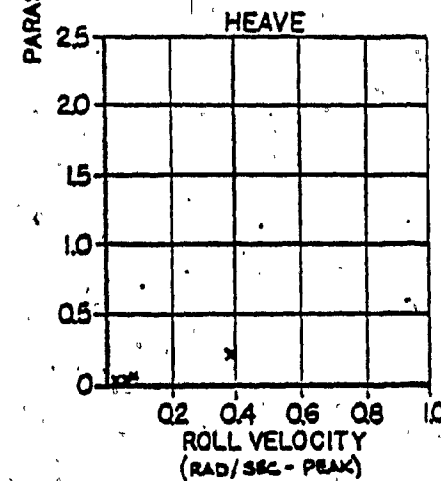
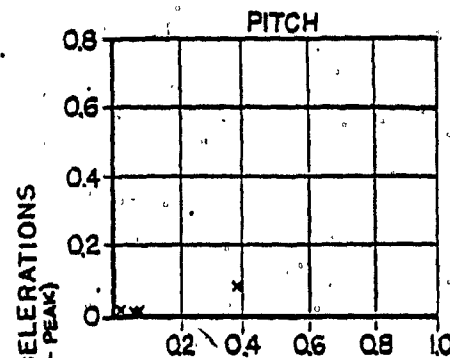
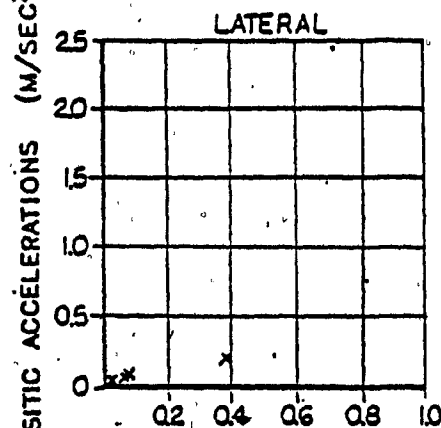
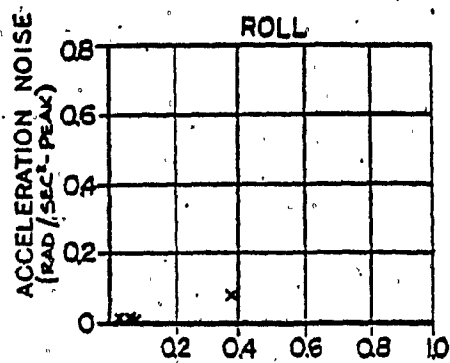
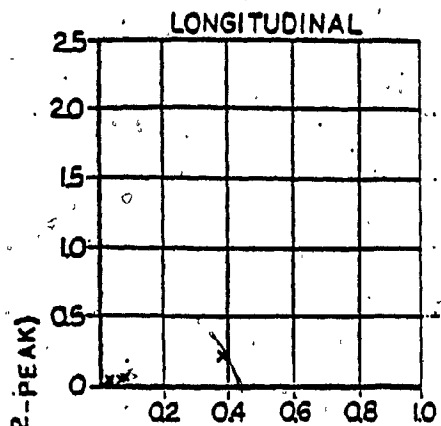


FIGURE 7.11 FREQUENCY RESPONSE, ELLIPTIC FILTER

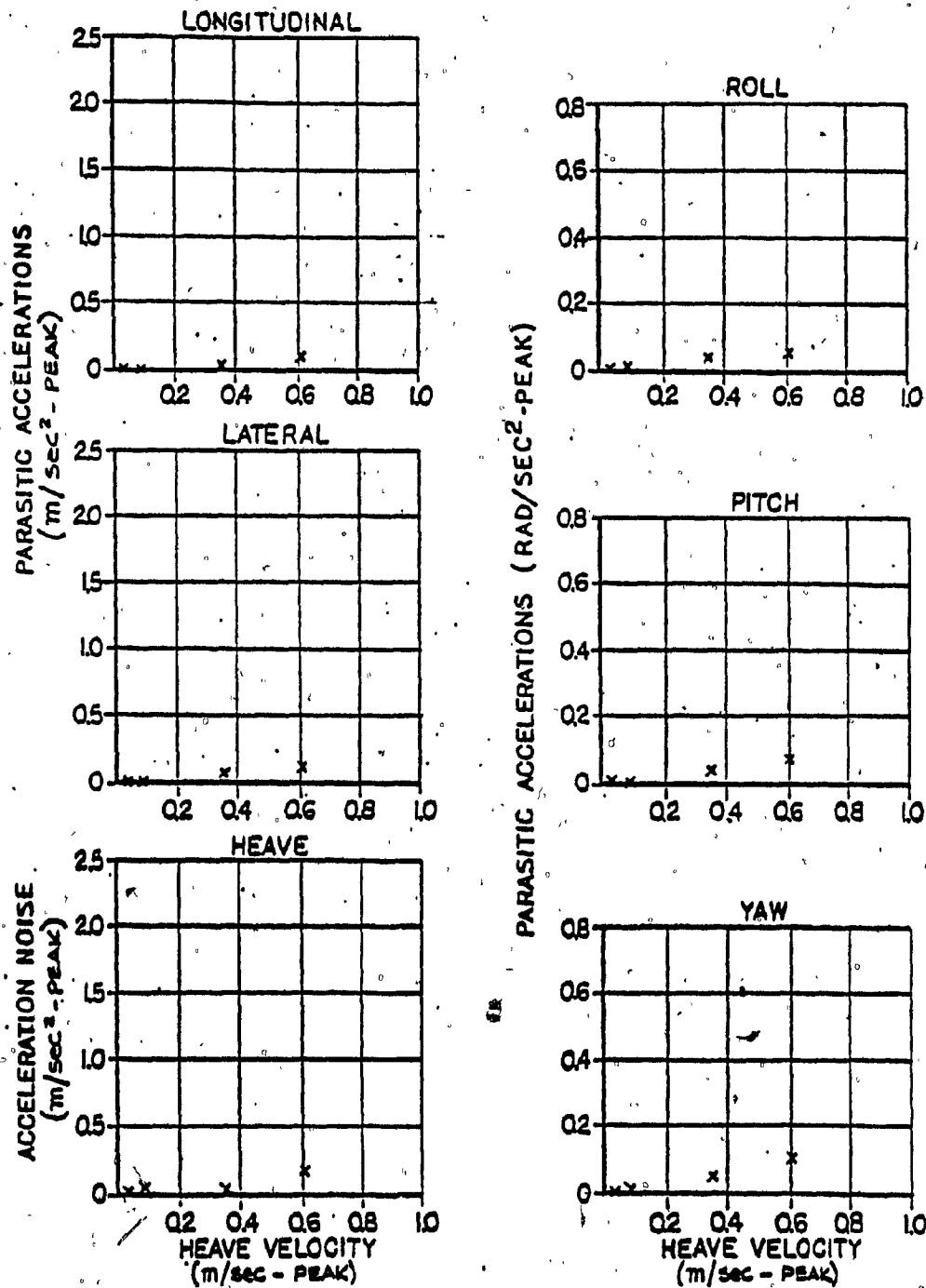
POOR COPY  
COPIE DE QUALITEE INFERIEURE



ACCELERATION NOISE FOR 0.5Hz EXCITATION OF  
THE CAE SERIES 500 (6-DOF) MOTION SYSTEM

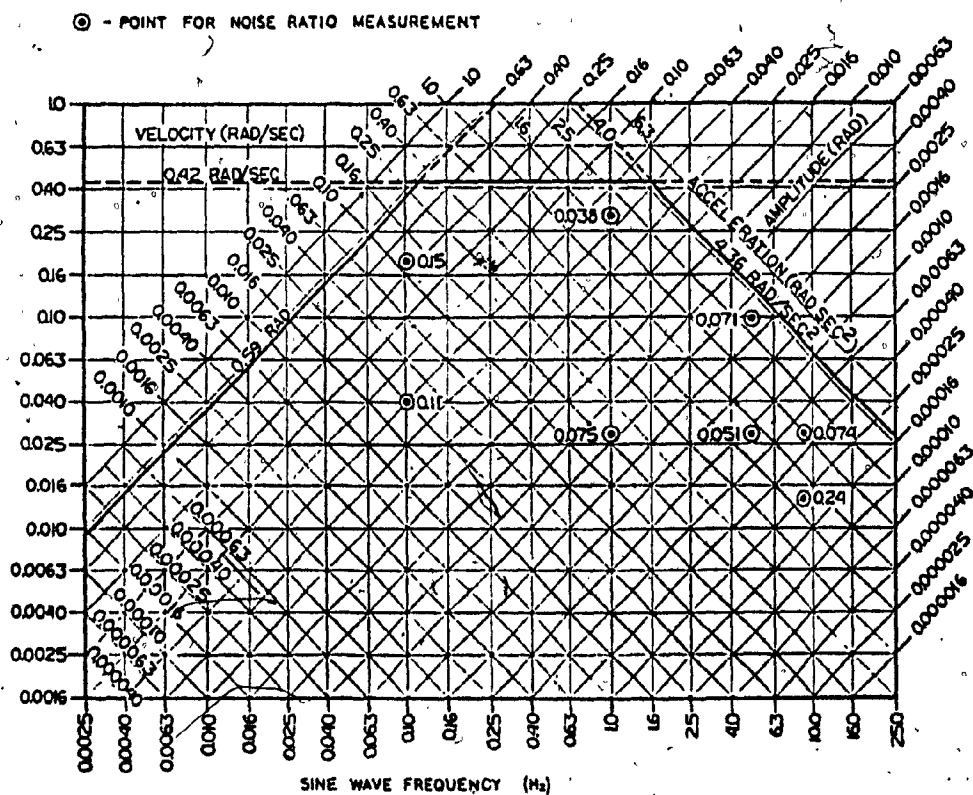
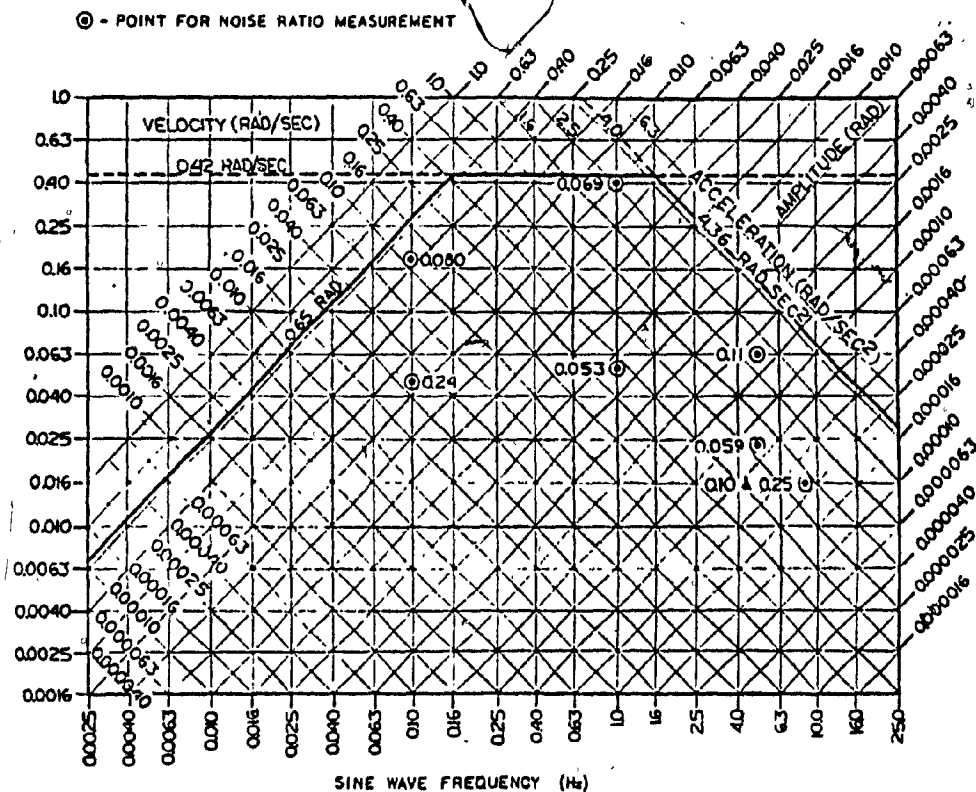
FIGURE 7.12 - EXCITATION MODE: ROLL





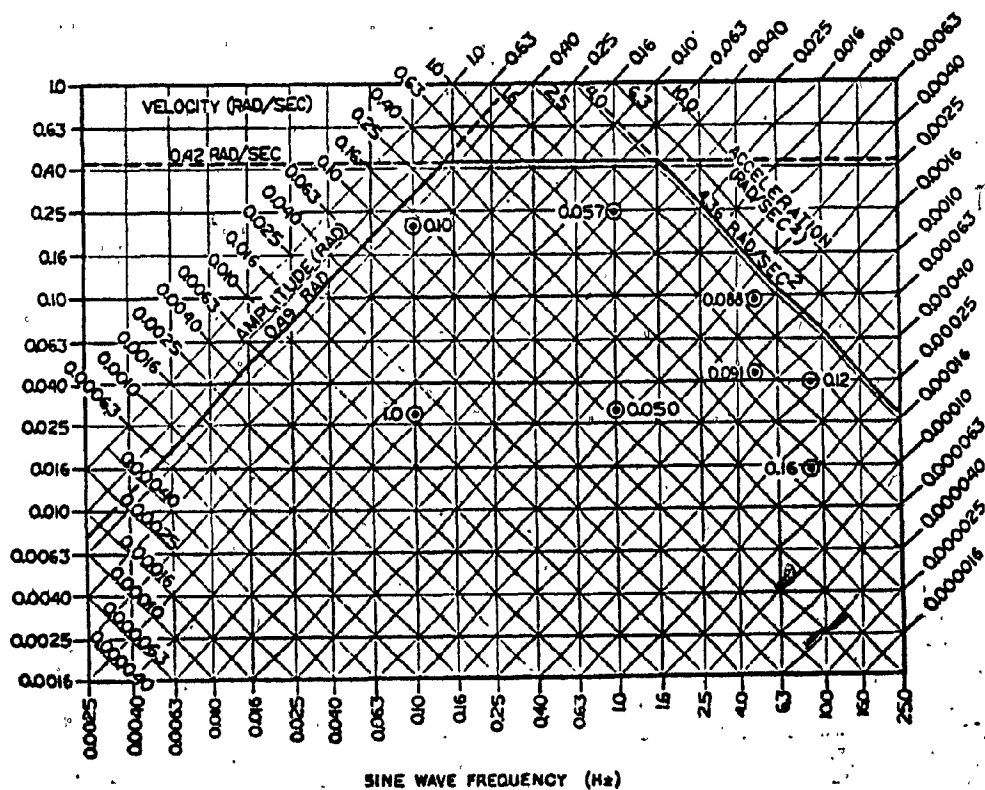
ACCELERATION NOISE FOR 0.5 Hz EXCITATION OF  
THE CAE SERIES 500 (6-DOF) MOTION SYSTEM

FIGURE 7.13 - EXCITATION MODE: HEAVE



[illegible]

⑥ POINT FOR NOISE RATIO MEASUREMENT



167'

⊙ - POINT FOR NOISE RATIO MEASUREMENT

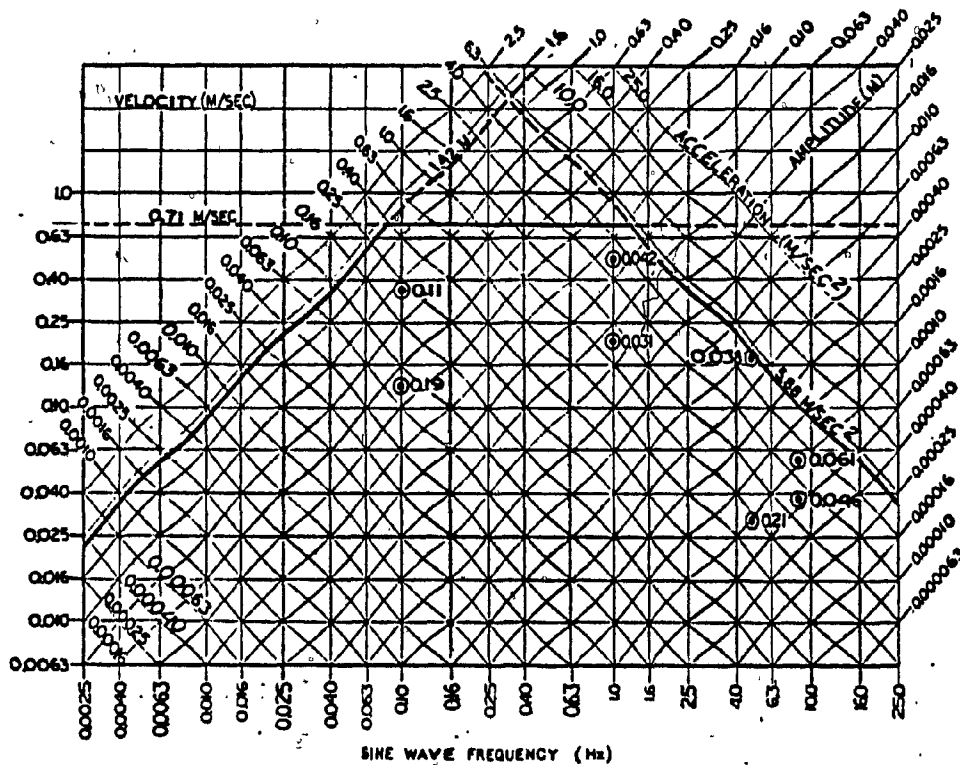


FIGURE 7.18 MOTION SYSTEM PERFORMANCE DIAGRAM - LONGITUDINAL MODE

⊙ - POINT FOR NOISE RATIO MEASUREMENT

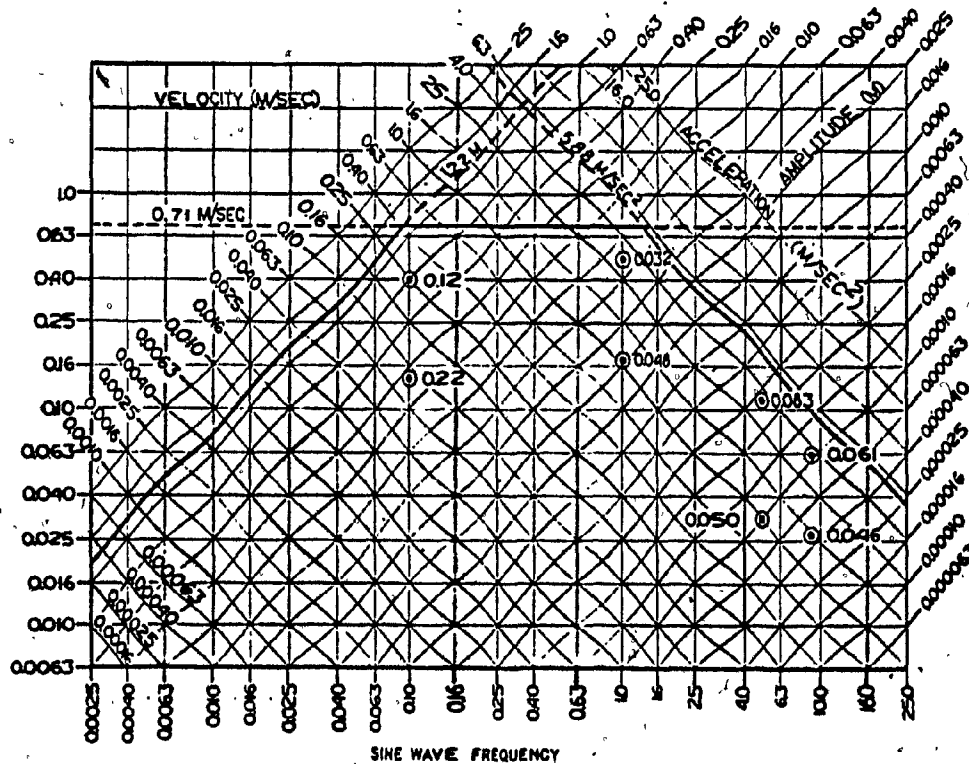


FIGURE 7.19 MOTION SYSTEM PERFORMANCE DIAGRAM - LATERAL MODE

Maximum position, velocity and acceleration can be inferred as shown by the grid. The physical limits are shown by the dark line, i.e. up to 0.08 Hz the system is limited by available travel, between 0.08 and 1.2 Hz by velocity, and from 1.2 Hz upwards by acceleration.

The noise to signal ratios show the performance that can be achieved at various points within this operating envelope.

Figure 7.20 shows the impulse response used in flight simulation primarily to indicate the delay time or latency. It is important that the delay time be compatible with those of the other cueing devices in the simulator, in particular with the visual system. In addition, the delay time should be short relative to the characteristic response time of the pilot to avoid induced oscillations.

Current simulator regulations require a maximum latency of 150 msec from control input to response; however, delays inherent in the aircraft may be added. The delay in the Series 500 motion system hardware is approximately 68 msec, so that an overall delay of 150 msec is achievable, provided good programming techniques are maintained.

Figure 7.21 shows the Series 500 motion system for KLM DC10 simulator which was used during performance testing.

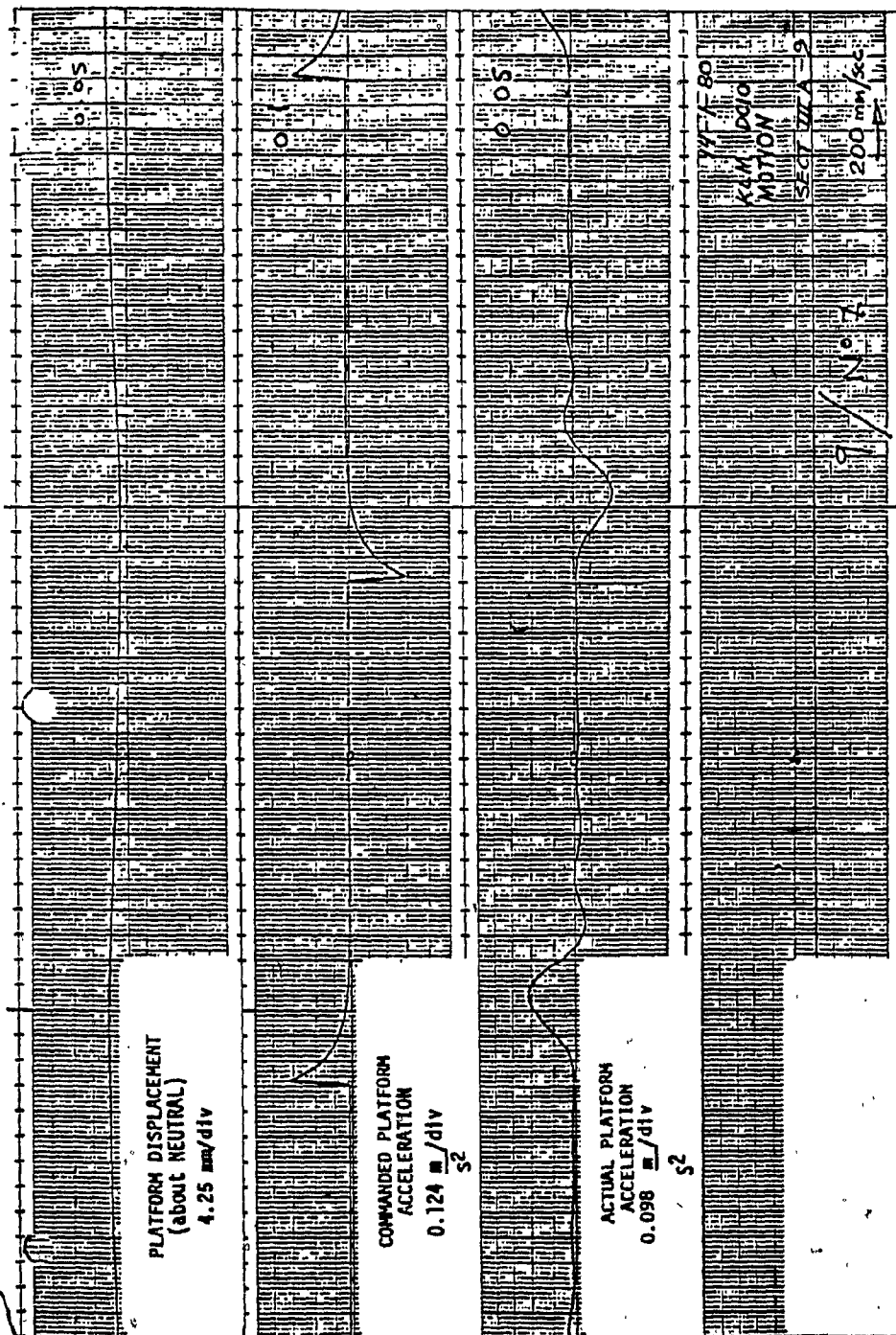


FIGURE 7.20 IMPULSE RESPONSE

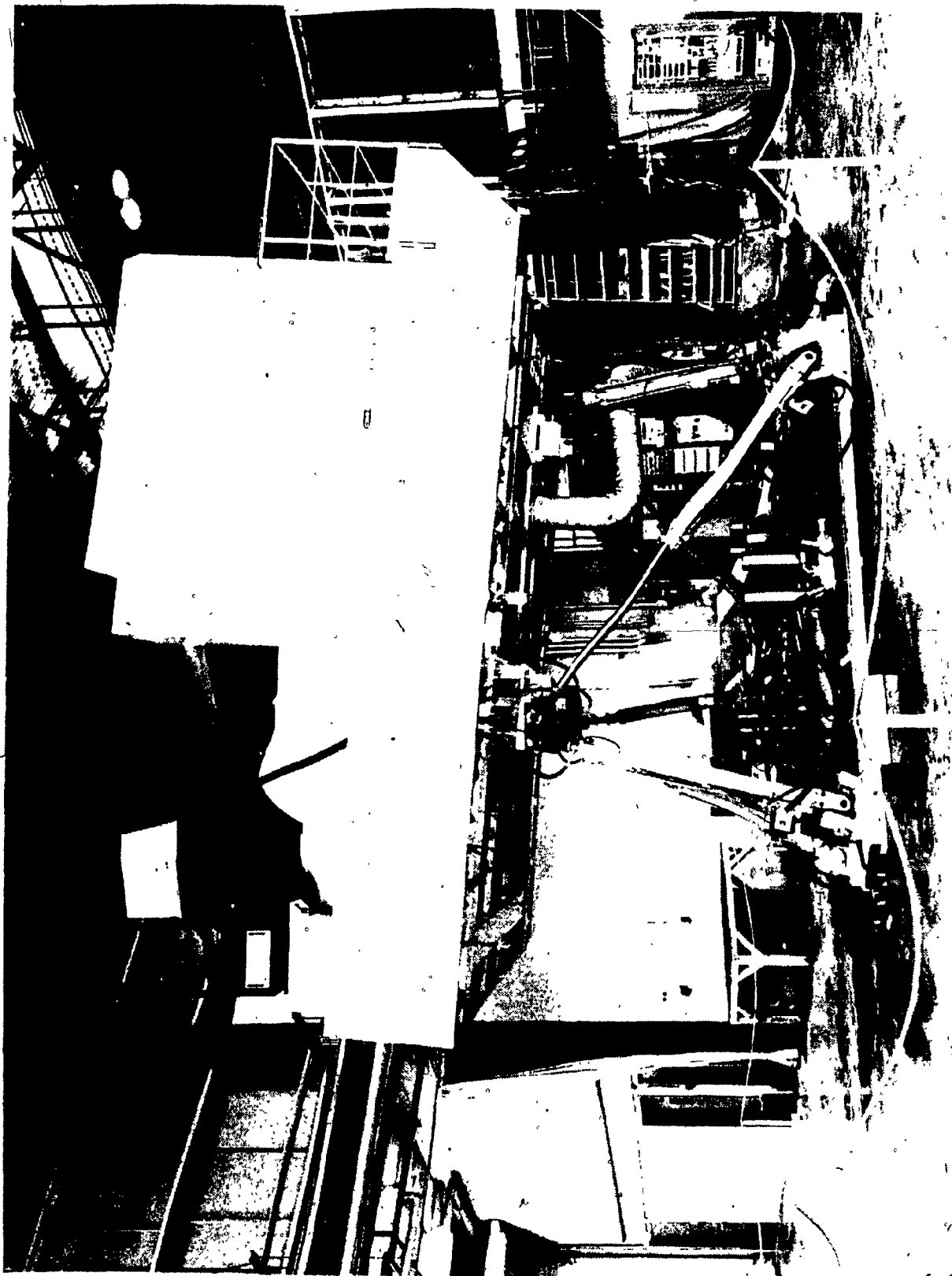


FIGURE 7.21 KLM DC10 SIMULATOR WITH SERIES 500 MOTION SYSTEM

## 7.2 Conclusion

A high performance hydraulic servo-actuator was designed and tested.

One of the major improvements over conventional actuators is the introduction of the hydrostatic piston and sleeve bearings that reduce the static and coulomb friction to 30 lbs, from the 300 lbs friction experienced with the conventional actuators.

Another anticipated advantage of the hydrostatic bearing design, is an extended actuator life due to the absence of mechanical contact. A nominal leakage flow of 1 U.S. gallon per minute is supplied to each hydrostatic bearing.

The reduction in friction imposed a requirement for further development in servovalve design and drive circuit implementation.

The servovalve port opening areas are underlapped and matched to the actuator differential areas, thus, eliminating reversal bump around the neutral position and, in general, reducing the amplitude of unwanted acceleration disturbances.

The introduction of the magnetostrictive position transducer in the piston rod eliminated the rack driven potentiometer that was relatively noisy.

A force transducer, mounted in the upper attachment point of the actuator to the flight compartment provides a force signal which is used to compensate for the load variations which occur due to the six degrees of freedom configuration, and to compensate for the load related valve non-linearities.



The tapered slotted spears at both sides of the piston provide adequate cushioning at both extremities of stroke, thus, eliminating the external deceleration valve.

Pressure transducers installed at both cylinder ports are used as a maintenance aid to monitor piston friction levels.

The use of the hydrostatic bearings reduced the hydraulic stiffness of the actuator, thus, a force forward compensation technique in the design control circuit is used to increase the apparent stiffness of the servo-actuator. This technique has proved effective in increasing the bandwidth.

Improvements in the drive circuit were achieved by introducing acceleration control at high frequencies, and position control at low frequencies. Acceleration control is effective, since, it is changes in acceleration that are perceived as motion cues by the human sensory systems. Position control is used to ensure that mechanical limits of the motions system are respected and to slowly reposition the flight compartment to its neutral position.

Compensating terms for force related non-linearities in the servo-valve and mid-range compensation to ensure a smooth transition between the position and acceleration regimes are included in the drive circuit. Experimental optimization provided a flat frequency response to 10 Hz in comparison to the previous system where the flat frequency response was in the range of 1 Hz.

The mechanical design of the actuator was predicated upon a safety factor of 4.0 based on worst case conditions. The actuators of the motion system were pin jointed at the two ends, so, that no external bending moments were applied although tranverse dynamic loads are generated through the inertia load of the actuator itself. A twisting load, which occurs if one actuator is bottomed while another moves, was limited by the design of the hydrostatic piston.

In the design process, which evolved from the previous conventional design, all dimensional changes were such as to increase strength to improve safety and performance by stiffening the actuator and hence raising its natural frequency.

The improvements were achieved with no significant increase in manufacturing cost as compared to the conventional actuator which was replaced. To date some one hundred and fifty actuators have been produced and installed in the field. Predictions of maintenance free operation and long life appears to be valid as no mechanical problems have been encountered to date and the system requires little calibration or adjustment.

## 8.0 REFERENCES

1. STRESS ANALYSIS OF TIE RODS IN CYLINDER.  
John F. Berninger, Cylinder Division,  
Parker Hannifin Corporation  
National Conference on Fluid Power, 1975.
2. STRESS ANALYSIS OF HYDRAULIC CYLINDERS:  
K.L. Seshasai, Dr. W.P. Dawkins, S.K.R. Iyengar  
Oklahoma State University  
National Conference on Fluid Power, 1975.
3. MACHINE DESIGN, Schaum's Outline Series,  
McGraw-Hill Book Company.
4. MECHANICS OF MATERIALS, 2nd Edition  
A. Higdon, E.H. Ohlsen, W.B. Stiles, J.A. Weese  
John Wiley and Sons Inc., New York, P.433.
5. VIBRATION MODES OF AN AIRCRAFT SIMULATOR MOTION SYSTEM.  
R. Hoffman, McGill University, Montreal  
M.G. McKinnon, CAE Electronics, Montreal.
6. ANALYSIS, SYNTHESIS AND DESIGN OF HYDRAULIC SERVOSYSTEMS.  
T.J. Viersma, Delft University of Technology.
7. TAILOR YOUR SHOCK ABSORBER TO FIT YOUR NEEDS.  
L.M. Polentz, Hydraulics and Pneumatics, May 1973.
8. AN ANALYSIS OF HYDRAULIC CYLINDER CUSHIONING.  
Dr. B.N. Murals  
HOW TO SPECIFY CUSHIONING IN MILL-TYPE CYLINDERS.  
G. Hoobler  
Hydraulics and Pneumatics, May 1979.
9. HYDRAULIC CYLINDER CUSHIONING, DESIGN FOR EFFECTIVE DECELERATION.  
Parker Series 2H Catalogue 1110  
Parker Hannifin Corporation.
10. UNDERSTANDING SERVOVALVES AND USING THEM PROPERLY.  
F.J. Niemos, Jr. Hydraulics and Pneumatics  
October 1977, November 1977, December 1977.
11. KEY PARAMETERS FOR SERVOVALVE SELECTION.  
Catalogue 801 1177, Moog Inc. Industrial Division.

12. SERVOVALVE OPERATION, MODELS AND PERFORMANCE.  
Catalogue PSV-277, Koehring Pegasus Division.
13. REPORT UA-00-12 ON MOTION ACCELERATION SERVO SYSTEM  
FOR 6 DOF MOTION SYSTEM  
W.J. Lam, W.L. de Vries  
Fokker-VFW.BV.
14. REPORT ON DESIGN OF A HYDROSTATIC ACTUATOR FOR USE IN  
FLIGHT SIMULATOR MOTION SYSTEMS.  
G.M. McKinnon, C. Calogeropoulos  
CAE Electronics Ltd.  
6th International Fluid Power Symposium, 1981.

9.0 BIBLIOGRAPHY

1. SERVOMECHANISM PRACTICE  
William R. Ahrendt  
McGraw Hill Book Company
2. FLUID POWER CONTROL  
J. F. Blackburn, Gerhard Reethof, J. Lowen Sheaver  
The M.I.T. Press
3. CONTROL OF FLUID POWER  
D. McCloy, H. R. Martin  
Longman Group Ltd.
4. FEEDBACK AND CONTROL SYSTEM  
Joseph J. Distefario, Allen R. Stubberud, I. Williams  
Schaum's Outline Series,  
McGraw Hill Book Company
5. STRENGTH OF MATERIALS, Parts I and II  
S. Timoshenko  
D. Van Nostrand Company Inc.
6. MACHINE DESIGN, 3rd Edition  
Paul H. Black, O. Eugene Adams, Jr.  
McGraw Hill Book Company
7. HYDRAULIC SYSTEM ANALYSIS, 2nd Edition  
G.R. Keller  
Published by the Editors of  
Hydraulics and Pneumatics Magazine, 1978.